TECHNISCHE UNIVERSITÄT MÜNCHEN

Lehrstuhl für Genetik

Crybb2, a new candidate gene for Schizophrenia?

Minxuan Sun

Vollständiger Abdruck der von der Fakultät Wissenschaftszentrum Weihenstephan für Ernährung, Landnutzung und Umwelt der Technischen Universität München zur Erlangung des akademischen Grades eines

Doktors der Naturwissenschaften

genehmigten Dissertation.

Vorsitzender: Univ.-Prof. Dr. S. Scherer

Prüfer der Dissertation:

1. apl. Prof. Dr. J. Graw
2. Univ.-Prof. Dr. M. Klingenspor

Die Dissertation wurde am 14.07.2011 bei der Technischen Universität München eingereicht und durch die Fakultät Wissenschaftszentrum Weihenstephan für Ernährung, Landnutzung und Umwelt am 14.10.2011 angenommen.

I dedicate this work to my parents.

Index

Zusammenfassung

βB2-Kristallin wurde ursprünglich als ein Strukturprotein der Augenlinse beschrieben; Mutationen im für βB2-Kristallin kodierenden Gen *Crybb2* führen generell zu Katarakten. Darüber hinaus erfolgt eine Expression im Gehirn, wobei die dortige Funktion des βB2-Kristallins noch nicht aufgeklärt werden konnte. Die in dieser Arbeit durchgeführten Untersuchungen mit der im *Crybb2* – Gen mutierten Mauslinie *O377* zeigten eine veränderte Struktur sowie ein verringertes Volumen des Hippocampus im Vergleich zu Wildtyp-Kontrollmäusen. Im Gegensatz dazu waren Struktur und Volumen des Hippocampus in der mutierten *Philly* – Mauslinie nicht signifikant verändert. Als weiteres Ergebnis wurde eine *Crybb2* – Expression innerhalb bestimmter Gehirnregionen sowie in verschiedenen GABA-ergen Interneuronen nachgewiesen. Im ventralen Hippocampus zeigte sich eine altersabhängige Verringerung der Zelldichte von Parvalbumin positiven GABA-ergen Interneuronen. Dies wurde jedoch nicht im prefrontalen Cortex beobachtet. Darüber hinaus zeigte sich eine verringerte Komplexität der Dentriten bei Neuronen des Hippocampus sowie eine reduzierte Reifung der Astrocyten in adulten *O377* – Mäusen. Diese pathologischen Phänotypen könnten durch die beobachtete Überexpression von *Capn3* und *Tmsb4x* aufgrund einer erhöhten Calciumkonzentration in Neuronen des Hippocampus verursacht werden.Die Ergebnisse dieser Arbeit deuten auf eine wesentliche Funktion von *Crybb2* im Gehirn hin. Es stellt daher ein neues Kandidatengen für psychiatrische Studien dar, speziell für die Erforschung von Schizophrenieerkrankungen.

1 Abstract

βB2-crystallin is presently described as a structural protein of the ocular lens. Mutations in the corresponding gene, *Crybb2*, cause cataracts. Although βB2-crystallin is reported to be expressed in the brain, its function there is still unknown. In the present study, I demonstrate that in *Crybb2* mutant mice, *O377*, structure of hippocampus is altered and hippocampal volume is reduced compared with wild type, while in the *Philly* mouse; another *Crybb2* mutant mouse, the hippocampus structure and volume do not show significant difference compared with wild type. In addition, βB2-crystallin is shown to be expressed in parvalbumin positive GABAergic interneurons, calretinin positive GABAergic interneurons and somatostatin positive GABAergic interneurons. Furthermore, the cell density of parvalbumin positive GABAergic interneuron is reduced in an age-dependent manner, specifically in ventral hippocampus, but not in the prefrontal cortex. Loss of dendritic complexity in hippocampal neurons and less astrogensis in adult *O377* mutants are also observed. Up-regulation of *Capn3* and *Tmsb4x* caused by increase of calcium concentration in hippocampal neurons is associated with losses of parvalbumin positive GABAergic interneurons and reduced dendrtic comlexity. All results suggest that *Crybb2* plays an important role in the brain, and it is a new candidate gene for psychiatric disorders, especailly for schizophrenia.

2 Introduction

Crybb2 is mapped to chromosome 5 (60cM) in mouse while the human homolog is located on chromosome 22 (22q11.2-12) (Hulsebos *et al.*, 1995; Kerscher *et al.*, 1995). The corresponding protein, βB2-crystallin, is one of the main structural proteins of the vertebrate ocular lens, and plays an important role in refraction of light and maintain the opacity of lens, together with other crystallins. *Crybb2* is expressed in retina, brain and testis (Magabo *et al.,* 2000). Mutations in *Crybb2* are associated with hereditary cataracts (Graw 2009). A Cataract is a clouding affecting passage of light that develops in the crystalline lens of the eye or in its envelope. Recent reports suggest additional functions of βB2-crystallin in testis and brain (Duprey *et al.,* 2007; Ganguly *et al.,* 2008). My study indicates that *Crybb2* plays an important role in the brain. In this chapter, I mainly focus on the crystallins, βB2-crystallin and its related functions in human and mouse.

2.1 Crystallins

Crystallins account for 30–35% of the entire mass of the transparent lens, and up to 90% of the entire protein of the lens. All the crystallins are derived from only one cell type, the ectoderm of the lens placode and are important in maintaining the lens transparency and flexibility,. They were first discovered by Mörner in 1893 and are named α-, β- and γ-crystallins. Mutations in crystallins are linked to the loss of transparency in the lens, leading to cataract. In addition, crystallins are associated with axon outgrowth, non-syndromic deafness and neurodegenerative diseases (for reviews: Graw, 2009; Graw, 2004; Bhat *et al.*, 2003).

2.1.1 α-Crystallins

There are two types of α-crystallins, αA-crystallin and αB-crystallin, which are encoded by *Cryaa* and *Cryab* respectively (in human *CRYAA*, *CRYBB*). *Cryaa* and *Cryab* are located on chromosome 17 (31.8) and chromosome 9 (50.6 cm) respectively in mouse, while the human homologs are located on chromosome 21q22 and chromosome 11q22 respectively (Graw, 2009).

Mutations in *CRYAA (Cryaa)* lead to recessive and dominant cataracts. Since Litt first described a family with autosomal dominant cataract due to a single missense mutation in αA-crystallin (Litt *et al.*, 1997), several mutations in αA-crystallin leading to cataracts in the human population have been reported (Graw, 2009). In

additionally to cataract, microcornea and microphthalmia have also been reported to be caused by mutations in *CRYAA* (Devi *et al*., 2008; Khan *et al*., 2007; Hansen *et al*., 2007). Mutations in *Cryaa* in mouse also cause cataract. Up-to-now, four mouse mutants have been characterized, and all of them develop cataract.

αA-crystallin is mainly expressed in the lens but also detectable in brain and retina. αB-crystallin is essentially considered to be a ubiquitous protein, since it is highly expressed in heart, skeletal muscle and kidney, and is also detected in skin, lung, placenta, and brain (Graw, 2009).

αA-crystallin is considered to have anti-apoptotic properties by binding to Bax and Bcl-S. αA-crystallin homozygous mouse mutants result in small eyes caused by an increase in cell death by apoptosis (Xi *et al*., 2008). Most recently, Ninkovic and colleagues showed that the transcription factor Pax6 regulates the survival of dopaminergic neurons in olfactory bulb by directly regulating the expression of αA-crystallin, which blocks apoptosis by inhibition of procaspase-3 activation (Ninkovic *et al*., 2010). Moreover, they also demonstrated that re-expression of *Cryaa* fully rescued survival of Pax6-deficient dopaminergic interneurons *in vivo* and knockdown of *Cryaa* by shRNA in wild-type mice reduced the number of dopaminergic interneurons in olfactory bulb. Although, *Cryaa* has often been reported to be expressed and play a role outside the lens, only cataract is reported to be associated with mutations in the αA-crystallin encoding gene.

In contrast to αA-crystallin, only a small percentage of mutations in αB-crystallin cause dominant cataracts in human, but most of the mutations are suggested to cause also for desmin-related myopathy or dilated cardiomyopathy (Graw, 2009; Horwitz, 2003). Even the homozygous *Cryab* knock-out mouse mutants do not display an overt disease phenotype (Brady *et al.,* 2001).

Interestingly, αB-crystallin is associated with several neurological disorders. As early as 1988, αB-crystallin was reported to be up-regulated in scrapie infected hamster brain (Duguid *et al*., 1988). This was further confirmed by a proteomics study for neurodegeneration diseases (Zabel *et al.*, 2006). Moreover, αB-crystallin accumulates in the brain of patients with Alexander's disease. Alexander's disease is a neurodegeneration disease caused by mutations in *GFAP* gene (coding for the glial fibrillary acidic protein). The characteristic neuropathological feature of all forms of Alexander's disease is the presence of Rosenthal fibres. The up-regulation of αB-

crystallin was also reported in response to stress in GFAP expressing glioma cells. Therefore it is functionally related to the development of Alexander's disease (for reviews see: Quinlan, 2007; Graw, 2009). Additionally, αB-crystallin is reported to accumulate with β-amyloid peptide in Alzheimer's diseases (Lowe *et al.*, 1990), α-synuclein in Parkinson's disease (Braak *et al.*, 2001), prion protein in Creutzfeldt-Jakob disease (Kato, 1996), and huntingtin in Huntington's disease (Jackson *et al.*, 1995). In all these diseases, the deposits or plaques contain the proteins in an amyloid fibrillar form. The up-regulation of αB-crystallin in these diseases implies an important role for the heat shock proteins in amyloid diseases, indicating that they are one of the first lines of defence for the cell in its attempt to mitigate amyloid fibril formation by the particular disease-associated protein (Ecroyd and Carver, 2009). However, the correlation between αB-crystallin up-regulation and its co-localization with amyloid fibril deposits in various protein conformational diseases remains unclear. The precise role of αB-crystallin in interacting with the aggregation target protein and the subsequent effect on its toxicity remains controversial (Laskowska et al., 2010; Quinlan, 2007).

2.1.2 β/γ crystallins

There are acidic (βA-) and basic (βB-) crystallins. Each subgroup has three genes (*Cryba1*, *2*, *4*; *Crybb1*, *2*, *3*); only *Cryba1* is encoding two proteins (βA1- and βA3-crystallins). This feature is conserved among all mammals, birds and frogs (Graw, 2009). In human, a particular duplication of *CRYBB2* gene was found. As no transcript of this particular gene is detected; therefore, it is referred to as a pseudogene (Brakenhoff *et al*, 1992). In mouse and human, the *Cryb* genes are distributed on three different chromosomes (Table 2.1). It is interesting that the *Cryba4/Crybb1* genes are present as a head-to-head manner, while the other pair of *Cryb* genes has a head-to-tail orientation. The γ-crystallin encoding genes (*Cryg* genes) are organized as a cluster of five genes (γA-γE-crystallin; gene symbols *Cryga-Cryge* respectively) within approximately 50 kb; these genes are all arranged in a head-to-tail orientation. Only the sixth gene (*Crygf*) is separately located but close to this cluster (Table 2.1). This gene cluster is found on chromosome 1 in mouse and chromosome 2 in human (for more reviews about β/γ crystallins see: Graw, 2009; Bhat, 2003).

A typical *Cryb* gene has 6 exons, in which the last 4 exons encode 4 different Greek

key motifs. While a typical *Cryg* gene consists of 3 exons, each of the second and third exons are responsible for two Greek key motifs. The β-crystallins are characterized as oligomers (the molecular weight of the monomers is between 22 and 28 kDa) with native molecular masses ranging up to 200 kDa, while the native γ-crystallin proteins are characterized as monomers with molecular weights of 20 kDa (Graw, 1993, Moerner, 1893).

Table 2.1: The gene symbol, chromosome location and protein of β/γ- crystallins (Reproduced from Graw, 2009)

Gene	Chromosome		Protein
	Mouse (MB)	Human (MB)	
Cryba1	11 (77.5)	17q11 (24.6)	βA1/A3-crystallin; 215aa, 23/25 kDa
Cryba2	1 (74.9)	2q34 (219.6)	βA2-crystallin; 196aa, 22 kDa
Cryba4	5 (112.7)	22q11 (25.4)	βA4-crystallin; 186aa, 22 kDa
Crybb1	5 (112.7)	22q11 (25.3)	βB1-crystallin; 252aa, 28 kDa
Crybb2	5 (113.5)	22q11 (23.9)	βB2-crystallin; 205aa, 23 kDa
Crybb3	5 (113.5)	22q11 (23.9)	βB3-crystallin; 211aa, 24 kDa
φCRYBB2	-	22	Additional pseudogene
CrygN	5 (24.3)	7q36 (150.8)	γN-crystallin; 182aa, 21 kDa
Crygs	16 (22.8)	3q27 (187.7)	γS-crystallin; 178aa, 21 kDa
Cryga/Crygd	1 (65.1)	2q33 (208.7)	γA/gD-crystallin; 175aa, 21 kDa
Cryge	1 (65.0)	-	γE-crystallin; 174aa, 21 kDa
φCRYGE	-	2q33	γE-crystallin; pseudogene
Crygf	1 (65.9)	-	γF-crystallin; 174aa, 21 kDa
φCRYGF	-	2q33	γF-crystallin; pseudogene

Expression pattern of β-crystallins varies among the individual β-crystallins. In general, β-crystallins' expression starts from the early developmental stages and rises after birth; the highest concentration of β-crystallins are usually found in the lens cortex (Aarts *et al.*, 1989; Graw, 1997). The *Cryg* genes are expressed in mouse lens

from E13.5 in the primary fibres and later on in the secondary fibre cells. *Cryg* genes are most expressed in new born mice, and decreases during the first weeks after birth while the *Cryg* expression is detected only during the prenatal development stage in human (Graw, 2009).

The β- and γ-crystallins share a common structure of 4 different Greek key motifs (Jaenicke and Slingsby, 2001). The name Greek key motif comes from its similarity to paintings on ancient Greek pottery (Figure 2.1 B). Greek key motifs are organized by anti-parallel β-sheets linked with random coils, which allows the dense packing of the protein in the lens (Figure 2.1 A). Within the β/γ crystallins family, the Greek key motifs form two different domains that are linked by an 8–10 amino acid inter-domain connecting peptide. Members of β/γ crystallins have been shown to have calcium binding ability and putative calcium binding sites within Greek key motifs that were suggested in different proteins (Jobby *et al.*, 2007; Rajini *et al.*, 2001, Sharma *et al.*, 1996; Sharma *et al.*, 1989).

A   **B**
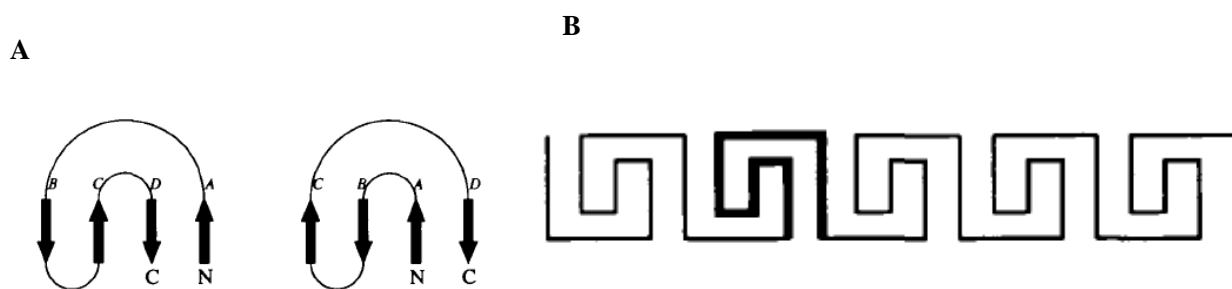
Figure 2.1 (A) Topology of the four strands common to all Greek key motifs. There are two possible topologies (left and right diagrams). (B) The design on Greek vases after which Greek keys were named. Four strands with the Greek key topology are indicated by thicker lines (Reproduced from Hutchinson *et al*., 1993).

Several mutations affecting *Cryb* genes have been reported both in mouse and in human, since the first mutation was described in *Crybb2* in the mouse (Chambers and Russell, 1991) and the first mutation in the human *CRYBA1* gene causing congenital zonular cataract. Interestingly, there are two mutational hot spots in human *CRYBA1*, position 1 of its 3rd intron, which is affected in seven distinct families all over the world, and the ΔG91 mutation occurs in four different families (for more details please see chapter 2.2).

Until now, various mutations in the *Cryg* genes leading to different forms of cataract have been reported (Graw, 2009). The first mutation in *Cryg* was found in the *Elo*

mutant. It is caused by 1 bp deletion which shifts the reading frame, affecting the fourth Greek key motif of the protein (Cartier *et al.*, 1992). Today, more than 20 mutations in all of the six genes of the *Cryg* have been detected. All of these are dominant cataracts and the phenotypes of these mutants vary significantly. In contrast to mouse, mutations in *CRYGC* and *CRYGD* genes are reported only in human. However, the cataract phenotypes are quite different from case to case, as the same situation in mouse (Graw, 2009).

β/γ-crystallins were also found in tissues other than the lens. β/γ-crystallins transcripts were detected in the mouse retina by microarray and RT-PCR. The corresponding proteins were also detected to be expressed in its outer and inner nuclear layer as well as in the inner segments of the photoreceptors by immunostaining (Xi *et al.,* 2003). In addition, *Cryba1* is expressed in retinal astrocytes; the mutation in *Cryba1* destroys their normal structure and function leading to abnormalities in the development and maturation of the retinal vasculature. Moreover, these retinal abnormalities were observed only in the homozygous mutants indicating a recessive mode of inheritance, while the cataracts were present in both the heterozygotes and homozygous as a dominant feature (Sinha *et al.*, 2008). Most recently, βγ-crystallins were reported to be expressed in the cornea of mice and human (Ren *et al.*, 2010). Additionally, congenital cataract and microcornea in a Chinese family were also reported by a mutation (c.225G>T) in exon 4 of *CRYBA4* (Zhou *et al.*, 2010)

2.1.3 Enzyme crystallins

Enzyme crystallins are expressed at relatively high levels in the lens, they are characterized by their strong relationship to well known enzymes. They are also referred as taxon specific-crystallins (for reviews: Wistow and Kim, 1993; Piatigorsky, 1998). δ–crystallins in the lens are restricted to birds only, which evolved from a Argininosuccinate lyase (ASL). Like other crystallins, mutations in δ -crystallin lead to cataract formation (Graw, 1997). μ-crystallin (gene symbol: *Crym*) was first identified in eye lens of several Australian marsupials like kangaroos (Wistow *et al.*, 1991). μ-crystallin was also detected in human retina, brain, muscle and kidney. Later, μ-crystallin was characterized as an NADPH-dependent cytosolic 3, 3', 5-triiodo-L-thyronine (T3) binding protein (Vie *et al.*, 1997). *CRYM* has been discussed to be causative for non-syndromic, dominant deafness but no other pathological effects in

other organ including the eye (Abe *et al.*, 2003; Oshima *et al.*, 2006). ξ-crystallin (encoding gene *Cryz*) was first detected in guinea pig lens, then it was also detected in camels, cattle, mouse and human (Rao *et al.*, 1997; Gonzalez *et al.*, 1994; Garland *et al.*, 1991; Huang *et al.*, 1987). ξ-crystallins protein show an oxido-reductase activity, but it requires NADPH as a co-factor (Rao *et al.*, 1997. Mutations in *Cryz* lead to cataract in guinea pig (Rodriguez *et al.*, 1992; Huang *et al.*, 1990). Most recently, ξ-crystallin is observed to be involved in bcl-2 over-expression in T-cell acute lymphocytic leukemia by acting as a mRNA binding protein in human (Lapucci *et al.*, 2010).

2.2 βB2-crystallin

2.2.1 *Crybb2* gene and expression

βB2-crystallin (Gene symbol *Crybb2*) is a member of the β-crystallin family. It is one of the main structural proteins of the vertebrate eye lens, which plays an important role in light refraction and maintaining transparency of the lens, together with other crystallins. *Crybb2* is one of the typical *Cryb* that has 6 exons, in which the last 4 exons encode 4 different Greek key motifs（Figure 2.2）.
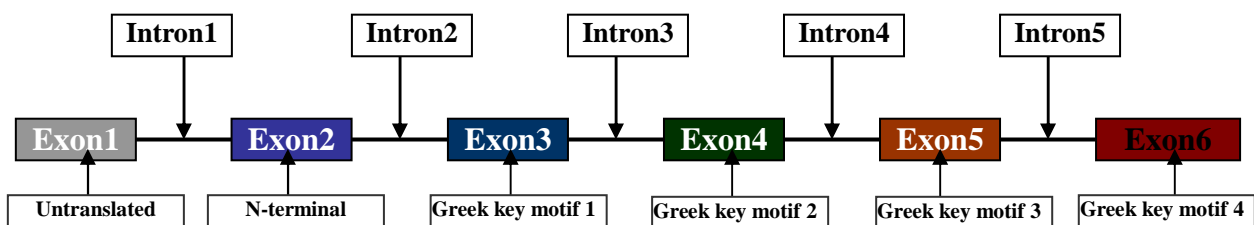
Figure 2.2: Schematic structure of the *Crybb2* at the genomic level. The βB2-crystallin protein consists of two domains; each domain consists of two Greek key motifs; each Greek key motif consisting of four anti-parallel β-strands.

The regulation of βB2-crystallin has been studied in rat (Dirk *et al.*, 1996). The rat βB2-crystallin gene is active only during a specific stage of the differentiation of rat lens fiber cells directed by basic fibroblast growth factor. The regulatory elements that determine the transient activity of this gene are located in the -750/-123 region and in the first intron. These regions together constitute an enhancer only during specific stages of lens differentiation. Otherwise, they act individually as silencers. An additional silencer is found between -123 and -77. The proximal promoter region contains a Pax-6 binding site at -65/-51; however, it is not confirmed by *in vivo*

footprinting experiments.

Maf responsive elements (MARE) have been detected in the promoter of rat βB2-crystallin. Even though c-Maf was suggested to be a common regulator of the eye lens crystallin genes, it is not proven to play a major role in regulating the βB2-crystallin promoter activity. It was also suggested that the putative *Sox2* binding site at -164/-159 and a positive element at -14/-7 are the primary regulatory elements (Doerwald *et al.*, 2001).

2.2.2 βB2-crystallin and calcium binding

In the βγ-crystallin family, γ-crystallins were first reported to have calcium binding ability (Sharma *et al.*, 1989). Greek key motifs in the protein were suggested as a potential binding site for calcium. Carver and his colleagues used both two-dimensional NMR spectroscopic studies to determine the calcium binding of the homodimer of βB2-crystallin (Carver *et al.*, 1993). No difference in chemical shift were observed in the total correction spectroscopy spectra of β-homodimer that suggested that terminal extension of βB2-crystallin is not involved in calcium binding.

Using calcium-binding assays such as ^{45}Ca overlay, terbium binding, calcium sensitive dye and isothermal titration calorimetry, Jobby and his colleage demonstrated that βB2-crystallin binds calcium with moderate affinity (Jobby and Sharma, 2007). There was no significant change in their conformation upon binding of calcium as monitored by fluorescence and circular dichroism spectroscopy. However, ^{15}N-^{1}H heteronuclear single quantum correlation NMR spectroscopy of βB2–crystallin with and without calcium revealed that amide environment of several residues underwent changes after addition of calcium suggesting calcium ligation. In a further study, the N/D-N/D-#-I-S/T-S domain in Greek key motif (Asn/Asp- Asn/Asp-#-Ile-Ser/Thr-Ser) was suggested to be a conserved Ca^{2+}-binding domain among the βγ-crystallin family. The second Greek key motif of βB2-crystallin retains the canonical domain (91-TDSLSS-96), which could be the reason that βB2-crystallin has moderate calcium affinity (Aravind *et al.*, 2009).

2.2.3 βb2-crystallin is causative for cataracts in human

Mutations in *CRYBB2* lead to cataracts in human. Among the reported mutations, the most frequent mutation in the *CRYBB2* gene is a conversion to its pseudogene. Gene conversion is a kind of homologous recombination that the newly generated gene copies have the tendency to unequal reciprocal crossover because of the high

degree of homology between these two genes (Chen *et al.*, 2007). It is exactly the situation of the *CRYBB2* gene and *CRYBψB2* in some mutations. In these mutations, a part of the *CRYBB2* sequence acts like an 'acceptor' and is replaced by a sequence that is copied from the 'donor', *CRYBψB2*. For consequence, the 9–104 of the original bases in the *CRYBB2* gene is replaced. The replacement leads to a stop codon (Q155X), and it is causative for the cataract (Graw, 2009).

Gene conversion in *CRYBB2* gene was first observed in a large Indian family (Vanita *et al.*, 2001). An autosomal dominant sutural cataract with punctuate and cerulean opacities affects this family. Progressive polymorphic congenital cataracts affecting a large five-generation Chinese family were also found to be caused by gene conversion in the *CRYBB2* gene (Yao *et al.*, 2005). The opacification of the lens was bilateral in all affected family members. However, the appearance of white opacities distributed in the nucleus and cortex were highly variable. The shapes of the opacities include pulverulent, dot, strip, sheet and star-like. In addition, gene conversions are reported in a large Chilean family with autosomal dominant cataracts (Bateman *et al.*, 2007) and in another five-generation Chinese family with autosomal dominant progressive polymorphic congenital coronary cataracts (Li *et al.*, 2008). All cataracts caused by gene conversion in *CRYBB2* demonstrated distinct clinical entities, which suggest unidentified modifying factors influencing cataract formation.

Besides gene conversions, other mutations in *CRYBB2* also are causative for human cataracts.

In an American family, an autosomal dominant cerulean cataract was mapped to a region of human chromosome 22 containing βB2-crystallins and two other crystallin genes (Litt *et al.*, 1997). In molecular analysis, it has been found to be associated with a chain termination mutation in the *CRYBB2* (477G>A). As a consequence, the βB2-crystallin polypeptide lost 51 of the 55 amino acid residues normally encoded by exon VI. The visual acuity in this family is reduced in adulthood, even though opacity could also be observed during fetal development and childhood.

A substitution (W151C) in exon VI of *CRYBB2* has been identified as causative mutation underlying the phenotype of central nuclear cataract in all affected members of an Indian family (Santhiya *et al.*, 2004). The mutation may affect the solubility of the mutant protein and hence contribute to cataract formation.

Cataracts characterized as nuclear with an additional ring-shaped cortical opacity were reported in a German family (Pauli et al 2007). Congenital cataracts were observed in a daughter of healthy parents and their two children. A sequence variation in exon 5 (383A>T) of *CRYBB2* gene were identified. It represents the first mutation outside exon 6 of the human *CRYBB2* gene.

Four generations of a Chinese family affected with bilateral congenital posterior subcapsular cataracts were also identified (Yao *et al.*, 2011). Sequencing of the candidate genes detected a heterozygous 5C>T change in the coding region of the *CRYBB2*, resulting in the substitution of a highly conserved amino acid 'Ala' to 'Val'. Visual acuity was affected in all the family members with different degrees. Most affected individuals noticed their visual impairments in their twenties, and then their visual acuity decreased gradually.

All of those clinical observations in human suggest that mutations in *CRYBB2*, especially the mutations in exon 6 because of gene conversions, are highly involved in the pathogenesis of cataracts.

2.2.4 *Crybb2* mouse mutants

Philly mouse is the earliest and best-studied *Crybb2* mutant mouse. Its cataract is characterized as 'anterior and posterior subcapsular opacity', which is inherited as an autosomal dominant trait (Kador *et al.*, 1980). The cDNA of *Crybb2* from the *Philly* contains an in-frame deletion of 12 bp resulting in a loss of 4 amino acids. The deletion of 4 amino acids is close to the carboxy-terminus which is essential for the formation of the tertiary structure of the βB2-crystallin protein (Sergeev *et al.*, 1998; Chambers *et al.*, 1991). The formation of cataract begins after the first postnatal week and continues progressively.

The second reported *Crybb2* mutant, *Aey2*, was found during an ethylnitrosourea (ENU) screening. This mutation is due to a T → A exchange at position 553bp in the *Crybb2* gene, leading to an exchange of amino acid 'Val' for 'Glu'. It affects the same region as the *Philly* allele. However, compared to the *Philly* mouse, the *Aey2* mutant showed a slower progression of the opacification, which terminates between 8 and 11 weeks of age. The slower progression in cataractogenesis may be due to a smaller molecular lesion in the *Aey2* mice than in the *Philly* mouse (Graw *et al.*, 2001).

The third *Crybb2* mutant, *O377*, was discovered in the offspring of male mice

exposed to 3 Gy X-ray irradiation. This mutation was characterized as an A→T substitution at the end of intron 5 of the *Crybb2* gene. It led to alternative splicing with an insertion of 57-bp in the mRNA and to 19 additional amino acids in the protein. It affects the same region as *Philly* and *Aey2*. The cataractogenesis in *O377* mutant is very similar to the *Philly* mutant. *O377* mice lenses develop like wild type mice until the first postnatal week, when particles appear in the anterior cortex that extends, by the 10th day, to the anterior subcapsular area. Moreover, *O377* mice also lack the lens denucleation process like in *Philly* mice (Ganguly *et al.*, 2008).

A *Philly*

| Exon1 | Exon2 | Exon3 | Exon4 | Exon5 | 12bp Exon6 |

B *Aey2*

553bp T→A

| Exon1 | Exon2 | Exon3 | Exon4 | Exon5 | Exon6 |

C *O377*

| Exon1 | Exon2 | Exon3 | Exon4 | Exon5 | 57bp | Exon6 |
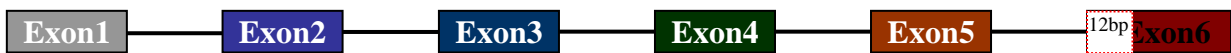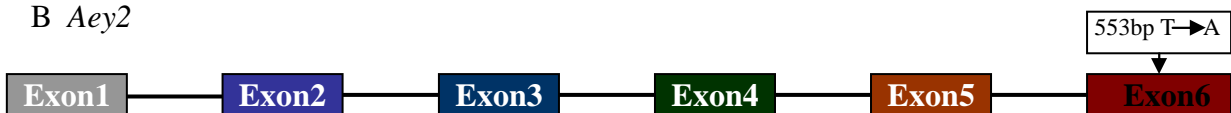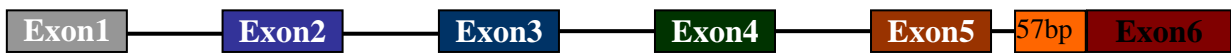
Figure 2.3: Schematic structure of the *Crybb2 mutants Philly* (A)*, Aey2* (B)*, O377* (C) at the genomic level.

Recently, knockout mice of *Crybb2* were generated (Zhang *et al.*, 2008). A relatively slower cataractogenesis procession compared to *Philly* and *O377* mutants was observed. The lens appeared to develop well in the first months of life. A punctuate cataract was first observed in the posterior portion of the cortex at 6 to 8 weeks of age and became more obvious at 4 months. In older animals, the weight and axial diameter of the knockout mice lenses were significantly smaller than in wild-type mice.

2.2.5 *Crybb2* expression in the retina

Crybb2 expression was also detected outside the lens. *Crybb2* mRNA was detected in rat brain, rat testis, and human retina by RT-PCR. In addition, βB2-crystallin protein was purified from lens and its identity was confirmed in rat brain, rat testis, and bovine retina (Magabo *et al.*, 2000). Adult retinal ganglion cells (RGCs) can regenerate their axons *in vitro*. *Crybb*2 was found to be clearly up-regulated in the

regenerating retina compared to the un-regenerated retina. The expression of *Crybb*2 within the retina, including filopodial protrusions and axons of RGCs, was detected by Immunohistochemistry. Overexpression of *Crybb2* in RGCs and hippocampus neurons increased axonogenesis. It is suggested that *Crybb2* is involved in axonal regeneration in the retina (Liedtke *et al.,* 2007).

2.2.6 *Crybb2* in the brain

Crybb2 transcripts were detected in the brain during postnatal development through adolescence and diminish thereafter in both wild type and *O377* mutants. Immunohistochemistry demonstrated that *Crybb2* is widely expressed in neurons of the olfactory bulb (mitral cell layer and glomerular layer), hippocampus (pyramidal cells of the CAI, CAII, CAIII regions and granule cells of the dentate gyrus), cerebral cortex (pyramidal cells throughout all layers), and cerebellum (Purkinje cells and stellate cells of the molecular layers) (Ganguly *et al.,* 2008). To assess global changes in gene expression levels in the brains of *O377* mutants, expression-profiling experiments using genomewide DNA microarrays were performed (Ganguly *et al.,* 2008). 6 genes were observed to be upregulated and seven genes down-egulated in the whole brains of homozygous mutants (Figure 2.4). Among these genes, *Capn3*, *Cr536618* and *Tmsb4,* are the most up-regulated ones. Therefore, I analyzed their expression pattern during this study*.*

Calpain-3 (encoded by *Capn3*) is a widely expressed calcium dependent protease, which plays important roles in a variety of pathophysiological conditions including necrotic and apoptotic cell death (Verkhratsky, 2007; Liu et al., 2008). One well-known target of calpains are the NMDA receptor subunits (Bi *et al.*, 1998; Araújo *et al.*, 2005, Wu *et al.*, 2005). Interaction of calpain and NMDA receptor have been involved in neurodegenerative disorders (Goni-Oliver *et al.*, 2009; Nimmrich *et al.*, 2008).

NMDA receptors are major synaptic plasticity mediators that play very important roles in learning, memory and cognition in central nervous systems. Deletion of NMDA receptors subunits or blocking NMDA receptors by NMDA antagonists caused the loss of GABAergic interneurons, especially loss of parvalbumin positive GABAergic interneurons (Rujescu *et al.*, 2006; Belforte *et al.*, 2010). Loss of parvalbumin positive GABAergic interneurons is often detected in psychiatric disorders, especially in schizophrenia.

Rank	Min abs.	Mean abs.	Ratios of 15 Chip Experiments	Lion ID	Gene symbol
1	1.8	3.45		MG-16-176k15	Capn3
2	1.45	1.93		MG-6-3c22	Tmsb4x
3	1.41	2.17		MG-3-19k2	1700065I16Rik
4	1.37	1.82		MG-6-2a13	2510049I19Rik
5	1.32	1.72		MG-16-10o9	D12Ertd647e
6	1.24	2.44		MG-15-70b2	CR536618
7	1.24	1.89		MG-14-40o13	Sgne1
8	1.2	1.61		MG-6-55e7	Atp6v0a1
9	1.18	1.45		MG-14-31j9	1810006K23Rik
10	1.15	1.33		MG-3-3k20	Stmn1
11	1.15	1.45		MG-12-1k15	Mrpl48
12	1.13	1.45		MG-3-5b7	BC061236
13	1.13	1.75		MG-13-61g11	Rab9

mouse #1   #2   #3   #4

Figure 2.4 RNA expression profiling. Fifteen dual-color DNA chip hybridizations from 1-month-old homozygous mutant brains against a pool of four strain-matched wild-type brains were performed. Expression ratios are depicted in red (up regulated in mutant) and green (downregulated in mutant) in the heat plot. The colored scale bar on the left shows the related color code for the ratio. All genes shown in this figure have reproducible upregulation or downregulation in all 15 chip experiments (Reproduced from Ganguly *et al.*, 2008).

β-thymosins are a family of actin monomer (G-actin) sequestering proteins, widely expressed in different regions of mouse and human (Ericksson-Viitanen *et al.*, 1983). *Tmsb4x* (thymosin β4) is a small polypeptide having one of the highest expression levels among the thymosin family (Yu *et al.*, 1993). As a cytoskeleton protein, thymosin β4 was reported to be involved in axonal outgrowth (Yang *et al.*, 2008; Mollinari *et al.*, 2009). Thymosin β4 was found to be highly expressed in glia cells and related to gliosis (Vartiainen *et al.*, 1996; Anadon *et al.*, 2001). Furthermore, thymosin β4 was also related to cell migration, apoptosis, wound healing, angiogenesis and tumor growth (Philp *et al.*, 2004; Reti *et al.*, 2008; Qiu *et al.*, 2009; Crockford *et al.*, 2010).

CR536618 is an anonymous mRNA, which is also oberved to be up regulated in brain of *O377* mutants compared to wild-type, and it was detected in neuronal tissues like retina and brain (NCBI databank http://www.ncbi.nlm.n ih.gov/nuces t/4991 2395? rid= ue1gw152011&blast_rank=1&log$=nucltop&report=genbank).

2.3 Schizophrenia

Schizophrenia is a chronic, debilitating psychiatric disorder affecting approximately 0.3–0.7% of the world population. Prenatal and early childhood factors, environment, genetics, psychological and social processes have been reported to be important contributory factors, some recreational and prescription drugs appear to cause or worsen symptoms (van and Kapur, 2009; Tamminga and Holcomb, 2005)

Schizophrenia is characterized by a disintegration of the process of thinking and of emotional responsiveness. Three distinct symptoms in schizophrenia have been demonstrated during analysis of several schizophrenic patients: positive symptoms, negative symptoms and cognitive dysfunction (Tamminga and Holcomb, 2005). Positive symptoms are symptoms that most people do not experience but are present in people with schizophrenia, such as hallucinations, delusions, and disorders of thought, speech, and movement. Negative symptoms are characterized by deficits of normal emotional responses or of other thought processes including lack of emotions, social withdrawal and thought poverty. Cognitive dysfunction is characterized by abnormalities in attention, working memory, and executive function. Schizophrenia is not curable till now. Even though many pharmacological and nonpharmacological methods of treatment have been used, these drugs fail to significantly ameliorate the negative symptoms and cognitive dysfunction (Tandon *et al.*, 2008).

2.3.1 *Crybb2* is associated with schizophrenia related phenotype in mouse and human

Crybb2 was demonstrated to be expressed in different regions of the brain (Ganguly *et al* 2008); mutation in *Crybb2* may lead to behaviour changes. Therefore, behavior studies were performed in *O377* mutants compared to wild type. The most impressive finding in behavior tests is that homozygous *O377* mutants showed a clear increase in prepulse inhibition compared to wild type (personal communication by Dr. Sabine Hölter, unpublished data). Prepulse Inhibition is a neurological phenomenon that a weaker prestimulus (prepulse) inhibits the reaction of an organism to a subsequent strong stimulus (pulse). In the experiemnt of *O377* mutants, acoustic stimuli were used in the prepulse inbition. However, tactile stimuli and light stimuli are also used in other prepluse inhibition expreiments. Abnormalities in prepulse inhibition demonstrate the organism is not able to filter out the useless information. The observed prepulse increase indicates altered sensorimotor gating, which is normally

found in neuropsychiatric disorders especially schizophrenia (Koch, 1999; Swerdlow *et al* 2001).

One genome scan meta-analysis of schizophrenia shows that the human chromosomal region harbouring *CRYBB2* (22q11.2) is linked to schizophrenia, as well as to schizophrenia-related intermediate phenotypes of reduced P50 suppression (sensory gating) and altered antisaccade eye movement (Lewis et al., 2003). The P50 suppresion and the antisaccade eye movement are two common ways to study deficits in the brain functions of schizophrenia patients. The P50 suppression is used to identify deficits in the early stages of information processing. It is the positive component of the event-related potential that occurs about 50 msec after an auditory stimulus. The deficits in the P50 suppression indicate the abnormalities in sensory gating. Patients with schizophrenia have significantly lower P50 suppression compared with health control (Braff and Geyer, 1990). While the antisaccade eye movement is a very senstive tool to investigate the problem in the congitive process of scchizophrenia patients. In the antisaccade task, a participant is required to refrain from looking at a target appearing unpredictably in a right or left peripheral location, and instead, make a rapid voluntary eye movement (saccade) to the opposite peripheral location. Generation of a reflexive saccade in direction of the peripheral target is considered an error (Hutton and Ettinger, 2006).

In addition, associations of haplotypes with sensory gating, antisaccade eye movements and the quantity of *CRYBB2* mRNA in lymphocytes were demonstrated. Antisaccade eye movements related to lower mRNA expression of *CRYBB2* in lymphocytes were observed in carriers of two different haplotypes, while altered sensory gating was found in carriers of another haplotype (personal communication by Prof. Dr. Dan Rujescu, unpublished data). Those data demonstrated an association of schizophrenia-related intermediate phenotypes with genetic variations in human *CRYBB2*.

2.3.2 Hypothesis of schizophrenia

Schizophrenia is a multifactorial psychiatric disorder, for which the real cause of this disease is still uncertain. However, different research groups basing on different research and clinical studies present many hypothesis about schizophrenia. These include dopamine hypothesis of schizophrenia (Jentsch and Rothe, 1999, Lieberman et al., 1987) and glutamate hypothesis of schizophrenia (Coyle, 2006).

Dopamine hypothesis of schizophrenia

As early as 1963, Carlsson and Lindqvist suggested that a hyperactivity of dopamine transmission is associated with positive symptoms of schizophrenia (Carlsson and Lindqvist, 1963). It is the original idea of the dopamine hypothesis of schizophrenia. Then it was supported by further clinical and pharmacological evidence that antipsychotic drugs could effectively block dopamine D2 receptors (Creese *et al.*, 1976; Seeman and Lee, 1975). Moreover, chronic or sustained use of psychostimulants, acting by releasing biogenic amines from their storage sites in presynaptic nerve terminals, has been shown to induce a toxic psychosis closely resembling the positive symptoms of schizophrenia (Lieberman *et al.*, 1987). However, several postmortem studies in human have challenged the dopamine hypothesis. Inconsistent results have been yielded when dopamine and its metabolites were checked in schizophrenia patients (Davis, 1991). Moreover, neuroleptic drugs like Compazine could up-regulate dopamine D2 receptors and dopamine D2 receptor D2-like receptors that result in an increase in dopamine D2 receptors and dopamine D2 receptor are difficult to interprete (Seeman, 1987). With development of imaging techniques, positron emission tomography (PET) or single photon emission computerized tomography (SPECT) have been used for *in vivo* study of dopamine receptor and dopamine release. However, *in vivo* studies of dopamine D2 and dopamine D2-like receptor density in schizophrenic patients have generally been negative (Nord *et al.*, 2010; Graff-Guerrero *et al.*, 2009).

Glutamate hypothesis of schizophrenia

Kim and colleagues initiated the glutamate hypothesis of schizophrenia in 1980. They found low glutamate levels in cerebrospinal fluid (CSF) of schizophrenia patients (Kim *et al.*, 1980). Until recently, the glutamate hypothesis of schizophrenia has been considered as a valuable model. The glutamate hypothesis suggested a hypofunction of glutamatergic signaling via NMDA receptors. NMDA receptors are the major subtype of glutamate receptors, based on a set of clinical, neuropathological and genetic findings. Using NMDA receptor antagonists such as phencyclidine (PCP) or ketamine could produce "schizophrenia like" symptoms in healthy individuals (Krystal *et al.,* 1994, Javitt *et al.*, 1991). Symptoms produced by these drugs include positive symptoms, negative symptoms and cognitive dysfunctions of schizophrenia, as well as disruptions in smooth-pursuit eye movements and prepulse inhibition of startle.

Moreover, blockage of NMDA receptors could disinhibit GABAergic inputs to the glutamate-containing neurons, thereby enhancing the firing rate of these glutamatergic neurons. In the mean time, inhibition of NMDA receptors could increase the targeted neuronal release of glutamate through presynapses, which is toxic to postsynaptic neurons. Consequently, blockage of NMDA receptors could produce schizophrenia like phenotype in human and in mouse models (Belforte *et al.*, 2010; Rujescu *et al.*, 2006; Moghaddam *et al.*, 1997). Postmortem studies in schizophrenia patients show changes in glutamate receptor related proteins like NF-L, PSD95 and SAP102 in different regions of the brain (Kristiansen *et al.*, 2010; Clinton *et al.*, 2004). *In vivo* study by PET and SPECT also directly confirmed NMDA receptor deficiency in schizophrenic patients (Vyas *et al.*, 2001; Pilowsky *et al.*, 2006).

2.3.3 Structural and functional abnormalities of brain in schizophrenia

Schizophrenia is associated with structural and functional changes in the brain. Recent improvement in neuro-imaging has enabled a very effective step in exploring the brain structure and functional abnormalities in human. Structural and functional abnormalities in different regions of the brain including prefrontal cortex, gray matter, superior temporal gyrus, amygdala, and hippocampus have been reported in schizophrenia patient (Karlsgodt *et al.*, 2010; Marić *et al.*, 2003; Kucharska-Pietura *et al.*, 2003). In this overview, I mainly focus on the prefrontal cortex and hippocampus, which are also two of most frenquently studied region in schizophrenia studies (Rujesscu *et al.*, 2006; Lodge *et al.*, 2009).

Prefrontal cortex is one of most important brain regions responsible for cognitive behaviors, personality expression and decision-making. In schizophrenia patients the most prevalent as well as the most devastating symptom is cognitive impairment. Therefore, prefrontal cortex is much compromised in schizophrenia. Accumulating magnetic resonance imaging data reveals that the total volume of prefrontal cortex is decreased in schizophrenia patients in comparison to healthy control (Schobel *et al.*, 2009; James *et al.*, 2004; Buchanan., *et al* 1998). Moreover, postmortem studies in schizophrenia patients exhibit layer-specific reductions in neuronal size and density in the prefrontal cortex (Rajkowska *et al.*, 1998), while loss of inter-neuron and glial cells were also observed (Farkas *et al.*, 2010; Sakai *et al.*, 2008).

Beneath the cortical surface, hippocampus is a paired structure, with mirror-image halves on the left and right sides of the brain. It has been widely accepted that

hippocampus is very important for spatial memory formation, learning, memory and anxiety related behavior (O'Keefe *et al.*, 1978; Eichenbaum, 2000; Squire *et al.*, 2004). One of the most consistent brain morphological changes in schizophrenia patients is the hippocampus volume reduction. A meta-analysis compared 54 independent studies in schizophrenia showed a reduction of approximately 6% in the left and 7% in the right hippocampus of patients with schizophrenia (Wright *et a.,l* 2000). A more recent meta-analysis of patients including 52 cross-sectional and 16 longitudinal investigations (Steen *et al.*, 2006) suggests bilateral hippocampal volume reductions of about 8%. Consistent with hippocampal volume loss, postmortem studies revealed cytoarchitectural changes in the hippocampus of schizophrenia patients, including decreased neuronal density, glial density and decreased expression of synaptic proteins like NMDA receptors (Gothelf *et al.*, 2000; Harrison *et al.*, 2004). As in prefrontal cortex, the specific loss of GABAergic interneurons especially parvalbumin positive interneurons, is consistently observed in hippocampus of schizophrenia patients (Tooney *et al.*, 2004; Reynolds *et al.*, 2001; Beasley *et al.*, 1997).

2.3.4 Loss of GABAergic interneurons in schizophrenia

GABAergic interneurons are neurons, which are present throughout the central nervous system, expressing the compound γ-aminobutyric acid. Previous studies have classified interneurons in 13 different classes in monkey and in human brain by using Golgi staining and immunohistochemistry, according to the morphological and biochemical characteristics (Mrzljak *et al.*, 1992, Lund *et al.*, 1993). Three types of these most important interneurons are basket neurons, double-bouquet cells, and chandelier cells. Basket cells are identified by their multipolar shape and big soma; double-bouquet neurons with long descending vertical bundles of axons; while chandelier cells are characterized by their dendritic arborisations and short, vertically oriented rows of punctuate structures (Reynolds *et al.*, 2001; Benes *et al.*, 2001).

Different GABAergic interneuron subpopulations can also be identified by their expression of neurochemical markers such as calcium binding proteins and neuropeptides. Moreover, by those neuron markers, different types of GABAergic interneurons have been characterized via anatomical, biochemical and electrophysiological methods (Reynolds *et al.*, 2001; Kawaguchi *et al.*, 1997).

Parvalbumin positive GABAergic interneurons are mainly found in chandelier and basket cells, and they are distinguished from other GABAergic interneurons by their electrophysiological properties, named as "fast-spiking" neurons. Compared with other neurons, parvalbumin positive GABAergic interneurons have shorter duration of action potentials with shorter duration after-hyperpolarizations, negative resting potentials and lower input resistance. Parvalbumin positive GABAergic interneurons also have been demonstrated to be connected to each other both by chemical synapses and through electrical synapses. Most recently, a few research groups have confirmed that parvalbumin positive GABAergic interneurons contribute to the synchronized oscillation of cortical and hippocampal neurons (Sohal *et al.*, 2009; Wulff *et al.*, 2009).

Calretinin positive GABAergic interneurons are mainly found in double bouquet *and* biopolar cells. By their electrophysiological characteristics calretinin positive GABAergic interneurons are kind of "regular spiking" cells. Small populations of calretinin positive cells are suggested to be non-inhibitory interneurons, as this subpopulation of calretinin positive GABAergic interneurons have synapses with pavalbumin positive GABAergic interneurons and other GABAergic interneurons (Kawaguchi and Kubota 1996). Somatostatin positive GABAergic interneurons are also "regular spiking" cells. Different subgroups of somatostatin positive GABAergic interneurons were found to express also vasoactive intestinal polypeptides and Calretinin.

In postmortem study of schizophrenia patients, GABAergic interneurons, especially parvalbumin positive GABAergic interneurons, have been reported to be consistently reduced in hippocampus (Tooney *et al.*, 2004; Woo *et al.*, 1997) as well as in some cases of prefrontal cortex (Reynolds *et al.*, 2001; Beasley *et al* 1997). A reduction in parvalbumin positive GABAergic interneurons is also observed in many animal models of schizophrenia, including methylazoxymethanol acetate (MAM) treated rats (Lodge *et al.*, 2009; Penschuck *et al.*, 2006), phencyclidine (PCP) treated rats (Rujescu *et al* 2006), rats reared in isolation (Harte *et al.*, 2007) and the amygdala activation model (Berretta *et al.*, 2004). In addition, specific loss of parvalbumin positive GABAergic interneurons is also observed in the postnatal NMDA ablation mouse, which is also a promising model for schizophrenia (Belforte *et al.*, 2010). The specific loss of positive GABAergic interneurons in schizophrenia mouse models is

caused by NMDA receptor blockage or depletion (for more detail please see chapter 2.3.1).

2.3.5 Neuronal morphology changes in schizophrenia

Neurons are morphologically characterized based on the presence of axon, soma and dendrites. The vast majority of synapses throughout the nervous system are present on dendrites. The dendrite complexity is the major indication on how neurons integrate and process incoming information, and thus, they play a vital role in the functional properties of neural circuits. During the last years, varieties of studies have documented considerable evidence that dendritic complexity (dendritic length and branches) is relatively dynamic (Gao et al., 2007; Leuner and Gould 2010). In early studies in animals exposed to enriched environment, dendrites of neurons in cortical and subcortical areas showed increased complexity compared with the animals housed in normal cages (Kolb and Whishaw, 1998). Changes in dendrite complexity could also be observed in human or animals with chronic drug exposure.

Reduction of dendritic complexity is consistently observed in postmortem studies in schizophrenia patients. A significant decrease occurs in the number of both primary and secondary basilar dendrites in both layer III and layer V of pyramidal neurons (Broadbelt et al., 2002). Another postmortem study in human patients also revealed a decrease in the length of basilar dendrites in cortical layer V neurons (Black et al., 2004). Alteration in dendritic complexity was suggested to be closely related to the dysfunction in cognition in schizophrenia patients. In schizophrenia-related mouse models, hippocampal neuron complexity is also reported to be reduced compared with wild type control (Kvajo et al., 2008). Moreover, several schizophrenia-related proteins, like Neuregulin1, Disrupted-In-Schizophrenia 1 and Reelin, have been reported to be involved in dendritic complexity (Chen Y et al., 2010; Hoe et al., 2009; Krivosheya et al., 2008; Duan et al., 2007).

Microtubule associated protein 2 (MAP2) is a cytoskeleton protein predominant localized in the neuronal dendritic compartment and weakly located in cell body (Huber et al 1984). MAP2 is closely related to the neuronal elongation, branching and neuronal plasticity (Chamak et al., 1987; Johnson et al., 1992). Therefore, MAP2 protein level is a very good indicator for neuron morphology and neuronal plasticity. Loss of MAP2 immunoreactivity was observed in the hippocampus and cortex of aged rats (Chuahan et al., 1997) indicating a putative relationship of hippocampus

and cortical functional impairment with aging. Both increased and decreased expression of MAP2 have been observed in many psychiatry disorders, especially in schizophrenia (Arnold *et al.*, 1991; Somenarain *et al.*, 2010; Rosoklija *et al*; 2005). Increase in overall MAP2 immunoreactive dendritic length in all hippocampal regions were observed in schizophrenia patients (Cotter *et al.*, 2000). However, the opposite results have also been observed. Reduced MAP2 immunoactivity has often been reported in schizophrenia patients (Somenarain *et al.*, 2010; Rioux *et al.*, 2004; Cotter *et al.*, 1997).

2.3.6 Genetics of schizophrenia

There is increasing number of evidences that the risk to develop schizophrenia is higher in relatives of a schizophrenia patient than the relatives of healthy controls (Ruderfer et al., 2011; Francois et al., 2010; Heydebrand, 2006). The recurrence risk ratio of schizophrenia for monozygotic twins is 3 times higher than first–degree relatives and 11 times higher than second-degree relatives (Moldin, 1998). Moldin also suggested that concordance rates for monozygotic twins are 3 times higher than the concordance rates for dizygotic twins even when reared in different families.

In addition, several studies have reported that the prevalence of schizophrenia is higher in biologic relatives than in adoptive relatives of schizophrenia patients (Kendler *et al.*, 1981; Kinney 2000).

Twins studies and adoption studies improved our understanding of genetics in schizophrenia, but the mode of inheritance is still unclear. Neither recessive nor dominant inheritance is conclusive for the mode of inheritance. It is suggested that the inheritance of schizophrenia involves contribution from multiple genes together with environmental factors (Krebs, 2002; Tsuang *et al.*, 1991).

Genetic factors highly contribute to the risk of schizophrenia (for more details: Harrison and Owen, 2003; Tiwari et al., 2010). In the past years, different methods including linkage analysis, association studies and resequencing approach were employed to identify schizophrenia risk genes and susceptibility loci on different chromosomes (Kim *et al.*, 2011).

Most of the genes associated with schizophrenia are neurotransmitter related genes, especially of the dopaminergic system or glutamatergic system. Most interestingly, energy-related gene (*ABCA13*), ion channel related gene (*KCNH2*), messenger molecule (*NOS1*) and neurotrophic factor (*BDNF*) are also demonstrated to be

related to schizophrenia (for more details see table 2.2).

Table 2.2 Genes associated with schizophrenia (adapted from OMIM: 181500)

Gene (Protein)	Locus	Comments
MTHFR (methylenetetrahydro-folate reductase)	Chromosome 1p36	*MTHFR* together with folate metabolism may contribute as schizophrenia risk factors.
NOS1AP (nitric oxide synthase 1)	Chromosome 1q23	Identified by association study in Chinese Han population and South American isolate (Antioquia).
RGS4 (G protein signaling-4 gene)	Chromosome 1q23	*RGS4* is associated with structural alterations in the dorsolateral prefrontal cortex
CHI3L1 (chitinase 3-like 1)	Chromosome 1q32	The presence of *CHI3L1* protein inhibits the activity of ASK1, which is pivotal for the transmission of stress-induced cellular responses, and protects the cells from undergoing apoptosis.
DISC1 (disrupted in schizophrenia 1)	Chromosome 1q42	*DISC1* regulates brain development. DISC1 interacted with a variety of cytoskeletal proteins and interacts with the UCR2 domain of phosphodiesterase-4B.
NRXN1 (neurexin1)	Chromosome2p16.3	*NRXN1* deletions affecting exons may confer risk of schizophrenia
ZNF804A (zinc finger protein 804A)	Chromosome 2q31	Identified by genomewide association study of schizophrenia. SNP rs1344706 in the *ZNF804A* gene is strongly assicated with schizophrenia .
ERBB4 (v-erb-b2 avian erythroblsastic leukemia viral oncogene homolog 4)	Chromosome 2q33	*Erbb4* localized at GABAergic terminals of rat prefrontal cortex and it is involved in regulation of GABAergic transmission.
DRD3 (dopamine receptor D 3)	Chromosome 3q13	*DRD3* is related to dopaminergic system in the brain. mRNA level of the *DRD3* is increased in lymphocytes of schizophrenia patients. Increased D3 receptor mRNA on blood lymphocytes can be used as a marker for identification and follow-up of schizophrenia.
SYN2 (synapsin 2)	Chromosome 3p25	*SYN2* is involved in to presynaptic function of neuron in the brain.
PMX2B (paired mesoderm homeobox 2B)	Chromosome 4p13	A possible interaction between PMX2B and other schizophrenia-precipitating factors, increasing the risk of the combined phenotypes
CLINT1 (clathrin interactor 1)	Chromosome 5q33	*CLINT1* encodes enthoprotin, which has a role in transport and stability of neurotransmitter vesicles at the synapses and within neurons.
DRD1 (dopamine receptor D 1)	Chromosome 5q35.1	Dopamine D1 receptors modulate NMDA glutamate receptor-mediated functions through direct protein-protein interactions.
DTNBP1 (dystrobrevin-binding protein 1)	Chromosome 6p22.3	The dysbindin-1 protein was located in presynaptic axon terminals of glutamatergic pathways. In schizophrenia cases, there was a significant reduction of dysbindin-1 in the terminal fields of intrinsic glutamatergic connections of the hippocampus compared to controls
NOTCH4 (NOTCH, Drosophila homolog of 4)	Chromosome 6p21	The *NOTCH* gene family encodes large transmembrane receptors that are components of an evolutionarily conserved intercellular signaling mechanism.
TAAR6 (trace amine-associated receptor 6)	Chromosome 6q23	*TRAR6* is preferentially expressed in different brain regions that have been implicated in the pathophysiology of schizophrenia.
ABCA13 (ATP-binding cassette, subfamily A, Member 13)	Chromosome 7p12.3	*ABCA13* carry out energy-dependent transport of substrate molecules.
KCNH2 (potassium channel voltage-gated subfamily H, member 2)	Chromosome 7q35-q36	*KCNH2* encodes a Ca (2+)-modulated potassium channel. It is associated with inefficient hippocampal activity in schizophrenia patients
NRG1 (Neuregulin-1)	Chromosome 8p22-p11	*NRG1* regulates GABAergic transmission.
PPP3CC (protein phosphatase 3, catalytic subunit, gamma isoform)	Chromosome 8p21.3	It is involved in a wide range of biologic activities, acting as a Ca(2+)-dependent modifier of phosphorylation status.

24

Gene (Protein)	Locus	Comments
SMARCA2 (SWI/SNF-related, matix-associated, actin-depend regulator of chromatin, subfamily A, member 2)	Chromosome 9p24.3	*SMARCA2* have been implicated in the regulation of gene expression, cell cycle control, and oncogenesis.
GRIN1 (N-methyl-D-aspartate, subunit 1)	Chromosome 9q34	Glutamate receptors are the predominant excitatory neurotransmitter receptors in the mammalian brain and are activated in a variety of normal neurophysiologic processes.
TPH1 (Tph1tryptophan hydroxylase 1）	Chromosome 11p15.3 -p14	Tph1tryptophan hydroxylase 1 is essential for serotonin biosynthesis.
BDNF (brain-derived neurotrophic factor）	Chromosome 11p13	*BDNF* is a prosurvival factor induced by cortical neurons that is necessary for survival of striatal neurons in the brain
DRD2 (dopamine receptor D2)	Chromosome 11q23	The D2 dopamine receptor is a G protein-coupled receptor located on postsynaptic dopaminergic neurons that is centrally involved in reward-mediating mesocorticolimbic pathways
DAO (D-amino acid oxidase)	Chromosome 12q24	D-amino acid oxidase oxidizes D-serine, a potent activator of N-methyl-D-aspartate-type glutamate receptor
NOS1 (nitric oxide synthase 1)	Chromosome 12q24	Nitric oxide is a messenger molecule with diverse functions throughout the body. NO displays many properties of a neurotransmitter; it is implicated in neurotoxicity associated with many disease
HTR2A (5-hydroxytryptamine receptor 2A)	Chromosome 13q32	Serotonin (5-hydroxytryptamine; 5-HT) is involved in many physiologic processes Abnormality of the serotonergic system has been implicated in a number of human diseases.
DAOA (D-amino acid oxidase activior)	Chromosome 13q34	*DAOA* is an activator of *DAO*, work together with D-amino acid oxidase.
AKT1 (V-AKT murine thymoma viral oncogene homolog 1)	Chromosome 14q32	A decrease in *ATK1* protein levels and levels of phosphorylation of GSK3B at serine-9 in the peripheral lymphocytes is associated with schizophrenia
CHRNA7 (cholinergic receptor, neuronal nicotinic, alpha polypeptide 7)	Chromosome 15q14	The nicotinic acetylcholine receptors (nAChRs) are members of a superfamily of ligand-gated ion channels that mediate fast signal transmission at synapses.
SLC6A4 (solute carrier family 6, member 4)	Chromosome 17q11-q12	Following release, Serotonin is actively cleared from synaptic spaces by *SLC6A4*, a high-affinity, Na(+)- and Cl(-)-dependent transporter localized in presynaptic neuronal membranes.
GNAL (guanine nucleotide-binding protein, alpha-activating activity polypeptide, olfactory type)	Chromosome 18p	*GNAL* is subject to epigenetic regulation of potential significance in the etiology of schizophrenia.
APOE (apolipoprotein E)	Chromosome 19q13	Schizophrenia is associated with an increased E4 allele frequency.
C3 (complement component 3)	Chromosome 19q13	*C3* is expressed in neural progenitor cells and immature neurons. Mice lacking *C3* show decreased basal neurogenesis and impaired ischemia-induced neurogenesis.
OLIG2 (oligodendrocyte lineage transcription factor 2)	Chromosome 21q22	*Olig2* was required for oligodendrocyte and astrocyte development.
COMT (Catechol-O-methyltransferase)	Chromosome 22q11	*COMT* contributes to maintenance of steady-state levels of catecholamines and play a role in emotional and social behavior in mice.
ZDHHC8 (zinc finger DHHC domain-containing protein 8)	Chromosome 22q11	*Dhhc8* knockout mice had a deficit in prepulse inhibition, and a gene dosage-dependent decrease in exploratory activity in a new environment.
PRODH (proline dehydrogenase)	Chromosome 22q11	Prodh -/- mice had significantly decreased levels of glutamate, GABA, and aspartate in the hypothalamus and of GABA and aspartate in the frontal cortex.
RTN4R (reticulon 4 receptor)	Chromosome 22q11	It is involved in axonal regeneration in the adult vertebrate central nervous system

2.4 Aim of the study

The function of βB2-crystallin in the brain and the consequences of the mutation in *Crybb2* mutants are still unknown. To this end, I have confirmed whether the *Crybb2* is expressed in the brain and if it is only expressed at the postnatal stage of the brain. Which kinds of neurons are co-expressed with *Crybb2* have been examined in more detail. Therefore, I checked the coexpression of *Crybb2* and different GABAergic interneuron markers in different brain areas. In addition, the consequences of mutation in *Crybb2* mutants from molecular and cell biology level have been identified, such as those phenotypes related to behaviour changes in *Crybb2* mutants. For example, cell density of GABAergic interneurons and cell morphology and cytoskeleton changes were examined. Furthermore, the mechanisms that are involved in those changes have been studied. Especially, the calcium concentration and calcium related genes were checked, as βB2 crystallin was suggested as a calcium binding protein. The expression pattern and level of genes which were demonstrated to be up-regulated and down-regulated in *O377* mutants compared with wild type also have been assessed, which well expained phenotypes that found in *Crybb2* mutants.

3 Materials and methods

3.1 Materials

3.1.1 Equipment

Equipment	Manufacturer
Agarose-Gel electrophoresis: Horizon 11.14	Life Technologies, Karlsruhe, Germany
Cameras for light microscopes	Zeiss, Oberkochen, Germany
Centrifuge : Eppendorf 5415D	Eppendorf, Hamburg, Germany
Sigma 3K18	Sigma, Osterode am Harz, Germany
Confocal microscope: Olympus 8934	Olympus, Hamburg, Germany
Coverslips	Roth, Karlsruhe, Germany
Fluorescence microscope: Zeiss Axiovert 200	Zeiss, Oberkochen, Germany
Incubator: Celsius 2007	Memmert, Schwabach, Germany
Light Microsope:Zeiss Axioplan2	Zeiss, Oberkochen, Germany
LS50B spectrofluorimeter	Perkin Elmer, Roadgau, Germany
Microwave	Samsung, Hamburg, Germany
Microtome:Leica CM 1950	Leica Microsystems, Wetzlar, Germany
Millipore Water purification system	Millipore, Schwalbach, Germany
Nescofilm	Roth, Karlsruhe, Germany
PCR- thermal cycler : PTC-225	MJ Research, Hamburg, Biozym, Germany
Perfusion pump	Neolab, Heidelberg , Germany
Pipetman (2µl 10µl 20µl 200µl 1ml)	Gilson, Limburg-Offheim, Germany
SDS-Gel electrophoresis:	Bio-Rad, Munich, Germany
Stereo microscope: Zeiss Axioplan2 imaging	Zeiss, Oberkochen, Germany
Sliding Microtome	Leica Microsystems, Wetzlar, Germany

Slides: Superfrost® Plus	Gerhard Menzel Gmbh, Braunschweig, Germany
Step one Quantitative real time PCR system	Applied Biosystems, Darmstadt, Germany
Thermomixer 5436	Eppendorf, Hamburg, Germany
Vortexer: Vortex-2geni	Scientific Industries, Karlsruhe, Germany
15 ml Tubes & 50 ml Tubes	BD Falcon, Heidelberg, Germany
2ml Tube & 1.5 ml Tubes	Eppendorf, Hamburg, Germany

3.1.2 Software

stereological counting of cells and measure volume	Stereo investigator, MBF Bioscience, Magdeburg, Germany
Trace neuronal morphology	Neuron Lucida, MBF Bioscience, Magdeburg, Germany
analysis of confocal imaging	Fluoview: Olympus, Hamburg, Germany
DNA sequence and gene analysis:	http://www.ensembl.org/ http://www.ebi.ac.uk/Tools/clustalw2/index.html
Primer design and evaluation:	http://www.sigma-genosys.com/calc/DNACalc.asp /
Real time PCR data collection and anaylsis	StepOne Software, Applied Biosystem Deutschland GmbH, Darmstadt, Germany

3.1.3 Cell line

RGC5 cell: Retinal ganglion cell (gift from Prof. Dr. Solon Thanos, Unversity of Muenster); HEK-293 cell: Human Embryonic Kidney 293 cells.

3.1.4 Mice

Mice were kept at the Helmholtz Center Munich, Neuherberg, according to the Declaration of Helsinki and the regulations of the German Law on Animal Protection.

The *0377* mice have been characterized previously (Ganguly et al., 2008), the *Philly* mice were received from Melinda Duncan (University of Delaware, USA); both mutant lines were kept on C57BL/6J background for more than 10 generations.

3.1.5 Plasmids

pETM11 is gift from Prof.Dr. Michael Sattler's lab; pEGFP is from my previous study (Sun *et al.*, 2007).

3.1.6 Chemicals

All chemicals used in my work, if not specially declared, were purchased from Sigma-Aldrich (Deisenhofen, Germany), Biorad (Munich, Germany), Fluka (Deisenhofen, Germany), Invitrogen (Karlsruhe, Germany), Merck (Darmstadt, Germany), Roth (Karlsruhe, Germany), Riedel de Haen (Seelze, Germany), Serva (Heidelberg, Germany) Roche (Mannheim, Germany). $^{15}NH_4Cl$ were purchased from Sigma-Aldrich (Deisenhofen, Germany).

Home made MilliQ water was used for the generation of solutions (Millipore, Schwalbach, Germany).

Fetal Bovine Serum (FBS), Dulbecco's Modified Eagle Medium (DMEM), low Glucose (1g/l) and antibiotics used in the cell culture were from either PAA (Karlsruhe, Germany) or Invitrogen (Karlsruhe, Germany). Phosphate buffered saline (PBS) and Hank's Balanced Salt Solution (HBSS) used for cell culture is purchased from Invitrogen (Karlsruhe, Germany).

All restriction enzymes and their compatible buffers were purchased from Fermentas (St. Leon-Rot, Germany) and New England Biolabs (NEB) (Frankfurt am Main, Germany).

DIG RNA labeling mix and Sp6/T7 RNA polymerase were purchased from Roche (Mannheim, Germany) and Fermentas (St. Leon-Rot, Germany).

3.1.7 Commercial kits

DNA Midi Prep	Qiagen, Hilden, Germany
DNA Mini Prep	Nucleospin, Macherey-Nagel, Düren, Germany
Gel extraction	Nucleospin, Macherey-Nagel, Düren,

Germany

DNA purification kit	Nucleospin, Macherey-Nagel, Düren, Germany
PCR kit	Invitrogen, Karlsruhe, Germany
Eva Green real time PCR mix	Solis BioDyneBi, Tartu, Estonia
PCR	Invitrogen, Karlsruhe, Germany
RNA extraction	Ams biotechnology, Germany
cDNA T-Primed First-strand Kit	Amersham Biosciences, Freiburg, Germany
FD Rapid Golgistain Kit	FD NeuroTechnologies, Karlsruhe, Germany
Polyfection transfection Kit	Qiagen, Hilden, Germany
RNA BEE	Ams biotechnology, Frankfurt, Germany

3.1.8 Buffers and solutions

Buffers and solutions for mouse perfusion, slices storage and immunohistochemistry:

4% Paraformaldehyd	Paraformaldehyd (PFA)	40 g/l
	Dissolve in 1xPBS	
0.2 M Phosphate buffer:	Sodium phosphate monobasic	16.56 g/l
	Sodium phosphate dibasic	65.70 g/l
	Disolve in H_2O	
	Adust pH to 7.4 with HCl	
Cryoprotect solution:	Glycerin	250 ml
	Ethylene Glycol	250 ml
	M Phosphate buffer	500 ml
	Disolve in H_2O adjust pH 7.0 with HCl	
Borate buffer:	Boric Acid	6.183 g/l

Dissolve in H$_2$O
Disolve in H$_2$O
adjust pH 8.5 with NaOH

TBS (10X) :	NaCl	80 g/l
	KCl	2 g/l
	1M Tris-Cl	100 ml/l
	Disolve in H$_2$O adjust pH 7.4 with HCl	

Buffers and solutions for *in situ* hybridization:

| Sodium citrate buffer: | Sodium Citrate | 2.94 g/l |
| | Disolve in H$_2$O adjust pH 6.0 with HCl | |

| 1M Tris-Cl : | Tris-base | 121.4 g/l |
| | Disolve in H$_2$O adust pH 7.4 with HCl | |

Denhardt's(50x) :	Ficoll,	10 g/l
	polyvinylpyrrolidone	10 g/l
	bovine serum albumin	10 g/l
	Disolve in H$_2$O	
	Filter and store at -20	

Hybridization solution:	50x Denhardt's	5 ml
	100mg/ml baker yeast tRNA	125 µl
	20x SCC	12.5 ml
	form amide	25 ml
	Fill up to 50 ml with DEPC treated H$_2$O	

SSC(20x) :	NaCl	175.3 g/l
	sodium citrate	88.2 g/l
	Add H$_2$O, adjust pH to 7.0 with HCl,	
	Treat with DEPC and autoclave.	
Buffer 1(1x) :	1 M Tris	100 ml/l
	NaCl	8.7 g/l
	Add milliQ-H$_2$O,adjust pH to 7.5	
	Treat with DEPC and autoclave.	
Buffer 2x:	1M Tris	100 ml/l
	NaCl	8.7 g/l
	1M MgCl$_2$	1 ml
	Add H$_2$O, adjust pH to 9.5 with HCl.	
1M MgCl$_2$:	MgCl$_2$.6 H$_2$O	60.99 g/l

10x TE:	1 M Tris	100 ml/l
	EDTA	3.72 g/l
	Add H_2O, adjust pH to 8.0 with HCl,	
	Treat with DEPC and autoclave.	

Color solution:	75 mg/ml NBT	45 l
	50 mg/ml BCIP-phosphate	35 µl
	Levamisole	2.4 mg
	In 10 ml buffer 2.	
	Prepare freshly, filter solution through a	
	0.22 um filter and store in darkness.	

Buffers and solutions for E.*coli* culture protein purification and labelling:

LB medium:	Bacto-Trypton	10 g/l
	Bacto-yeast extract	5 g/l
	NaCl	10 g/l
	Disolve in H_2O	
	autoclave (120 °C, 20 min)	

LB agar:	Bacto-Trypton	10 g/l
	Bacto-yeast extract	5 g/l
	NaCl	10 g/l
	Bacto-agar	15 g/l
	autoclave (120 °C, 20 min)	

Loading buffer:	Tris	50 mM
	NaCl	500 mM
	Glycerol	5%
	Imidazol	5 mM
	TCEP	1 mM
	Ajust pH to 7.4 with HCl	

Wash buffer:	Tris	50 mM
	NaCl	500 mM
	Glycerol	5%
	Imidazol	25 mM
	TCEP	1 mM
	Ajust pH to 7.4 with HCl	

| Trance elements: | Na_2EDTA | 150 mM |

	FeCl$_3$ .6H$_2$0	15 mM
	ZnCl$_2$	4 mM
	CuCl$_2$	1 mM
	CoCl$_2$.6 H$_2$O	1 mM
	H$_3$BO$_3$	2 mM
	MnCl$_2$.6 H$_2$O	60 mM
	Dissovle in the 100 ml MilliQ H$_2$O	
M9 medium	Na2HPO4	422.5 mM
	KH2PO4	220.6 mM
	NaCl	85.5 mM
	^{15}NH4Cl	46.7 mM
N15 component medium:	MilliQ H$_2$O	900 ml
	Trace elements	10 ml
	MgSO$_4$	1 mM
	CaCl$_2$	0.25 mM
	Biotin	1 mM
	Thiamin	1 mg
	Glucose	4 g
	M9 medium	100 ml

Buffers and solutions for SDS Gel Electrophoresis:

5x Sample Buffer:	SDS	10%
	Dithiothreitol	10 mM
	Glycerol	20 %
	Tris-HCl, pH 6.8	0.2 M
	Bromophenolblue	0.05%
Running Buffer:	Tris-HCl	25 mM
	Glycine	200 mM
	SDS	0.1%
Running Gel Solution:	H$_2$O	12.3 ml
	20% SDS	7.5 ml
	1.5 M Tris-HCl, pH 8.8	0.15 ml
	Acrylamide	0.8%
	ammonium persulfate (30%)	9.9 ml
	Tetramethylethylenediamine	0.15 ml
Stacking Gel Solution:	H$_2$O	3.075 ml

0.5 M Tris-HCl, pH 6.8	1.25 ml
20% (w/v) SDS	0.025 ml
Acrylamide (30%)	0.67 ml
10% ammonium persulfate	0.025 ml
Tetramethylethylenediamine	0.005 ml

Buffers and solutions for patch clamp:

Artificial Cerebrospinal Fluid(ACSF):	NaCl	125 mM
	KCl	2.5 mM
	$NaHCO_3$	25 mM
	$CaCl_2$	2 mM
	$MgCl_2$	1 mM
	D-glucose	25 mM
	NaH_2PO_4	1.25 mM
	Adjust pH to 7.4 with HCl	

Intracellular solution:	Mg-ATP	1 mM
	$CsCH_3SO_3$	100 mM
	CsCl	60 mM
	EGTA	0.2 mM
	HEPES	10 mM
	$MgCl_2$,	1 mM
	Lidocain N-ethyl-Chlorid,	5 mM
	Na_3GTP	0.3 mM
	Adjust pH to 7.4 with HCl	

Solution used for calcium measurement

HBSS++:	NaCl	137 mM
	KCl	5.8 mM
	HEPES,	10 mM
	glucose,	5 mM
	$CaCl_2$,	2.5 mM
	glycine,	10 µM
	$MgCl_2$	1 mM

3.1.9 Antibodies

Table 3.1 Primarily antibody

Target protein	Species	Dilution	Producer and catalog number
anti-DIG-AP Fab	Sheep	1:3000	Roche, Mannheim, Germany (11 093 274 910)
βB2-crystallin	Mouse	1:100	Dr.Kremmer Elisabeth, Helmholtz Zentrum

			München, Germany (clone 4C4)
BrdU	Rat	1:1000	AbD Serotec, Düsseldorf, Germany (MCA2060)
Calretinin	Rabbit	1:1000	Swant, Bellinzona, Switzerland (7699/3H)
Cleaved Caspase-3	Rabbit	1:200	BD Pharmingen, Heidelberg, Germany (559565)
Doublecortin	Goat	1:250	Santa Cruz Biotechnology, Heidelberg, Germany (sc-17320)
Glial fibrillary acidic protein (GFAP)	Rabbit	1:500	Sigma (G3893), Steinheim, Germany
Microtubule-associated protein 2 (MAP2)	Rabbit	1:100	Santa Cruz Biotechnology, Heidelberg, Germany (H300)
NeuN	Mouse	1:100	Hybridoma Bank, Iowa, USA (4D7/TAG1)
Neurofilament	Mouse	1:50	Abcam,Cambridge, UK (ab7795)
Parvalbumin	Rabbit	1:1000	Swant, Bellinzona, Switzerland (PV25)
Parvalbumin	Mouse	1:1000	Swant, Bellinzona, Switzerland (235)
Somastostatin	Rabbit	1:500	Enzo, Lörrach, Germany (SA1268)
Sox2	Goat	1:1000	Santa Cruz Biotechnology, Heidelberg, Germany (SC17320)

Table 3.2 Second antibody

Name	Species	Dilution	Producer
Alexa 488	According to primary antibody	1:250	Invitrogen, Karlsruhe, Germany
Cy3	According to primary antibody	1:250	Jackson Immunoresearch, Suffolk, UK
Cy5	According to primary antibody	1:250	Jackson Immunoresearch, Hamburg, Germany
FITC	According to primary antibody	1:250	Jackson Immunoresearch, Hamburg, Germany

3.2 Methods

3.2.1 Tissue preparation and dissection

Free floating section:

Brains were post-fixed in 4 % PFA overnight at 4℃ and were subsequently transferred to a 30% sucrose solution for 48 hours. 40 µm thick coronal brain sections were made using a sliding microtome (Leica Microsystems, Wetzlar, Germany).

Cryosection:

After sacrificed by CO_2, the mouse head was cut and the brain was taken out. Then, the brain was frozen in a block filled with OCT compound (Gene Research Lab,

Karlsruhe, Germany).

Paraffin section:

Mouse was sacrificed in an airtight box filled with CO_2. Then, mouse was transcardially perfused with phosphate-buffered saline at a speed of 12 ml/minute for 5 minutes followed by treatment with 4% paraformaldehyde (PFA) for 5 minutes. The head of the animal was cut and the brain was prepared. On the following day the brains were transferred into 70% ethanol and were subjected to graded dehydration in series of alcohol. Then the brains were embedded into paraffin. Afterwards, 8 µm thick sagittal sections were made using a microtome (Leica Microsystems, Wetzlar, Germany).

3.2.2 Fluorescent immunohistochemistry

Free floating sections were rinsed three times in 0.1 M Tris buffered saline (TBS) for 15 minutes each. After blocked in blocking solution TBS++ (containing TBS supplemented with 3% normal Fetal Bovine Serum, 0.25% Triton-X100), sections were incubated with primary antibody at the appropriate dilutions overnight at 4℃ on a shaker. Afterwards, they were rinsed three times in TBS for 15 minutes each. Sections were blocked in TBS++ for 30 minutes. Then brain slices were incubated in TBS++ containing the secondary antibody at a dilution of 1:250 for 2 hours at room temperature. Thereafter, brain sections were rinsed three times in 0.1 M Tris buffered saline (TBS) for 15 minutes each. In between, sections were rinsed in TBS containing a DAPI antibody for 5 minutes. Brain slices were transferred into 0.1 M phosphate buffer and mounted on superfrost slides using Aqua/Polymount. The whole procedure was done according to Lie et al (2005).

For BrdU labelling, antigen retrieval is necessary. After washing 3 times with TBS, sections were incubated in 2N HCl at 37℃ for 30 mi nutes. Slides were rinsed in 0.1 M borate buffer twice and then washed in TBS six times for a total of 90 minutes. Sections were then blocked as described above.

For the βb2-crystallin antibody, sections were boiled in 0.01 M citrate buffer at 95℃ for 20 minutes, cooled down to room temperature and then rinsed with TBS 3 times. Sections were then blocked 2 hours with TBS++. After incubation with primary antibody, all steps followed the immunohistochemistry procedure described above.

Confocal single plane images and Z-stacks were taken on an Olympus microscope

with a FluoView software.

3.2.3 Transformation of bacteria

Competent DH5α cells were thawed on ice. The DNA was added to the bacteria, mixed gently, and then incubated for 20 minutes on ice. The heat-shock was performed at 42℃ for 45-60 seconds. Cells were coo led down again on ice for 3 minutes and 400 µl of LB media was added. Thereafter, cells were put on a shaker at 37℃ for 40 minutes. Cells were plated out on agar plates with kanamycin for selection, and incubated over night at 37℃.

3.2.4 Isolation of plasmid DNA from *E. coli* (mini prep)

To isolate small amounts of plasmid DNA from *E.coli*, I used a kit from NucleoSpin. All reagents and columns used in the experiments are included in the kit. The procedure was done following the manufacture's protocol:

4 ml of saturated *E. coli* LB culture was spined down in a 1.5ml tube for 30 s at 11,000 x g. Supernatant was discarded and the liquid was removed as much as possible. Then 250 µl Buffer A1 (resuspension buffer) was added to resuspend the cell pellet completely by vortexing. After that, 250 µl Buffer A2 (lysis buffer) was added and mixed gently by inverting the tube 6 - 8 times. Sample was incubated at room temperature for 5 min. 300 µl Buffer A3 (neutralization buffer) was added to the sample, and mixed thoroughly by inverting the tube 6 - 8 times, and centrifuged for 5 min at 11,000 x g at room temperature. Then a Plasmid Column was placed in a collection tube and the supernatant was decanted from last step. A maximum of 750 µl of the supernatant were transferred onto the column, and centrifuged for 1 min at 11,000 x g. Then I discarded the flow-through and placed the Plasmid Column back into the collection Tube (2 ml). 600 µl Buffer A4 (wash buffer) were added and centrifuged for 1 min at 11,000 x g. Flow-through was discarded and Plasmid Column was placed back into the empty collection Tube (2 ml). Then, it was centrifuged for 2 min at 11,000 x g and the tube was discarded. Afterthat, 50 µl Buffer AE was added (elution buffer) to the column, which was a new 1.5 ml tube.The column with the tube was centrifuged for 1min at 11,000 x g. Finally, the plasimid was in the 1.5 ml tube, and it is ready to use.

3.2.5 Isolation of plasmid DNA from E. coli (Midi Prep).

To isolate the larger amounts of plasmid DNA from *E.coli* for transfection and

sequencing, I used a Midi Prep kit from Qiagen. All the reagents and column used in the experiment are included in the kit. The procedure was done following the manufacture's protocol:

A single colony was cultured in 3 ml LB medium containing the appropriate selective antibiotic. It was incubated on the shaker for 8 hours at 37°C with vigorous shaking. 50μl cultured LB media were transferred from last step to 25 ml new media culture on the shaker for 16 hours at 37°C with vigorous shaking. The cells were harvested by centrifugation at 6000 x g for 15 min in a 15 ml falcon tube. Bacterial pellet were resuspend in 4 ml Buffer P1 (resuspension buffer). 4 ml Buffer P2 (lysis buffer) were added and mixed thoroughly by vigorously inverting the sealed tube 5 times, and incubated at room temperature for 5 min. Then 10 ml of Buffer P3 (neutralization buffer) were added and mixed immediately, then thoroughly by vigorously inverting 5 times, and incubated on ice for 15 min. Mixture was centrifuged at 20,000 x g for 30 min at 4°C. The supernatant was transferred to anot her falcon tube. The supernatant was centrifuged again at 20,000 x g for 15 min at 4°C. After that, supernatant was transferred to another falcon tube very gently. A QIAGEN-tip 100 was equilibrated by applying 4 ml Buffer QBT (wash buffer), and column was allowed to empty by gravity flow. Then, the supernatant was applied from last step to the QIAGEN-tip and allowed to enter the resin by gravity flow. Then after, QIAGEN-tip was washed with 2 x 10 ml Buffer QBT, DNA was eluted with 5 ml Buffer QF (elution buffer). Then, 3.5 ml isopropanol was added and mixed, it was immediately centrifuged at 15,000 x g for 30 min at 4°C. The supernatant was trashed, while D NA pellet was washed with 2 ml of room-temperature 70% ethanol, and centrifuged at 15,000 x g for 10 min. The supernatant was decanted without disturbing the pellet. The pellet was air-dried for 5–10 min, and redissolve the DNA in 100 μl TE buffer. The DNA was ready to use.

3.2.6 Isolation of RNA

RNA used for real time PCR or cloning was isolated using the RNA Bee. The protocol from the producer was followed when using this reagent. Briefly, brain tissue from hippocampus was homogenized in 0.8 ml of RNA-Bee. Homogenate was transferred to a 1.5ml tube, with 160 μl of chloroform, and the mixture were stored for 5 minutes at 4 °C. Then it was centrifuged at 10,000 x g for 15 minutes at 4°C, the aqueous phase was collected and mixed with 0.4 ml of isopropanol for 30 minutes at 4°C. RNA precipitate was centrifuged at 10,000 x g for 10 minutes at 4°C. The pellet was

washed once with 75% ethanol. The pellet was dried for 10 minutes and dissolved in 30 µl MilliQ water.

3.2.7 cDNA synthesis

I started the cDNA synthesis immediately after I got the RNA. cDNA was synthesized using the cDNA T-Primed First-strand Kit following the manufacturer's protocol:

5µg RNA sample (or the control mix) was brought to a volume of 33 µl in an RNase-free microcentrifuge tube using DEPC- treated water; the mixture was heated to 65°C for 5 min. Then I transferred the RNA solution to a 37°C bath and incubated for 5 min. At the same time, I incubated the first-strand reaction mix at 37°C for 5 min. After that, I transferred the RNA solution to the first-strand reaction mix without any mixing and incubated it at 37°C for 5 min 37°C. Then, I mixed the contents of the tube by gentle vortexing or by repeatedly pipetting the mixture up and down. I centrifuged to collect the contents at the bottom of the tube. Afterwards, I incubated it at 37°C for another 60 min; the completed first-strand reaction was ready for use.

3.2.8 Extraction of DNA fragments from agarose gels

All the reagents and columns used in the experiment are included in the kit from NucleoSpin. A small piece of the agarose gel with the target DNA fragments were cut out of the agarose gel under the illumination of UV light and DNA was extracted using the NucleoSpin gel extraction Kit following the manufacturer's protocol:

The small piece of the agarose gel was mixed with 200 µl Buffer NT (binding buffer), and the sample was incubated for 10 min at 50°C. Th en I placed a column into a collection tube and loaded the sample. It was centrifuged for 1 min at 11000 x g. After that, I discarded the flow-through and placed the column back into the collection tube. Then, I added 700 µl Buffer NT3 (wash buffer) to the column, following by centrifugation for 1 min at 11,000 x g. Flow through was discarded and the column was placed back into the collection tube. The tube was centrifuged for 2 min at 11,000 x g to remove Buffer NT3 completely. Then I placed the column into a new 1.5 ml tube. 30 µl Buffer NE (elution buffer) were added to the 1.5ml tube and incubated at room temperature for 1 min. The 1.5ml tube was centrifuge for 1 min at 11,000 x g. Then the DNA was ready for use.

3.2.9 PCR

PCRs were performed using the *Taq* DNA polymerase (Invitrogen, Karlsruhe,

Germany); the PCR mixture was made following the manufacturer's instruction:

Table 3.3 Compents include in the PCR mixture

Components	Volume	Final Concentration
10x PCR buffer	10µl	1x
2mM dNTP	5 µl	0.1mM
50mM $MgCl_2$	3µl	1.5mM
Primer mix (10 µM)	5µl	0.5 mM
Template cDNA	2 µl	
Taq DNA polymerase(5U/µl)	1 µl	0.05U
MilliQ water	Up to 100µl	

PCRs were run on a thermal cycler. Primers were designed and evaluated using the online program http://www.sigma-genosys.com/calc/DNACalc.asp/. The initial denaturing step was performed at 94℃ for 4 minutes . The cycles consisted of the denaturing step at 94℃ for 30 seconds. In the expe riment of *Crybb2* expression study, PCR was run for 28 cycles and 35 cycles separately, in all others studies PCRs were run for 35 cycles.

Primers for amplification of wild-type and *O377 Crybb2* gene used for over-expression in RGC-5 cells and HEK-293 cells

Gene	Primer sequence	Product length
Crybb2	Forward: 5' AAGCTAGCATGGCCTCAGACCACCAG 3'	634bp or 691bp
	Reverse: 5' AAGGATCCGCTGGAGGGGTGGAAG 3'	
Gapdh	Forward: 5' ACGCTAGCATGGTGAAGGTCGGTGT 3'	1002bp
	Reverse: 5' AAGGATCCCTCCTTGGAGGCCATGT 3'	

Primers for amplification of wild-type and *O377 Crybb2* gene used in protein purification

Gene	Primer sequence	Product length
Crybb2	Forward: 5' AAATCATGA CCTCAGACCACCAGACAC 3'	639bp or 696bp
	Reverse: 5'AAAGCGGCCGCCTGCTGGAGGGGTGGAAG 3'	

Table 3.4 Parameters for PCR primers used in PCR study

Name	Annealing temp	Annealing Time	Extension temp	Extension time
Crybb2 (for expression in cells)	60°C	30 seconds	72°C	45 seconds
Gapdh	60°C	30 seconds	72°C	45 seconds
Crybb2 (for protein purification)	58°C	30 seconds	72°C	45 seconds

3.2.10 Cloning procedures

For cloning purposes, restriction digests were performed according to standard procedures or the manufacturer's protocol. Recognition sites for restriction endonucleases were checked and the appropriate plasmid maps were generated using the online service http://tools.neb.com/NEBcutter2/.

For over-expression wild-type and mutant *Crybb2* in *E.coli*, wild-type and mutant *Crybb2* with additional restriction endonuclease sites for *BspHI* and *NotI* were cloned in the expression vector pETM11 containing a 6x His-tag and a Tobacco Etch Virus protease cleavage site (TEV) (Figure 3.1 A).

In order to find out if the mutation in *O377* mutants could lead to aggregation, I over-expressed wild-type and mutant *Crybb2* in RGC-5 Cells and HEK-293 cells. Before the transfection, I cloned the wild-type and mutant *Crybb2* into the pEGFP. Briefly, the whole cDNA sequence of wild-type and *O377* mutant *Crybb2* with additional restriction sites for *NheI* and *BamHI*, but without the stop codon, were cloned and inserted into the pEGFP vector (Figure 3.1 B).
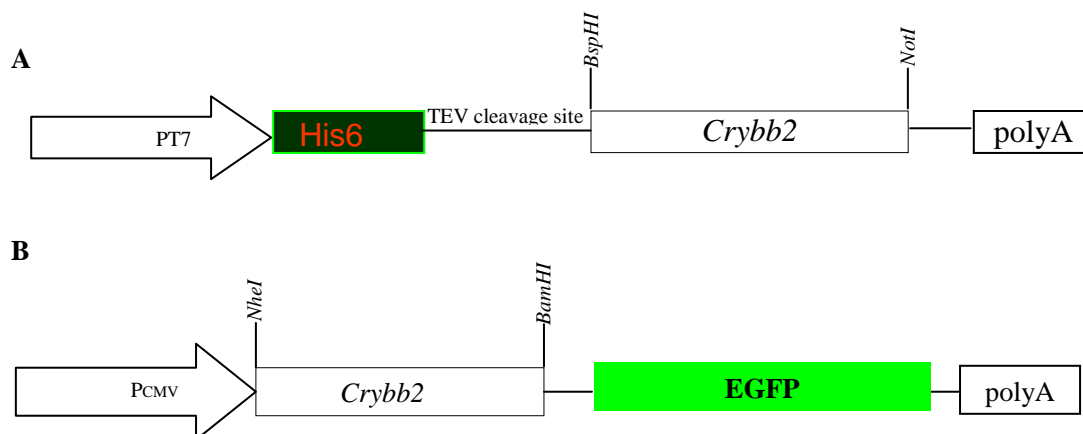
Figure 3.1 Cloning strategy for over-expression wild-type and mutant *Crybb2* in *E.coli* (A) and RGC-5 cells/HEK-293cells (B)

3.2.11 Quantitative real time PCR

Quantitative RT-PCR was performed on a StepOne instrument (Applied Biosystems, Unite states). The Online program http://www.sigma-genosys.com/calc/DNACalc.asp was used to design and evaluate primers for quantitative RT-PCR. For detection of cDNA, Eva Green qPCR Master Mix (Solis BioDyneBi, Tartu, Estonia) was used according to the manufacturer's protocol

Table3.5 components include in the qPCR mixture

Components	Volume	Final Concentration
5x Eva Green qPCR master mix	4 µl	1x
Primer mix (10µM each)	1µl	0.5mM
cDNA	0.5µl	
MilliQ water	14.5µl	

The running program for real time PCR was edited by the software compatible to step one. The initial denaturing step was performed at 94℃ for 15 minutes. The cycles consisted of the denaturing step at 94℃ for 30 seconds, annealing at 60℃ for 15 seconds, extension at 72℃ for 15 seconds, denat urizing 94℃ for 15 seconds and melting curve 60℃ for 15 seconds. In every run, *Tuba1a* was employed as an internal control present in every run. PCRs were run for 40 cycles. Analysis of relative gene expression data is according to the $2^{-\Delta\Delta ct}$ method as previously described (Livak and Schmittgen, 2001).

Primers for quantitative real time PCR:

Gene	Primer sequence	Product length
Capn3	Forward: 5' CTATGACATCATCACCATGCGCTA 3'	113 bp
	Reverse: 5' CATACATGGTAAGCTGCAGCCA 3'	
Grin1	Forward: 5' TTAAGGTGAACAGCGAGGAG 3'	181bp
	Reverse: 5' CAGGTTGGCAGTGTAGGAAG 3'	
Grin2a	Forward: 5' TCTCCTCACAGACTTTCATCCCC 3'	178bp
	Reverse: 5' GTGACCAAGGAGAAGACATGCC 3'	
Grin2b	Forward: 5' TGGGGGCTCATCTATGATAATGG 3'	188bp

Reverse: 5' GCGGATCTTGTTCACGAAGTC 3'

Grin2c	Forward: 5' CTCTGTGCCTTTTGTGGAGACC 3'	185bp
	Reverse: 5' GGTTGTAGCTGACAGGGCTGAA 3'	
Tuba1a	Forward: 5' CCAGATGCCAAGTGACAAGA 3'	117bp
	Reverse: 5' GTGGGTTCCAGGTCTACGAA 3'	

Table3.6 Parameters for PCR primers used in PCR study

Name	Annealing temp	Annealing Time	Extension temp	Extension time
Capn3	60°C	15 seconds	72°C	15 seconds
Grin1	60°C	15 seconds	72°C	15 seconds
Grin2a	62°C	15 seconds	72°C	15 seconds
Grin2b	62°C	15 seconds	72°C	15 seconds
Tuba1a	60°C or 62°C	15 seconds	72°C	15 seconds

3.2.12 Cell culture

RGC-5 and HEK-293 cells were kept under 37°C with 5% CO_2 in Dulbecco's modified Eagles's medium (DMEM) supplemented with 10% Fetal bovine serum and 1 x penicillin / streptomycin (50U of penicillin and 50µg of streptomycin per liter). When the cell grows to 80% confluence, cells were incubated with trypsin and splitted from 1 to 5.

3.2.13 Transfection

For over-expression of wild-type and *O377 Crybb2* in RGC-5 cell I performed transfection using a PolyFection kit (Qiagen, Hilden, Germany). The whole procedure was done according to manufacturer's protocol:

The day before transfection, cells were seeded in 24 well plate dishes in 1 ml of DMEM with 10% of FBS. The cells were cultured at 37°C and 5% CO_2. After the cell grew to 40–80% confluent, transfection was performed. I diluted 0.5 µg of DNA with cell growth medium containing no serum, proteins, or antibiotics to a total volume of 50 µl. The solution was mixed for a few seconds to remove drops from the top of the tube. After I added 5 µl of PolyFect Transfection Reagent to the DNA solution, I mixed by pipetting up and down 5 times. Then I incubated samples for 10 min at room temperature. At the same time, I gently aspirated the growth medium from the dish and added 125 µl of fresh cell growth medium. Then, I added it to the reaction tube

containing the transfection complexes. The mixture was immediately transferred to the cells in the 24 well plates. In addition, I gently swirled the plate to ensure uniform distribution of the complexes. Then, cells with the complexes were incubated at 37℃ and 5% CO_2 to allow gene expression.

3.2.14 SDS Gel Electrophoresis

SDS gel was prepared by using running gel solution and stack gel solution. Then, the protein was boiled for 5-10 mins after mixed with sample buffer. The prepared gel and running buffer was filled in the chamber according to the instructions for SDS-gel electrophoresis apparatus. The prepared samples and molecular weight standards were pipetted into the wells of the gel. Then, the SDS gel electorphoresis was run at 100V constantly till the blue dye fronts reach the bottom. Afterwards, the gel was removed and stained in Coomassie Brilliant Blue for visualization.

3.2.15 Protein isolation

For analyzing the protein of wild-type and *O377* βB2-crystallin, I expressed it in *E.coli* and purified the protein:

I transformed the plasmid with wild-type or *O377 Crybb2* to BL21 (DE3) competent cells in a plate with kanamycin antibiotics. Then, a colony was picked and cultured with 20 ml of LB with kanamycin on the shaker with 180 rpm. I transferred the 20 ml cultured *E.coli* to a bigger flask and filled it with 1L LB media. When the cells grew up to OD 600 nm of 0.8 to 1.2, 1 mM IPTG was added to the culture media to induce protein expression at 18 ℃ on the shaker with 180 rpm overnight. *E.coli* was collected with 10000 x g for 20 minutes. Then, the cells were resuspended in PBS and sonicated. After that, the mixture was centrifuged at 10000 x g for 45 minutes and supernatant was transferred to another falcon tube. Supernatant and pellet were checked the by SDS-PAGE. The mixture was passed twice through the Ni-column. Then the Ni-column was wahsed with loading buffer, 2 times with wash buffer and the protein containing His-tag was eluted with elution buffer. SDS-gel electrophoresis was used to make sure that the protein was in the elution buffer. Then, the protein was incuabed overnight at 4 ℃ with 1 mg/ml TEV pro tease to remove the His-tag. Afterwards, the mixture was passed through Ni-column to get the His-tag free protein. SDS-gel electrophoresis was run again to make sure that the protein was present in the pass through. Prepared protein was stored for further use. The E.coli containing

wild-type or *O377 Crybb2* was also cultured in N15 component medium for the heteronuclear single quantum correlation (HSQC) NMR spectroscopy.

3.2.16 Hippocampal neuron isolation

The hippocampal neurons were isolated according to a previous description (Nunez, 2008). Briefly, brains from E17.5-E18.5 of wild-type and *O377* embryos were removed and hippocampi were dissected free of meningeals and other brain regions. Hippocampi were cut into small pieces and digested with trypsin. Then cells were collected after all pieces of tissues are digested compeletly.

3.2.17 Calcium concentration measurement

Calcium measurement procedure is based on previous description (Grynkiewicz *et al*, 1985; Diaz-Hernandez *et al.,* 2002). Hippocampal neurons were washed twice in HBSS+ by resuspension and subsequent centrifugation (1000 x g, 10 min at RT). After cell counting and viability check in a Neubauer chamber using Trypan blue dye exclusion (0.2%), the cell concentration was adjusted to 1×10^6 cells/ml. Then the cells were incubated with 2.5 µM of the calcium dye Fura-PE3/AM for 30min at 37℃ in a humidified incubator with 5% O_2 and CO_2 95%. Afterwards, the extracellular dye was removed by two steps of HBSS+ rinsing and centrifugation. Before measurements, further dye desertification was allowed for further 30 minutes. For measurements, 2ml of the hippocampal neuron suspension at a concentration of 0.5×10^6 cells/ml were transferred to a cuvette, equipped with a magnetic stirrer and a thermostated waterjacket kept at 37℃. Fluorescence ratios (F380 nm/F340nm) proportional to Ca^{2+} concentration were monitored in a LS50B spectrofluorimeter. 50µM NMDA was used to open the NMDA receptor to influx calcium ions from environment to cell cytoplasm. After the stable Ca^{2+} level was obtained, 10µM Thapsigargin were added to allow an influx of calcium into the cytosol from endoplasmic reticula. The calibration was performed by adding 10µM of ionomycin (Rmax) and 5mM EGTA (Rmin). Ca^{2+} concentrations were calculated from the raw data by performing the Grynkiewicz calculation (Grynkiewicz *et al* 1985): $[Ca^{2+}]_i = k_d$ (Fmin, 380nm/ Fmax, 380nm)[(R-Rmin)/(Rmax-R)] using a $Kd = 146$ nmol/L for calculations.

3.2.18 Hematoxylin & Eosin Staining

As overexpression of the mutant *Crybb2* leads to protein aggregation in *vitro*, I also tried to check the aggregation *in vivo*. For detection of the aggregation of βB2-crystallin, we performed the H&E Staining according to manufacture's protocol:

The slices were first deparaffinized with 3 changes of xylene, 15 minutes each. Then, slices were re-hydrated in 2 changes of absolute alcohol, 5 minutes each, in 95% alcohol for 2 minutes, 90% alcohol for 2 minutes and 75% alcohol for 2 minutes. Then slices were washed in MilliQ water and stained with hematoxylin solution for 10 minutes. Then, slices were washed in warm runninng tap water for 10 minutes and in distilled water 2 times and in 95%, alcohol with 10 dips of HCl.

Slices were counterstained in eosin-phloxine B solution for 1 minute. The slices were dehydrated through 95% alcohol, 2 changes of absolute alcohol, and 5 minutes each. Slices were cleared in 3 changes of xylene, 5 minutes each. Slices were mounted with xylene based mounting medium.

3.2.19 Nissel staining

To better look at the morphology of the wild-type and *O377* hippocampal region, I performed the Nissel staining (cresyl violet staining) on every 12th slices. The whole procedure is done as previously decribed (Fernstrom, 1958).

Free floating slides were picked out (every 12th slide) and transferred on the slice by brush and made sure that it is even on the slices. Those slices were exposed to air to dry. The slices were passed through with 75% ethanol, 95% ethanol and 3 times 100% ethanol, with 3 times xylene, 3 times 100% ethanol, 1 time 95% and 1 time 75% ethanol, for each step 3 minutes. Then slices were transferred to MilliQ water for 30s. Afterwards, they were incubated in 0.1 % cresyl violet for 10min. The slices were destained with MilliQ H_2O with a few drops of HCl. Then, the slices were passed through with 75% ethanol, 95% ethanol, 3 times 100% ethanol and 3 times Xylene, for each time 3 minutes. Then the slices were covered with permount mounting media and a cover slip for inspection at the microspcope.

3.2.20 Whole-cell patch-clamp recording

To verify whether a decrease in the number of parvalblumin positive GABAergic interneurons and neurons with reduced dendrite complexity would result in functional changes in the dentate gryrus, I performed patch clamp whole cell recording in dentate gyrus. Briefly, wild-type and *O377* mice were decapitated, and brains were isolated. 400μm coronal brain sections were sliced rapidly by microtome in the oxygenated artificial cerebrospinal fluid (ACSF). Brain coronal slices were incubated in the ACSF for 30 min at 35℃. Then slices were pl aced in the recording chamber of the patch clamp set up and superfused with ACSF at a flow rate of 2 ml/min. For

whole-cell patch-clamp recordings, neurons in ventral dentate gryrus were visualized using infrared video-microscopy and the gradient contrast system (Dodt et al. 2002). The patch clamp experiment was performed at holding potential of -70 mV, and currents were recorded using a switched voltage-clamp amplifier. Series resistance was monitored continuously and compensated in bridge mode (Swandulla and Misgeld, 1990). Miniature inhibitory postsynaptic currents (mIPSCs) recording were made at holding potential of in the artificial cerebrospinal fluid (ACSF) with 5µM NBQX (2, 3-dihydroxy-6-nitro-7-sulfamoyl-benzo[f] quinoxaline-2, 3-dione, an AMPA Glutamate receptor antagonist), 50µM AP5 ((2R)-amino-5-phosphonovaleric acid; (2R)-amino-5-phosphonopentanoate, a NMDA channel blocker) and 1µM TTX (Tetrodotoxin, an action potential blocker).

3.2.21 DIG-labeling for *in situ* hybridization

In this study all the plasmids were from previous studies of the Molecular Eye Development group, the DIG mix was from Roche and the labeling procedure was done as previously decribed (Schaeren-Wiemers *et al.*, 1993).

As for every gene the template was constructed under either T7 or SP6 promoter with different restriction enzyme sites, I made the template for DIG labeling with 3µg DNA and digested it with the corresponding restriction enzyme. The mixture was incubated for 2 hours and digestion efficiency was checked by gel electrophoresis.

The digested DNA samples were transcribed with DIG mix, respective polymerase, RNA inhibitor and buffers in 37℃ for 2 hours. Fina lly, DNA was digested with 2µl DNase I for 15 min.

80µl TE, 10µl 5M LiCl and 300µl 100% ethanol were added to the transcription product to precipitate the RNA probes in -20℃ for 1 hour. Then I spined down the RNA probes for 20-25min at 10000 x g and 4℃. Then, the supernatant was discarded, and 200µl 75% ethanol was added, the mixture was centrifuged at 13000 x g for 15min. The pellet was collected and dissolved in 100µl TE, and RNA concentration was measured, the RNA was stored at -80 for long-term use.

3.2.22 *In situ* hybridization

In situ hybridization was performed in a close and clear environment to avoid the degradation of RNA. Cryosections were used for it. I followed a widely used protocol (Schaeren-Wiemers *et al.*, 1993; Giger et al., 1996; Pasterkamp *et al.*, 1999).

Slices were fixed for 20 min in 4% Paraformaldehyde in PBS (pH 7.4) and washed in PBS 3 times for 5 minutes. They were rinsed in MilliQ-H_2O for 5 min, followed by 10 min acetylation in 0.25% acetic anhydride. Then, cubes were washed in PBS.5 min and in 2x SSC (5 min).

Slices were incubated for 2 hours in hybridization solution (150µl/slide) covered with Nescofilm in a humidified chamber at room temperature.

200 ng /ml cRNA probe (sense or antisense) were added to hybridization solution on ice and the mixture was incubated for 5 min. 150 µl hybridization mixtures were added on each slices. Slides were hybridized overnight at 60 ℃ covered with Nescofilm in a humidified chamber.

The slices were washed in 5x SSC at 60 ℃ for 5 min , following with 1 min washing in 2x SSC at 60℃, 30 min washing in 0.2x SSC in 50% f ormamide (reuse this solution) at 60℃ and 5 min washing in 0.2x SSC at room tempe rature.

The slices from last step were washed in buffer 1 for 5 min and 1 h blocked in 1% blocking reagent in buffer 1 for 1 hour. Then, the slices were processed with 5 min washing in buffer 1 and 2 hours anti-DIG-AP Fab antibody incubation in a humidified chamber. Afterwards, the slices were washed twice in buffer 1 for 15 min, and 5 min wash once in buffer 2.

Slide colour solution was applied to slices for 1 h- 48 h within a humidified chamber. Then the colour reactions were stopped by washing in TE buffer for 10 min. The slices were dehydrated and mounted in aqueous mounting media.

3.2.23 Golgi staining

For Golgi staining, a kit "FD Rapid GolgiStain" was used. The mouse brains from wild type and *O377* were freshly prepared. Solutions A, B, C, D and E were from the kit. I followed the protocol from the kit:

Mouse brain was cut into two equal hemispheres. Brian hemispheres were immersed in a fixative, which was made up by mixing equal volumes of solution A and B and stored at room temperature overnight. The solution was replaced after 12 hours of immersion and stored at the room temperature for 2 weeks. Then brain hemispheres were transferred into Solution C and stored at room temperature for 4 days in the dark. Solution was replaced after 12 hours of immersion.

To avoid ice crystal damage, tissues were frozen rapidly in isopentane (isopentane

was precooled to -80℃) before sectioning. Sections of 80μm thickness were cut slowly on microtome with the chamber temperature set at -22℃. Each section should then be transferred with a glass specimen retriever and mounted with Solution C on slides. Then sections were air-dried at room temperature.

Sections were rinsed 2 times in distilled water, 2 minutes each. Then sections were washed in a mixture consisting of 1 part of Solution D, 1 part of Solution E and 2 parts of MilliQ water for 10 minutes. Afterwards, the slices were rinsed in distilled water 2 times, 4 minutes each (distilled water should be renewed frequently). The slices were dehydrated in 50%, 75% and 95% ethanol, 5 minutes each. The dehydrated sections were put 4 times in absolute ethanol, 4 minutes each, and cleared in xylene, 3 times, 5minutes each. All the sections were covered with coverslips in mounting medium.

4. Results

4.1 Hippocampal structure abnormality in the *O377* mutant

To investigate whether mutations in *O377* and *Philly* lead to changes in hippocampal structure, we performed crystal violet staining. To further analyse the difference in hippocampal structure, we also measured the hippocampal volumes of wild type, *Philly* mice and *O377* mutants.

4.1.1 Hippocampal ventral structural abnormalities in *O377* mutants

Crystal violet staining was used to analyze the differences of hippocampus morphology between 3-month-old *O377* mutants, *Philly* mice and wild type. The staining demonstrated that the ventral hippocampus of *O377* mutant was smaller (Figure 4.1 c4, c5) than wild type (Figure 4.1 a4, a5), while no obvious alteration was observed in the *Philly* mouse.
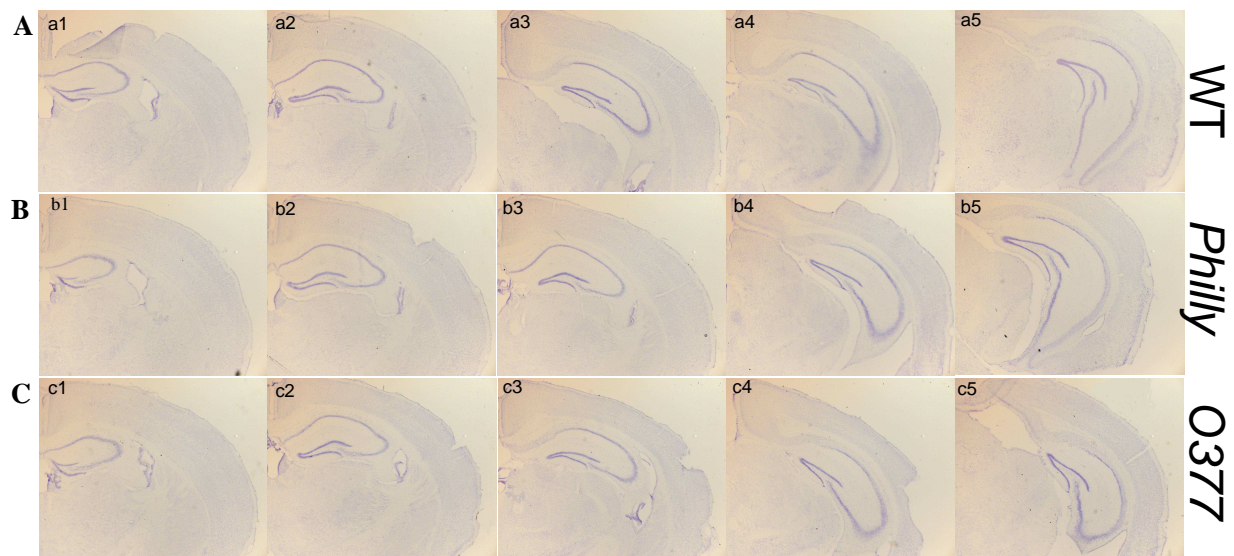
Figure 4.1 Crystal violet staining reveals hippocampal structure abnormality in the *O377* mutant. (A) a1 to a5 show from dorsal to ventral the hippocampal structure of 3-month-old wild type mice. (B) b1 to b5 show from dorsal to ventral the hippocampus structure of 3-month-old *Philly* mutant mice. (C) c1 to c5 show from dorsal to ventral the hippocampus structure of 3-month-old *O377* mutant mice.

4.1.2 Hippocampal volume reduction in *O377* mutants

To quantify the change in hippocampus of *O377* mice and *Philly* mice compared with wild-type mice at the age of 1-month and 3 month, crystal violet staining was used, and CA volume, dentate gyrus volume and whole hippocampus volume were determined (Table 4.1). In the *Philly* mutants, volumes of all regions of interest were

not significantly changed compared with the wild type. However, dentate gyrus volume of *O377* mutants was significantly smaller in comparison with wild type by 14.8% and 17.5% in mice at the age of one-month and 3-month respectively (Figure 4.2 B). CA volume decreased 12.2% and 17.1 % in one-month and 3-month *O377* mutant compared with wild-type separately (Figure 4.2 D), while the hippocampal volume decreased 18.4 % and 19.2% in one-month-old and 3-month-old *O377* mutants respectively (Figure 4.2 F).
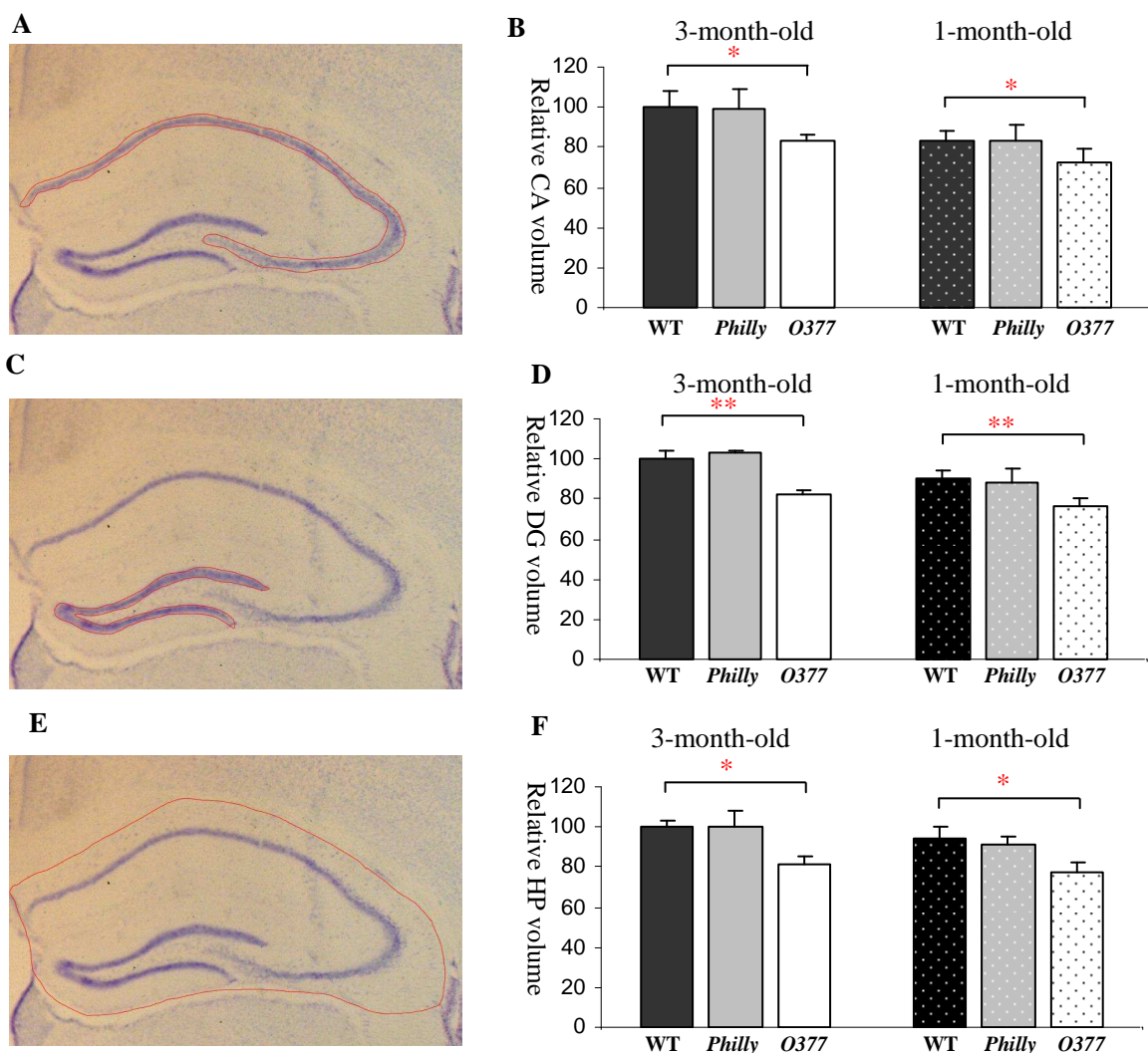
Figure 4.2 CA, dentate gyrus and hippocampus volumes reduction at one-month-old and 3-month-old *O377*. (A, C, E) Areas of interest are selected by Stereo Investigator when measured the volume of CA (A), dentate gyrus (C) and hippocampus (E). (B, D, F) Normalized CA (B), dentate gyrus (D) and hippocampus (F) volume. In each group, 3-month-old wild-type volume =100 (*$0.001 < P < 0.05$, ** $P < 0.001$, T-test, n=4-6). Err bar= ± standard deviation.

Table 4.1 CA, hippocampus (HP) and dentate gyrus (DG) volume (mm^3) in 3-month-old and one-month-old wild type and O377 mice

1-month-oldg	CA Volume	Dentate gyrus Volume	Hippocampus Volume
W T	1.115±0.061	0.489±0.021	12.578±0.757
Philly	1.108±0.106	0.481±0.034	12.184±0.536
O377	0.973±0.091	0.416±0.020	10.264±0.701
3-month-old	CA Volume	Dentate gyrus Volume	Hippocampus Volume
W T	1.336±0.110	0.543 ±0.023	13.339±0.407
Philly	1.328±0.133	0.558±0.008	13.346±1.033
O377	1.107±0.052	0.448±0.009	10.792±0.557

4.2 *Crybb2* is expressed in the brain

From the hippocampal structure analysis, *O377* mutants show significant differences compared with wild type, while *Philly* mouse show no significant difference. Therefore, we focus in the following chapters on the *O377* mutant.

4.2.1 *Crybb2* is expressed at different ages of the mouse brain

Crybb2 expression in mouse brain was analyzed by RT-PCR. To distinguish the different expression levels at different ages, 28 cycles and 32 cycles of RT-PCR were run and glyceraldehyde-3-phosphate dehydrogenase (*Gapdh*) was used to control the quality and equal mount of RNA. In the PCR with 28 cycles, I could detect an expected *Crybb2* band at 640 bp in one-month-old mice and in the positive control (a sequenced *Crybb2* in the pcDNA 3.1 plasmid), but not in other ages and in the negative control (Figure 4.3 A). In all groups, I could detect the *Gapdh* band at 1002 bp (Figure 4.3 A). In the PCR with 32 cycles, we could detect *Crybb2* in the positive control, all ages of wild type and *O377* mutants (Figure 4.3 B). These results indicate that *Crybb2* is expressed in the wild-type and *O377* mutants hippocampus from E14.5 to P30 and its expression reaches maximum at P30 within those ages.

A

B
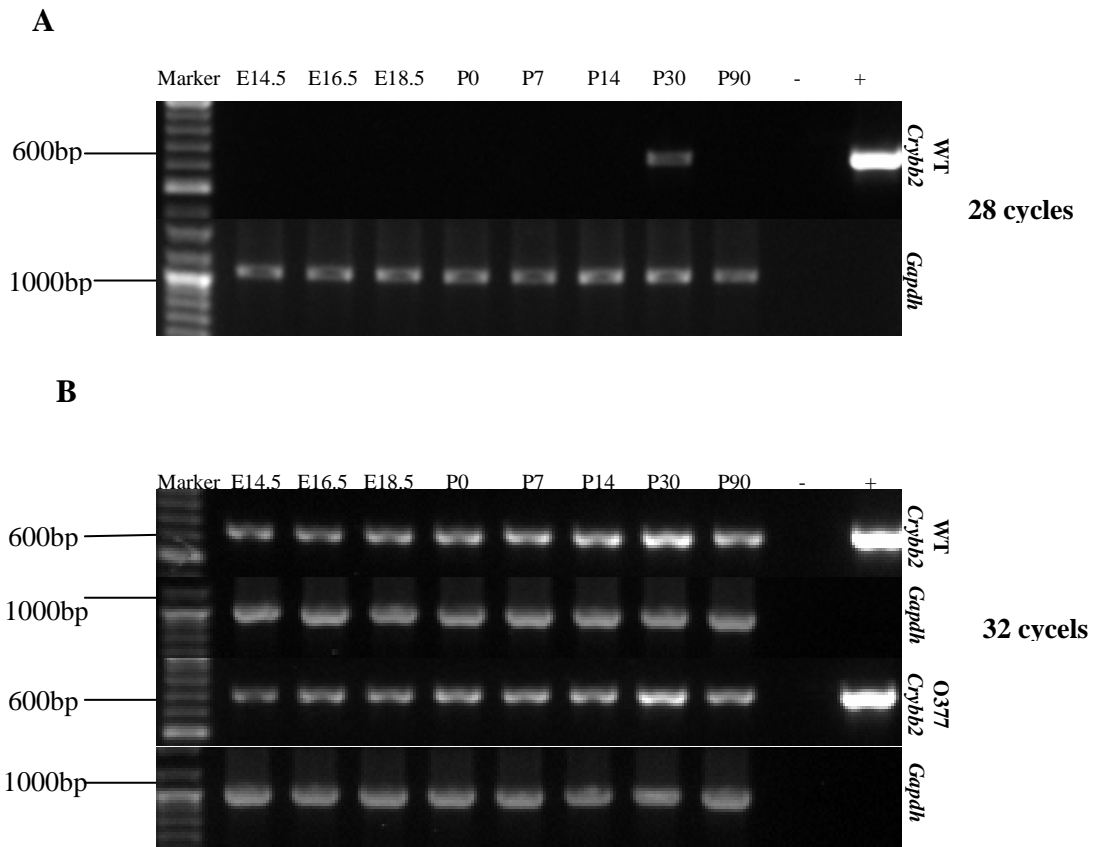
Figures 4.3 *Crybb2* was detected at different ages in mouse brain by RT-PCR. (A) RT-PCR was run for 28 cycles for detection of wild type *Crybb2* and *Gapdh* with a positive control (+) and negative control (-) **(B)** RT-PCR also was run with 32 cycles for detection of wild-type and O377 mutant *Crybb2* with a positive control (+) and negative control (-) and *Gapdh*.

4.2.2 *Crybb2* is expressed in different regions of 3-month-old wild-type and *O377* mutant brain

In situ hybridization was performed with 3-month-old wild type and *O377* mutant brains. The result demonstrated that *Crybb2* was expressed in Purkinje cells (PKC) and granular cells (GC) of cerebellum (Figure 4.4 B, B'); all layers of the cerebral cortex (Figure 4.4 C, C'); in CA1, CA2, CA3 and in the dentate gyrus of the hippocampus (Figure 4.4 D, D'); in the glomerular layer (GL), the mitral cell layer (MCL) and in the granule cell (GCO) of the olfactory bulb (Figure 4.4 E, E'). The expression pattern of 3-month-old wild type is similar to *O377* mutant. It indicates the expression pattern is not altered by the mutation.
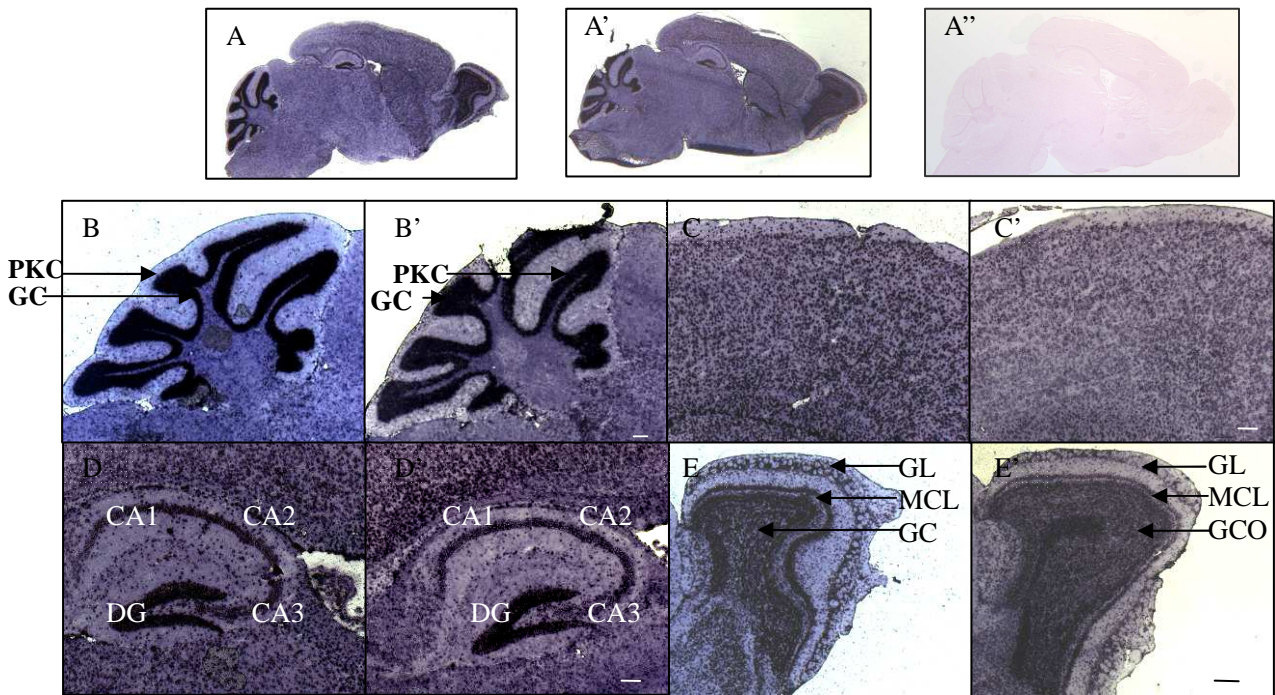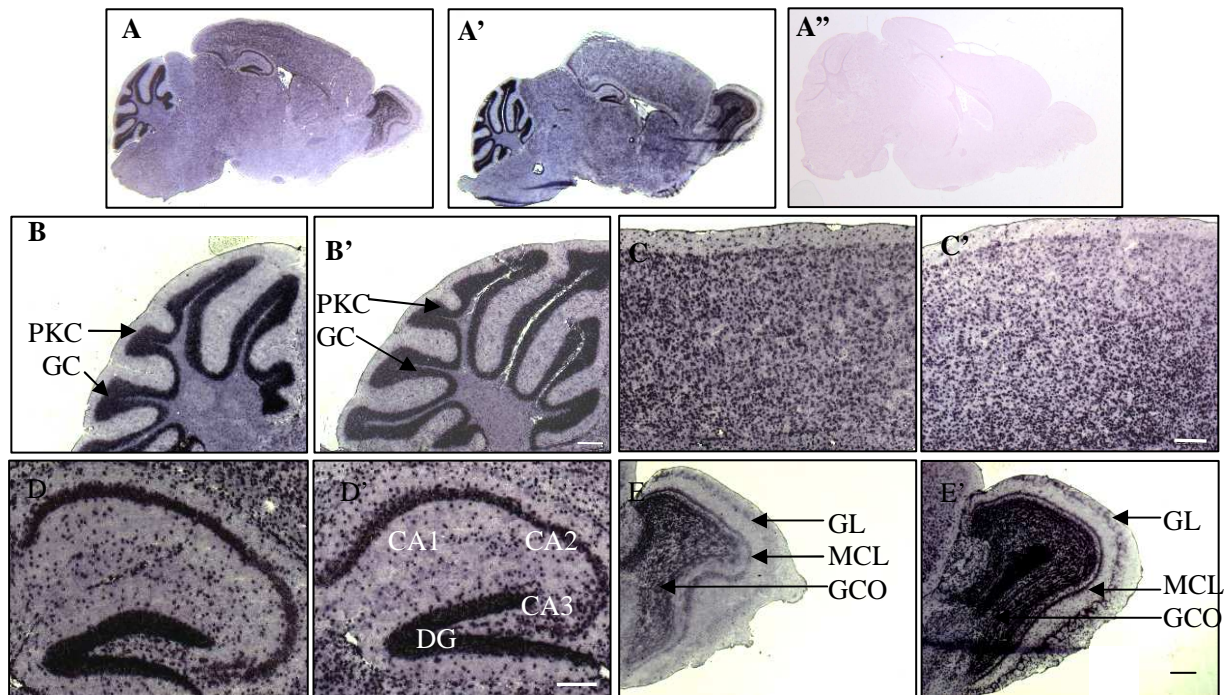
Fig 4.4 *Crybb2* is expressed in 3-month-old wild-type and *O377* mutant brain. *In situ* hybridization illustrate that *Crybb2* is expressed in different areas of the brain at wild type (A) and O377 (A'), including the Purkinje cells (PKC) and the granular cells (GC) of the cerebellum (B, B'); all layers of the cerebral cortex (C, C'); the CA1, CA2, CA3 and the dentate gyrus (DG) of the hippocampus (D, D'); the glomerular layer (GL), the mitral cell layer (MCL) and the granule cells of olfactory bulb (GCO) (E, E'). No staining is observed in the sense control (A''). Scale bar: 50µm.

4.3 Genes of interest are expressed in the brain

Capn3, *Cr536618* and *Tmsb4* were selected for further analysis based on previous results from expression arrays (for more details see chapter 2.2.6). In this chapter, we manily focus on the expression patern and expression stage of these genes in wild type and *O377* mutants.

4.3.1 *Capn3* is expressed in the brain

In situ hybridization at one-month-old wild type and *O377* mutant brain revealed the expression pattern of *Capn3*. *Capn3* is expressed in Purkinje cells and granular cells of cerebellum (Figure 4.5 B, B'); all layers of the cerebral cortex (Figure 4.5 C, C'); in CA1, CA2, CA3 and the dentate gyrus of the hippocampus (Figure 4.5 D, D') and in the glomerular layer, the mitral cell layer and the granule cell of olfactory bulb (Figure 4.5 E, E') in both wild-type and *O377* mutant brain. Completely overlapping expression patterns of *Capn3* and *Crybb2* indicated that *Capn3* might be functional connected to *Crybb2*.
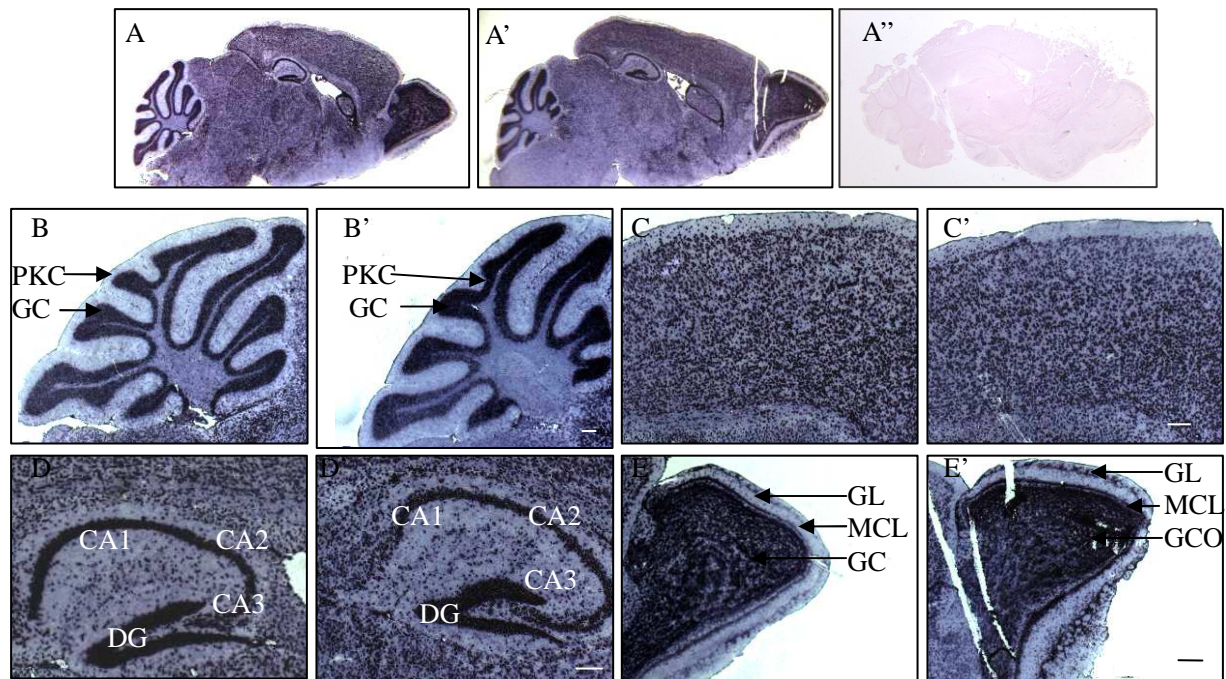
Fig 4.5 *Capn3* is expressed in 1-month-old wild-type and *O377* mutant brain. *In situ* hybridization shows that *Capn3* is is expressed in 1-month-old wild type (A) and O377 (A'), these areas include Purkinje cells (PKC) and granular cells (GC) of cerebellum (B, B'); in all layers of the cerebral cortex (C, C'); CA1, CA2, CA3 and the dentate gyrus (DG) of the hippocampus (D, D') and glomerular layer (GL), in the mitral cell layer (MCL) and the granule cell of the olfactory bulb (GCO) (E, E'). No staining is observed in the sense control (A''). Scale bar: 50μm.

In situ hybridization was also performed at 3-month-old wild-type and *O377* mutant brain sections. *Capn3* expression was detected in Purkinje cells and granular cells of cerebellum (Figure 4.6 B, B'); in all layers of the cerebral cortex (Figure 4.6 C, C'); in CA1, CA2, CA3 and the dentate gyrus of the hippocampus (Figure 4.6 D, D') and in the glomerular layer, the mitral cell layer and the granule cell of the olfactory bulb (Figure 4.6 E, E') in both wild-type and *O377* mutant brain. Expression patterns of *Capn3* in 3-month-old of both wild-type and *O377* mutant brains were almost the same as in 1-month-old wild type and *O377* mutants. This indicates that the *Capn3* expression pattern is not changed from premature stage to mature stage of wild-type and *O377* mutant brain. Eventhough, in some cases, differences in the intensity of *in situ* hybridization of *Capn3* could be observed in *O377* mutants compared with wild type (like Figure 4.6 C, 4.6 C'), the changes in the intensity of *in situ* hybridization is not constant. The unconstant staining of *in situ* hybridization may be caused by unstable experimental environment and different handling from time to time.

Fig 4.6 **Capn3 is expressed in 3-month-old wild type and *O377* mutant brain.** *In situ* hybridization illustrates that *Capn3* is expressed in different areas of the brain at 3-month-old wild type (A) and O377 (A'): these areas include the Purkinje cells (PKC) and the granular cells (GC) of the cerebellum (B, B'); all layers of the cerebral cortex (C, C'); CA1, CA2, CA3 and the dentate gyrus (DG) of the hippocampus (D, D'); the glomerular layer (GL), the mitral cell layer (MCL) and the granule cell of the olfactory bulb (GCO) (E, E'). No staining is observed in the sense control (A''). Scale bar: 50μm

Capn3 is expressed in different developmental stage of the brain

As we know from the *in situ* hybridization, *Capn3* is widely expressed in mouse brain, predominantly in hippocampus. Therefore, we detected the expression of *Capn3* in every stage of hippocampal development until mature by RT-PCR, *Gapdh* was used as internal control. *Capn3* was expressed in the hippocampus of wild type (Figure 4.7 A) and *O377* mutants (Figure 4.7 B) from E14.5 to P90. In addition, Judging from the intensity of band of wild-type and *O377* mutant from the electrophoresis, it is hard to tell whether in *O377* mutants *Capn3* expression is higher compared with wild type in different stages.

A

B
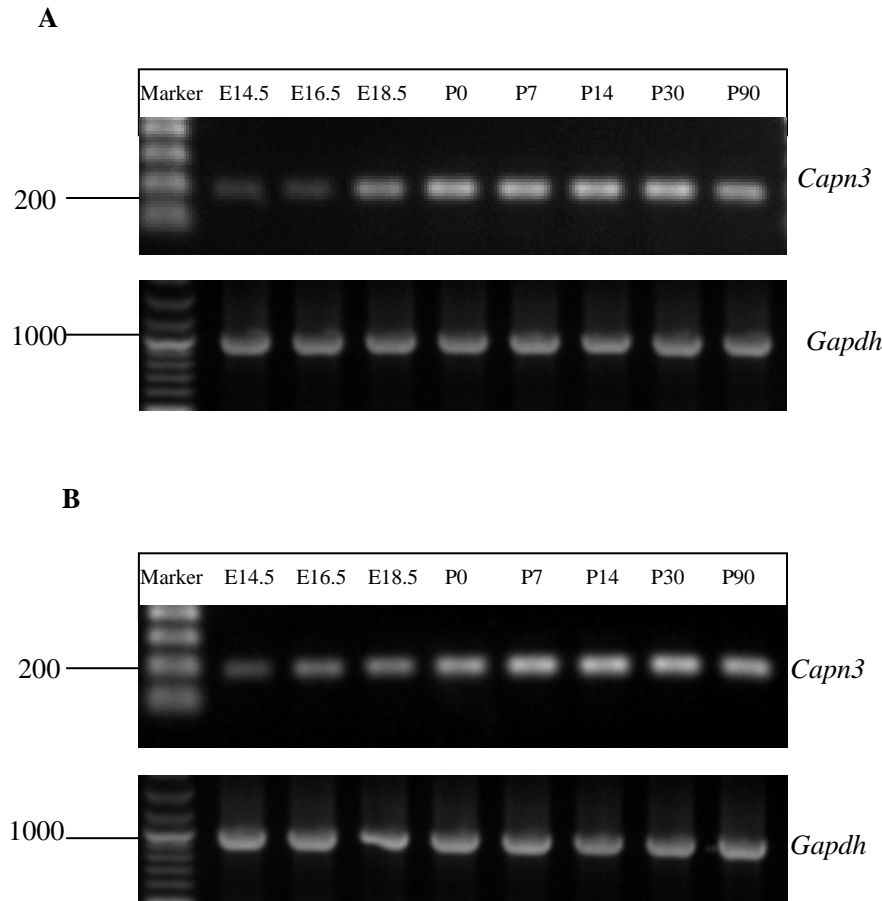
Fig 4.7 *Capn3* **is expressed at different ages of wild-type and** *O377* **hippocampus**. (A-B) *Capn3* is detected by RT-PCR in hippocampus of wild-type (A) and *O377* (B) at different ages together with *Gapdh* as loading control.

4.3.2 *Tmsb4x* is widely expressed in the brain

In situ hybridization was performed at 3-month-old wild-type and *O377* mutant brain sagittal sections. *Tmsb4x* was found to be expressed in Purkinje cells and granular cells of cerebellum (Figure 4.8 B, B'); in all layers of the cerebral cortex (Figure 4.8 C, C'); CA1,CA2,CA3 and the dentate gyrus of the hippocampus (Figure 4.8 D, D'); in the glomerular layer, the mitral cell layer and the granule cell of the olfactory bulb (Figure 4.8 E, E'); the rostral migratory stream (Figure 4.8 F, F') in both wild-type and *O377* mutant brain. The expression pattern of *Tmsb4x* in *O377* mutants was not altered compared with wild type. However, obvious higher expression of *Tmsb4x* was constantly detected in all the regions of interest at *O377* mutants (Figure 4.8 B'-F') compared with wild type (Figure 4.8 B-F). The expression pattern of *Tmsb4x* overlapped with expression pattern of *Crybb2* and up-regulation of *Tmsb4x* in *O377* mutants, indicating that *Tmsb4x* may be functional related to *Crybb2*.
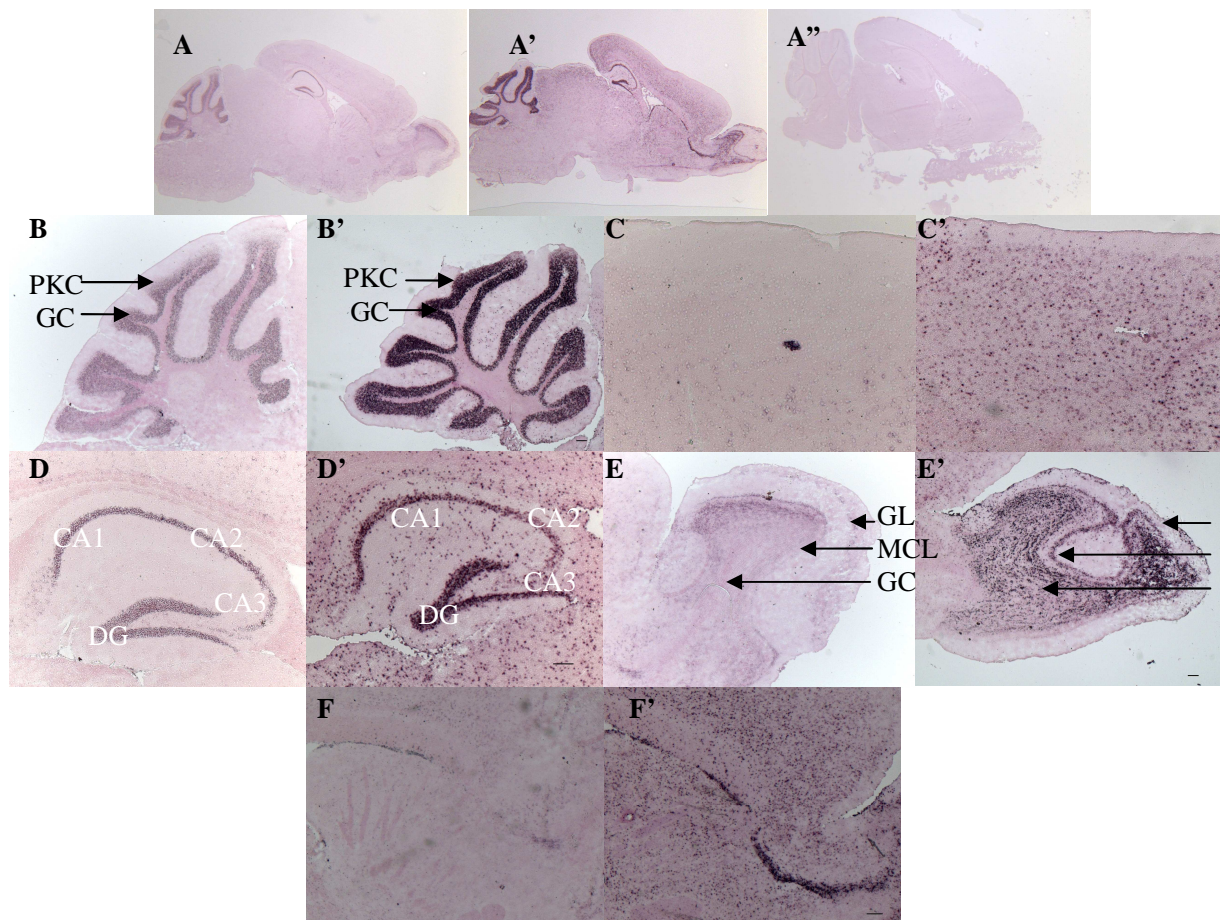
Figure 4.8 *Tmsb4x* is up regulated in 3-month-old *O377* brain. *In situ* hybridization shows that *Tmsb4x* is expressed in the brain of 3 month old wild type (A) and O377 (A'), and *Tmsb4x* is up regulated in all the region of *Tmsb4x* expressed. Those areas include Purkinje cells (PKC) of cerebellum (B, B'); all layers of cerebral cortex (C, C'); CA1, CA2, CA3 and dentate gyrus (DG) of hippocampus (D, D'); glomerular layer (GL), mitral cell layer (MCL) and granule cell of olfactory bulb (GCO) (E, E'); rostral migratory stream (F, F') in wild type (B, C, D, E, F) and O377 (B', C', D', E', F'). No staining is observed in the sense control (A"). Scale bar, 50µm.

Tmsb4x is expressed in different developmental stage of the brain

As we know from the in situ hybridization, *Tmsb4x* is widely expressed in mouse brain, especially in the hippocampus. Therefore, I also checked the expression of *Tmsb4x* in different stages of hippocampus development by RT-PCR. *Tmsb4x* expression were detected in different stages of wild-type (Figure 4.9 A) and *O377* hippocampus (Figure 4.9 B) with *Gapdh* as a loading control.
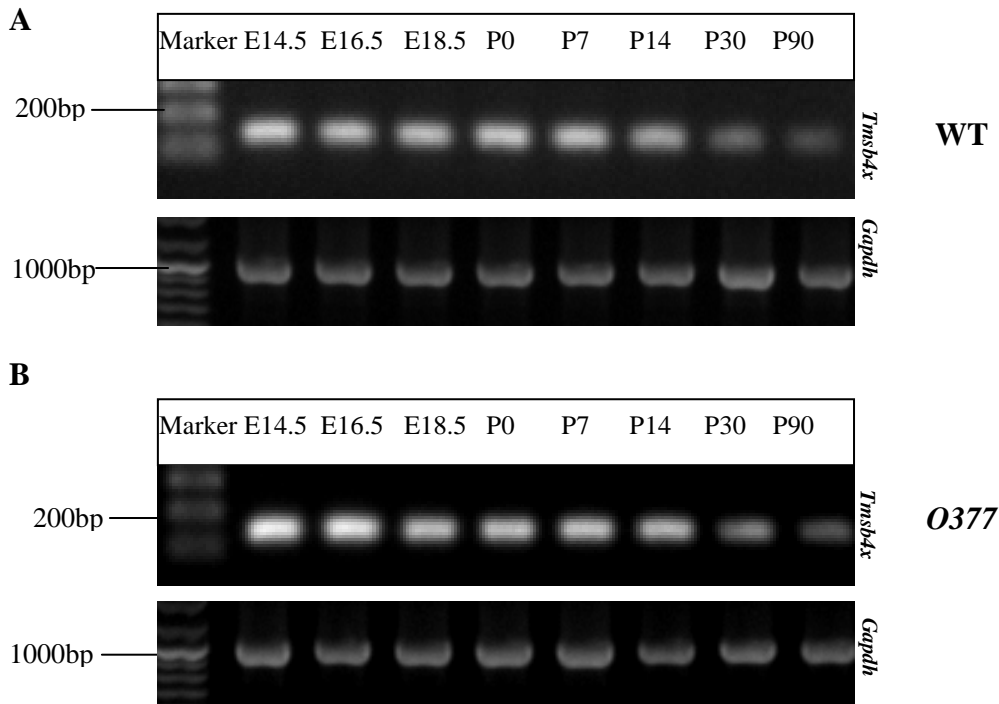
Figures 4.9 *Tmsb4x* is detected at different ages of wild-type and *O377* hippocampus by RT-PCR. RT-PCR for detection of *Tmsb4x* and *Gapdh* in wild-type (Figure 3.1 A) and *O377* hippocampus (B).

4.3.3 *CR536618* is expressed in the brain

In situ hybridization at one-month-old wild-type and *O377* mouse brain sagittal sections revealed the expression pattern of *CR536618*. *CR536618* is expressed in the Purkinje cells and the granular cells of cerebellum (Figure 4.10 B, B'); in all layers of the cerebral cortex (Figure 4.10 C, C'); in CA1, CA2, CA3 and the dentate gyrus of the hippocampus (Figure 4.10 D, D') ; the glomerular layer, the mitral cell layer and the granule cell of olfactory bulb (Figure 4.10 E, E') in both wild-type and *O377* mutant brain.

In situ hybridization was also done at 3-month-old wild-type and *O377* mutant brain sagittal sections. *CR536618* was illustrated to be expressed in Purkinje cells and granular cells of cerebellum (Figure 4.11 B, B'); all layers of cerebral cortex (Figure 4.11 C, C'); CA1,CA2,CA3 and dentate gyrus of hippocampus (Figure 4.11 D, D'); glomerular layer, mitral cell layer and granule cell of olfactory bulb (Figure 4.11 E, E') in both wild-type and *O377* mutant brain (Figure 4.11).

Eventhough, in some cases, differences in the intensity of *in situ* hybridization of *CR536618* could be observed in *O377* mutants compared with wild type (like Figure 4.10 E vs 4.10 E' and Figure 4.11 E vs 4.10 E'), the changes in the intensity of *in*

situ hybridization is not constant. The unconstant stainings of *in situ* hybridization are most likely caused by unstable experimental environment and different handling from time to time.
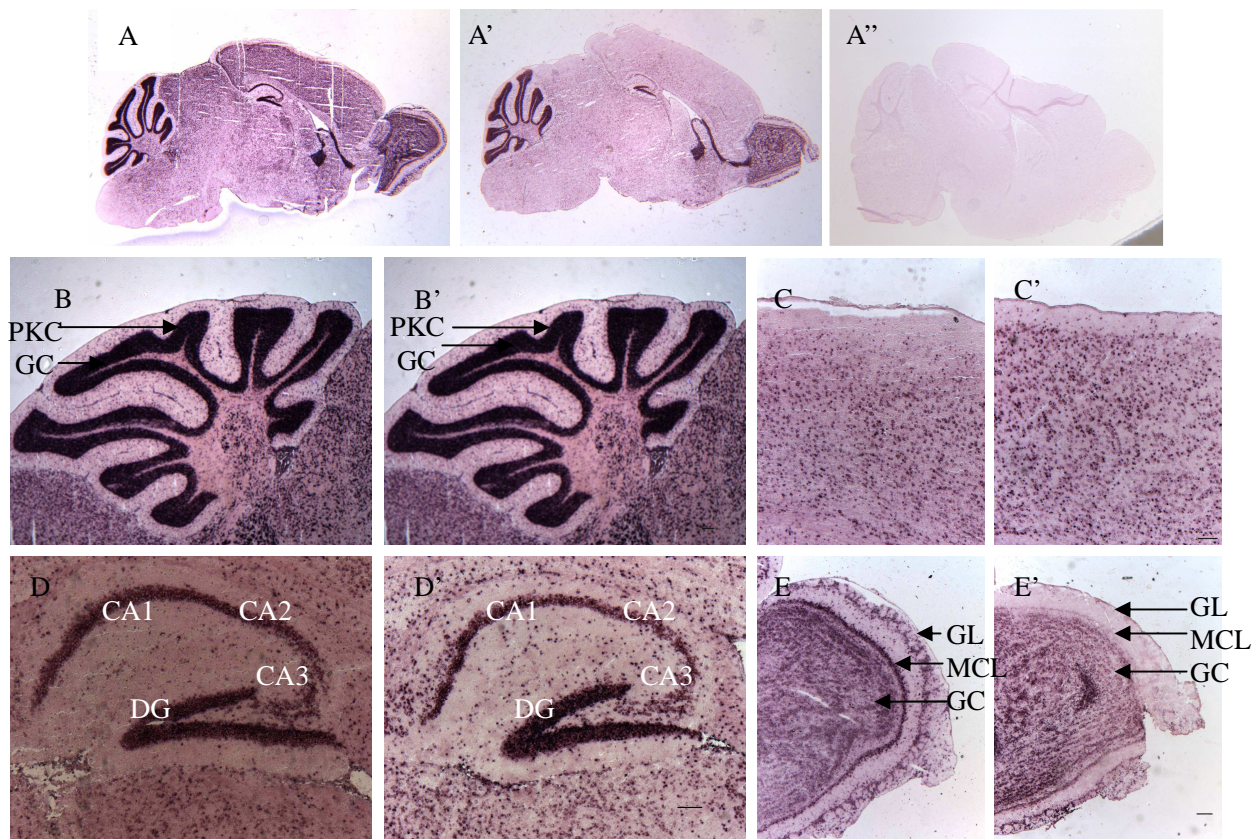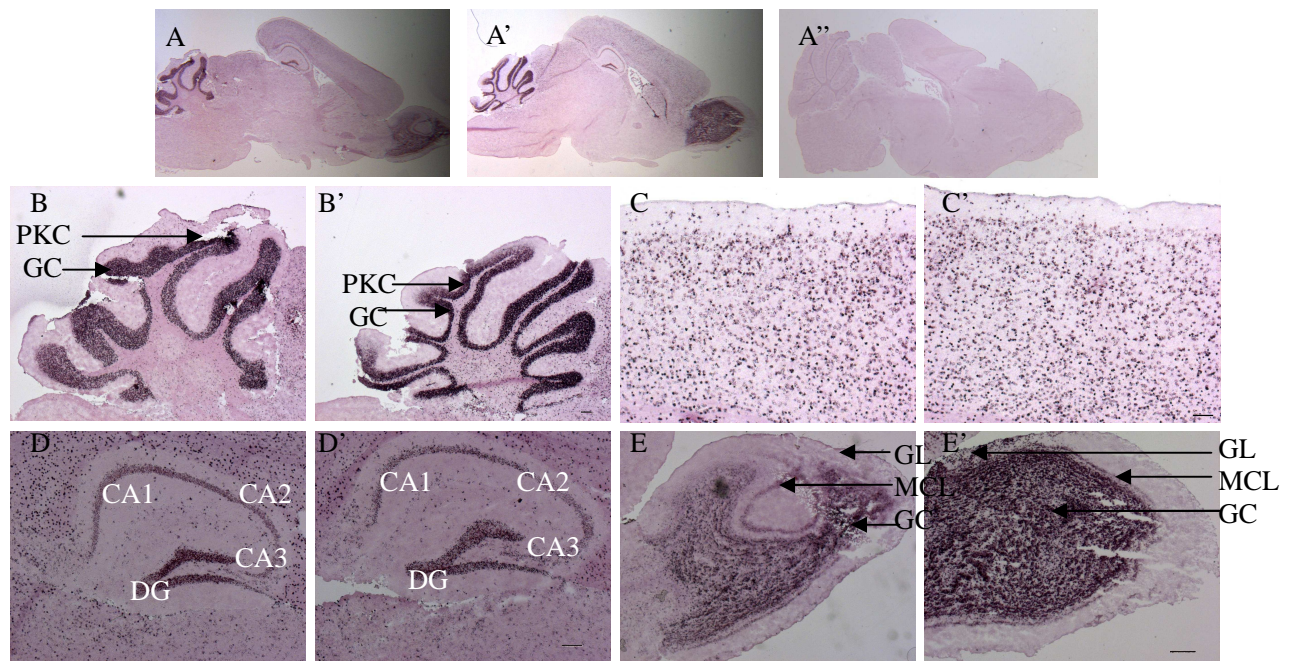

Figure 4.10 *CR536618* is expressed in 1-month-old wild type and *O377* brain. *In situ* hybridization shows that *CR536618* is widely expressed in 1-month-old wild-type (A) and O377 brain (A'), including in the Purkinje cells (PKC) and the granular cells (GC) of the cerebellum (B,B'); in all layers of the cerebral cortex(C,C'); in CA1, CA2, CA3 and the dentate gyrus of hippocampus (D,D'); the glomerular layer (GL), the mitral cell layer (MCL) and the granule cell (GC) of the olfactory bulb (GCO) (E,E') in wild type (B, C, D, E, F) and O377 (B', C', D', E', F'). No staining is observed in the sense control (A''). Scale bar, 50μm.

The expression patterns of *Capn3*, *Tmsb4x and CR536618* in wild-type and *O377* mutants were very similar to the expression pattern of *Crybb2*, suggesting that these genes may be functionally related to *Crybb2.* By *in situ* hybridization, the expression pattern of *Tmsb4x* is not altered in *O377* mutants compared with wild type, while the expression level was found to be obviously increased. In addition, the expression pattern of *Capn3 and CR536618* is not changed in *O377* mutants compared with wild type. No major difference in the intensity of *in situ* hybridization of *Capn3* and *CR536618* was observed in *O377* mutants compared with wild type. To verify the

expression level of *Capn3* and *CR536618* in *O377* mutants compared with wild type, we need to perform quantitative real-time PCR.

Figure 4.11 *CR536618* is expressed in 3-month-old wild-type and *O377* brain. *In situ* hybridization shows that *CR536618* is expressed in 3-month-old wild-type (A) and *O377* brain (A'). These area include the Purkinje cells (PKC) and the granular cells (GC) of the cerebellum (B, B'); all layers of the cerebral cortex (C,C'); CA1, CA2, CA3 and the dentate gyrus of the hippocampus (D, D'); the glomerular layer (GL), the mitral cell layer (MCL) and the granule cell (GCO) of the olfactory bulb (E, E') in wild type (B, C, D, E, F) and O377 (B', C', D', E', F'). No staining is observed in the sense control (A''). Scale bar, 50µm.

4.4 Calcium homeostasis is altered in *O377* mutants

The calcium binding ability of βB2-crystallin is still under discussion, therefore, it would be very interesting to determine the calcium binding ability of βB2-crystallin. It would be also very interesting for me to know if the mutation in *O377* will lead to alteration of calcium homeostasis in hippocampal neurons.

4.4.1 Alteration and shift in heteronuclear single quantum correlation spectra suggesting calcium binding of βB2-crystallin

Wild-type and mutant *Crybb2* were cloned in expression vectors pETM11 with a 6**x** His-tag and a Tobacco Etch Virus protease cleavage site (TEV) (for more details see chapter 3.2.10). Wild-type and mutant *Crybb2* were over-expressed as recombinant proteins in *E.coli*. Unfortunately, the expressed mutant proteins was completely

insolubly (Figure 4.12 A). Mutant protein was denatured by 8M urea in PBS, but it could not be refolded, eventhough many buffer conditions were screened (Table 4.2). However, wild-type βB2-crystallin recombinant protein was soluble purified. The His-tag of βB2-crystallin was removed by Tobacco Etch Virus (TEV) protease and further purified on the second Ni-column (Figure 4.12 B).
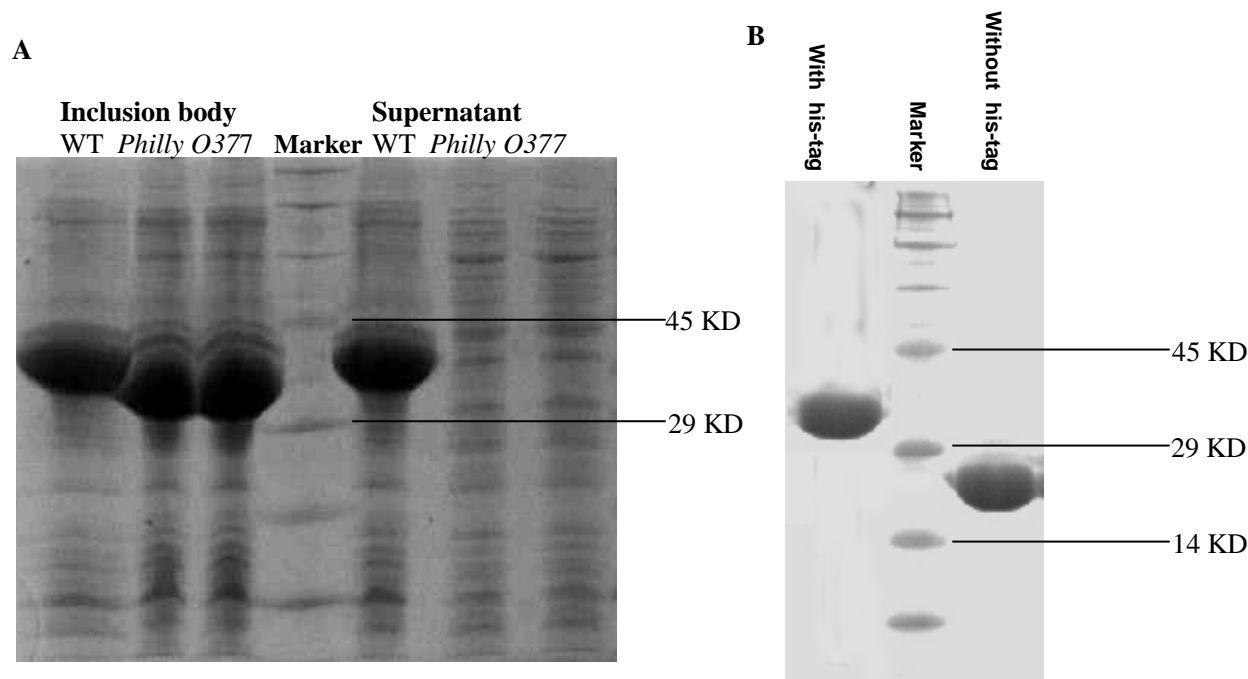
Figure 4.12 Purification of βB2-crystallin proteins (A) Plasmid construction for protein purification. (B) *Philly* and *O377* mutant protein was expressed completely in inclusion body but wild-type protein was expressed in both inclusion body and supernatant. (C) Purified wild type protein with His-tag or without His-tag after digestion with Tobacco Etch Virus protease.

Table 4.2 Buffers used for protein soluble. In the table A= 0.1 M NaAC; B=0.1 M Na2HPO4; C= 0.1 M Hepes; D= 0.1 M Tris; a1= 0.1 M NaCl; a2= 0.1 M NaCl+10% Glycerol; a3= 0.5 M NaCl; b1= 0.1 M Na2SO4; b2= 0.1 M Na2SO4+10% Glycerol; b3= 0.5 M Na2SO4; c1= 0.1 M NaAC; c2= 0.1 M Na2AC+10% Glycerol; c3= 0.5 M Na2AC; d1= 0.1 M (NH4)2SO4; d2= 0.1 M (NH4)2SO4+10% Glycerol; d3= 0.5 M(NH4)2SO4.

PH=4.5	A +a1	A +a2	A +a3	A +b1	A +b2	A +b3	A +c1	A +c2	A +c3	A +d1	A +d2	A +d3
PH=5.0	A +a1	A +a2	A +a3	A +b1	A +b2	A +b3	A +c1	A +c2	A +c3	A +d1	A +d2	A +d3
PH=5.5	A +a1	A +a2	A +a3	A +b1	A +b2	A +b3	A +c1	A +c2	A +c3	A +d1	A +d2	A +d3
PH=6.0	B +a1	B +a2	B +a3	B +b1	B +b2	B +b3	B +c1	B +c2	B +c3	B +d1	B +d2	B +d3
PH=6.5	B +a1	B +a2	B +a3	B +b1	B +b2	B +b3	B +c1	B +c2	B +c3	B +d1	B +d2	B +d3
PH=7.0	C +a1	C +a2	C +a3	C +b1	C +b2	C +b3	C +c1	C +c2	C +c3	C +d1	C +d2	C +d3
PH=7.5	D +a1	D +a2	D +a3	D +b1	D +b2	D +b3	D +c1	D +c2	D +c3	D +d1	D +d2	D +d3
PH=8.5	D +a1	D +a2	D +a3	D +b1	D +b2	D +b3	D +c1	D +c2	D +c3	D +d1	D +d2	D +d3

Without purified mutant protein, I was not able to compare the calcium binding ability of wild-type and mutant protein. However, it is still very interesting to confirm the previous reports that βB2-crystallin have calcium binding ability (Jobby *et al.*, 2006). Therefore, I performed ^{1}H, ^{15}N heteronuclear single quantum correlation (HSQC) NMR spectroscopy.
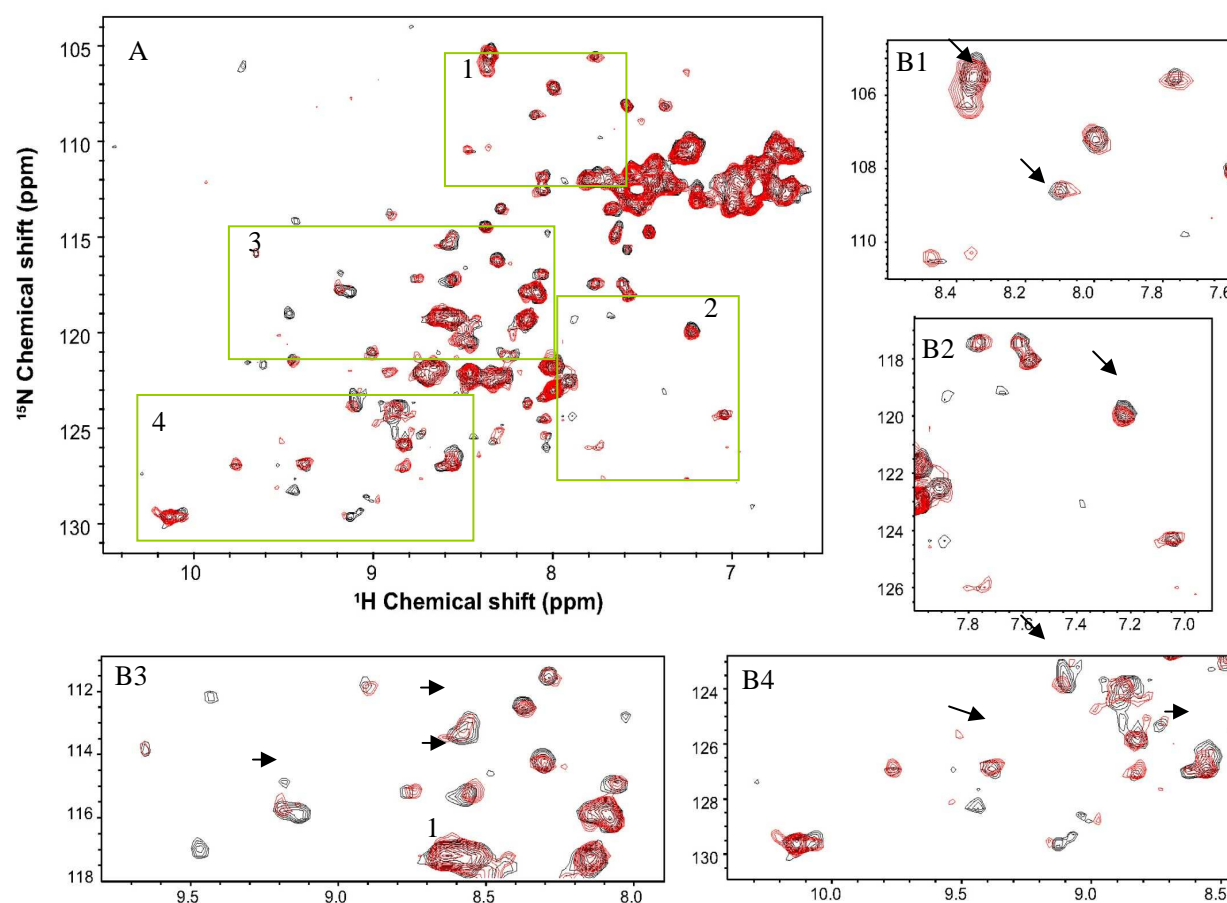
Fig 4.13   2D 15N-1H HSQC spectra. (A) Overview of HSQC spectra without calcium (black colored contours) and calcium-saturated ^{15}N-labelled βB2-crystallin (red colored contours). (B1, B2, B3, B4) Detail view of selected areas of 1, 2, 3, 4 in A. Arrows indicate shifts.

Each cross peak in the ^{1}H, ^{15}N (HSQC) NMR spectrum of a protein represents an amide group of the amino acids in the protein. Shift in these cross peaks upon ligand binding is an indication of changes in the microenvironment of this residue. We used

this technique to determine the changes in ^{1}H, ^{15}N HSQC spectra of the βb2-crystallin caused by calcium binding (Fig 4.13). To investigte the shift in the cross peaks after calcium binding of the protein, two spectra, free calcium and calcium-saturated, were recorded and overlapped for comparison. The overall spectral quality was very poor suggesting that the protein is not well-behaved under the conditions used, although signals observed suggest that there is a fraction of folded protein in the NMR sample. A few shifts were observed in the spectra of calcium saturated protein compared with spectra of free calcium protein. This may suggest calcium binding of βB2-crystallin (Figure 4.13). Similar NMR spectra have been reported previously (Jobby *et al.*, 2006).

4.4.2 Calcium concentration is increased in *O377* mutant hippocampus

The hippocampal neurons from E17.5-E18.5 wild-type and *O377* mutant mice were isolated and stained with the calcium sensitive dye, Fura-3PE. NMDA was used to open the NMDA receptor to influx calcium ions from environment to cell cytoplasm, while Thapsigargin were used to block the ability of the cell to pump calcium into the endoplasmic reticula and allow an influx of calcium into the cytosol.

Relative calcium concentrations at different stages were recorded by calcium spectrometry (Figure 14A). The basal calcium (Ca^{2+} basal) concentration in *O377* (129.62±13.526nM) is significantly increased compared with wild type (81.01±11.56nM). After stimulation with NMDA, the increase in calcium concentration of *O377* hippocampal neurons (13.56±2.47nM) was significantly higher than in wild type (7.20±1.21nM). However, the calcium concentration after stimulation by Thapsigargin in *O377* hippocampal neurons (31.11±13.91nM) was not significantly altered compared with wild type (37.75±6.72nM) (Figure 14B). It indicates that the mutation in *Crybb2* leads to an increase in the basal calcium concentration in *O377* hippocampal neurons compared with wild type hippocampal neurons. The increase of calcium concentration after NMDA stimulation suggests that NMDA receptors are functional altered.

A

B
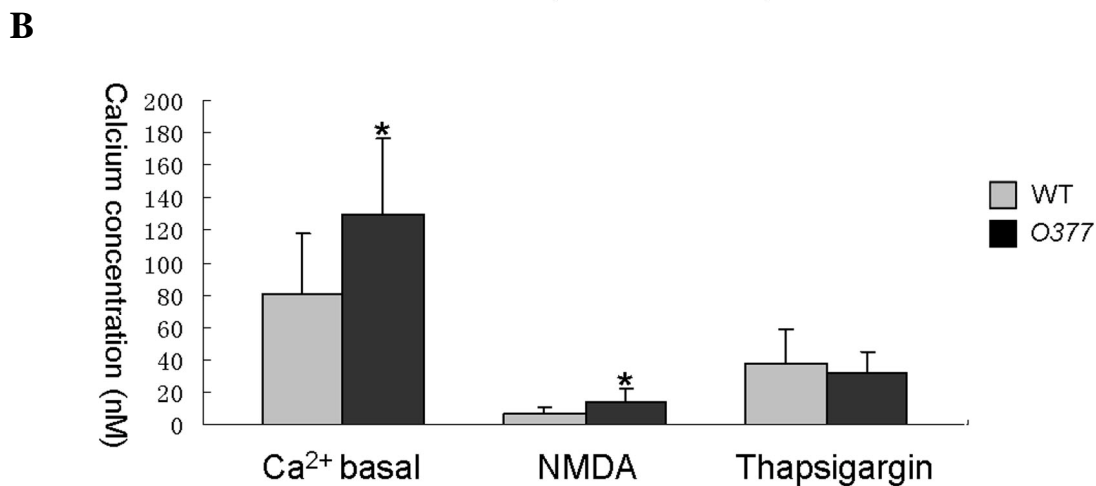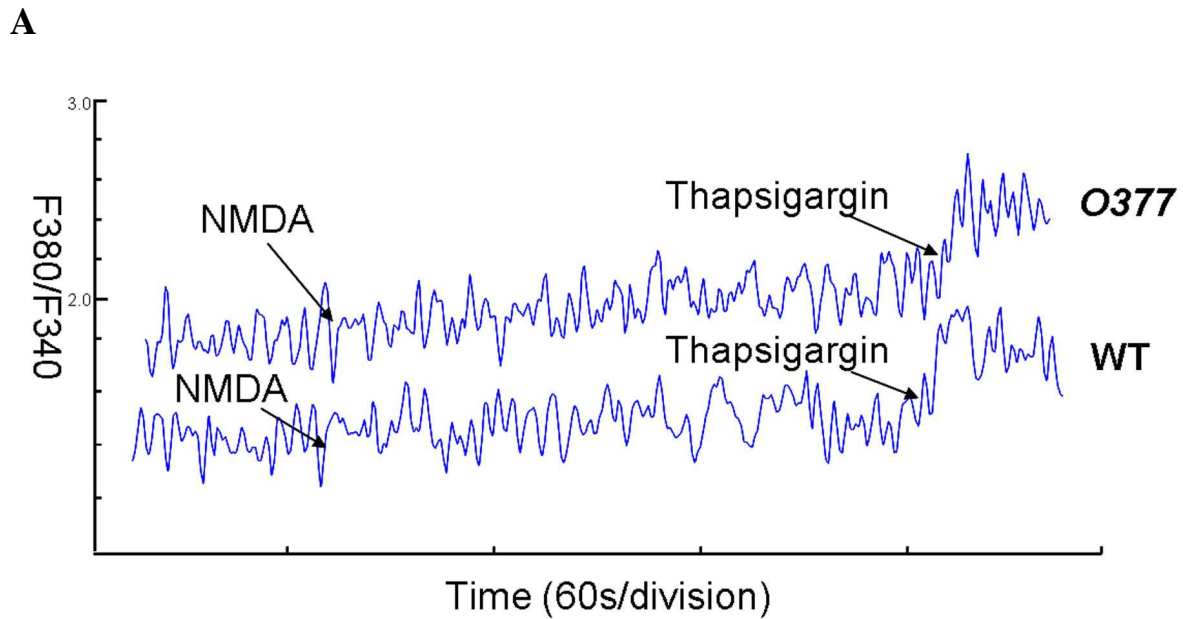
Figure 4.14 Calcium concentration is increased in hippocampal neurons of *O377* mutants. (A) Representative calcium recording in hippocampal neurons of wild type and O377 mutants. (B) Basal Calcium concentration and calcium increase after stimulated by NMDA and Thapsigargin in hippocampal neurons of wild type and *O377* mutants. $P \leq 0.05$, student T-test, $n \geq 10$. Err bar=± SEM. For details of calculation, please see chapter 3.2.17.

4.5 Mutation in *O377* leads to aggregation *in vitro* but not *in vivo*

As the mutant βB2-crystallin expressed in *E.coli* remained insoluble, I also want to know if the mutant in *Crybb2* leads to aggregation *in vitro* and *in vivo*.

4.5.1 Mutant in *Crybb2* leads to aggregation *in vitro*

In order to find out if the mutation in *O377* mutants could lead to aggregation, I over-expressed wild-type and mutant *Crybb2* in RGC-5 Cells. Briefly, the whole cDNA sequence of wild-type and *O377* mutant *Crybb2* without stop codon were cloned and inserted into the pEGFP vector (for more details see chapter 2.2.10). Then pEGFP, p*Crybb2* EGFP and p*Crybb2*^{O377} EGFP were transfected into RGC-5 cells. Shrinked

green protein with cell death was observed in p*Crybb2*^{O377} EGFP transfected RGC-5 cells 48 hours after transfection (Figure 4.15 C), while cells transfected with pEGFP and p*Crybb2* EGFP were nicely expressing EGFP (Figure 4.15 A, C). The shrinked green protein suggests the mutant protein with EGFP tag is aggregated. In addition, almost half of the cells transfected with p*Crybb2*^{O377} EGFP were disattached from the dish 48 hours after transfection, while no dissattched cells could be observed in cells transfected with pEGFP and p*Crybb2* EGFP. It indicates that aggregation in cells will cause the cell death.

Over-expression p*Crybb2*^{O377} EGFP in HEK-293 cells also caused aggregation and cell death (Figure 4.15 F). HEK-293 cells transfected with pEGFP and p*Crybb2* EGFP were expressing EGFP normally as RGC-5 cells transfected with pEGFP and p*Crybb2* EGFP (Figure 4.15 D, E).
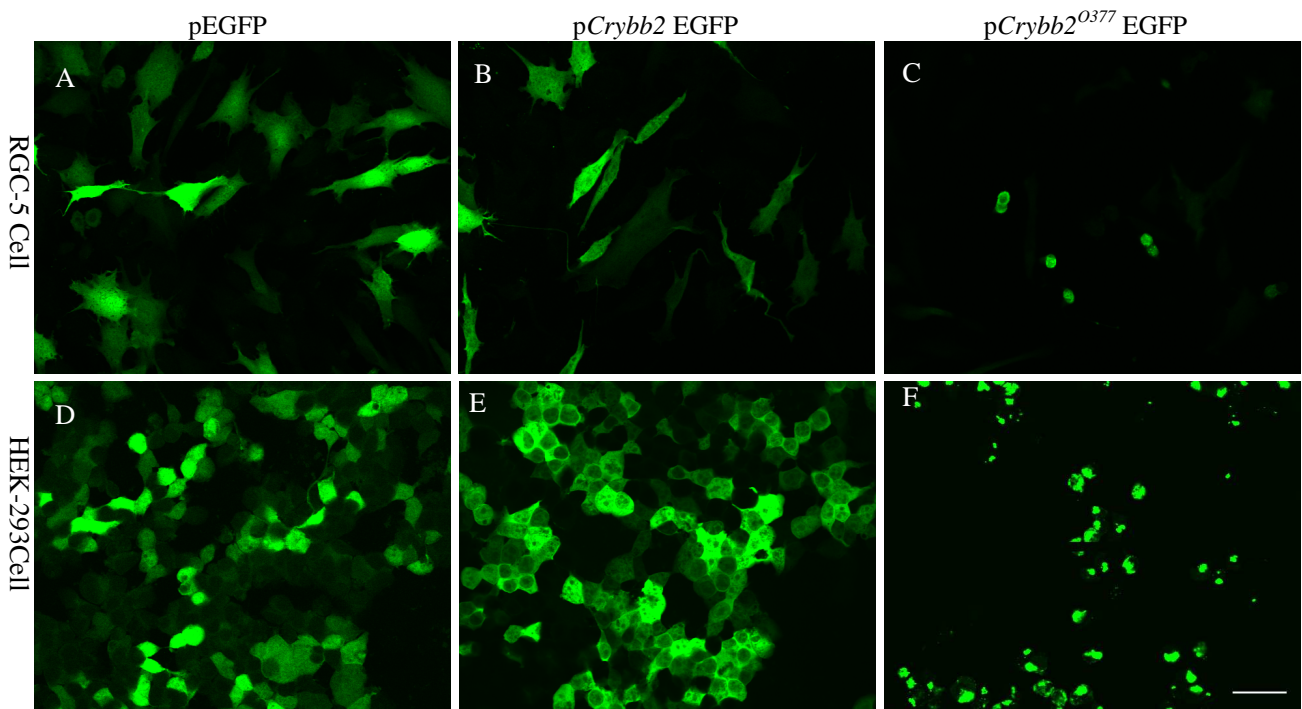
Figure 4.15 Over-expression mutant *Crybb2* in RGC-5 leads to aggregation. (A-C) Representative pictures of RGC5 transfected with pEGFP (A), p*Crybb2* EGFP (B) and p*Crybb2*^{O377} EGFP (C) after 48 hours. (D-F) Representative pictures of HEK-293 cells transfected with pEGFP (D), pCrybb2 EGFP (E) and pCrybb2 $_{O377}$ EGFP (F) after 48 hours. Scale bar, 40μm.

4.5.2 No aggregation is detected at brain area of *O377* mutants

To investigate whether the mutation in O377 also cause aggregation *in vivo*, I performed immunohistochemistry against *Crybb2* (Figure 4.16 A-D)*;* there is no aggregation oberserved in *O377* brain tissue. Hematoxylin and eosin staining was also used to check the aggregation in *O377* mutants. No aggregation was observed

in the *O377* mutants (Figure 4.16 F). However, it is not very certain for us whether there is any inclusion body in the brain of *O377* mutants, as the inclusion body positive tissue is not available.
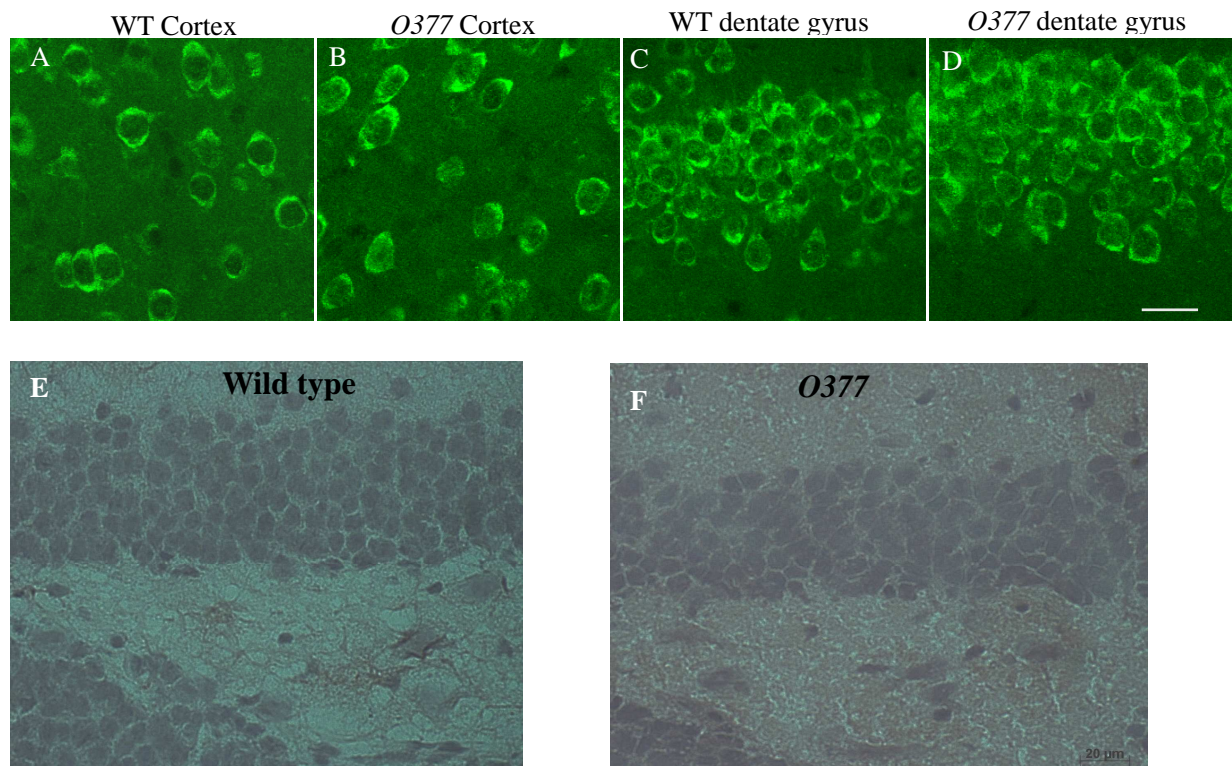
Figure 4.16 No aggregation is detected in *O377*. (A-D) immunohistochemistry of *Crybb2* at wild type cortex (A), wild type dentate gyrys, *O377* cortex (C) and dentate gyrys (D). (E-F) Hematoxylin and eosin staining of wild type dentate gyrus (E) Hematoxylin and eosin staining of *O377* dentate gyrus (F). Scale bar=20µm.

4.6 Adult neurogenesis study in *O377* mutants and wild-type mice

In my study, the hippocampus volume and the dentate gyrus volume are found to be reduced in O377 compared with wild type (for detail see chapter 4.1). In addition, *Tmsb4x* is up regulated *in O377,* which has been suggested to be involved in neurogenesis and differentiation (for detail see chapter 2.3). In order to check the possibility that the mutation in *Crybb2* might leads to change in proliferation and differentiation in hippocampus, I investigated neurogenesis in adult O377 mutants and wild type.

4.6.1 Proliferation is not altered at adult dentate gyrus of *O377* mutants

8-weeks-old *O377* mutants and wild-type C57BL6 mice (5 animals in each group) were injected once a day in continual five days with bromodeoxyuridine (BrdU). Then,

animals were perfused one month after the first injection (Figure 4.17 A). BrdU positive cells in the granular cell layer and sub-granular cell layer of dentate gyrus were counted (Figure 4.17 B C). No significant difference in the cell density of BrdU positive was detected between *O377* mutants (3375 ± 514cells/mm^3) and wild type (3098 ± 550cells/mm^3) (Figure 4.17 D).

A

B   **C**

D
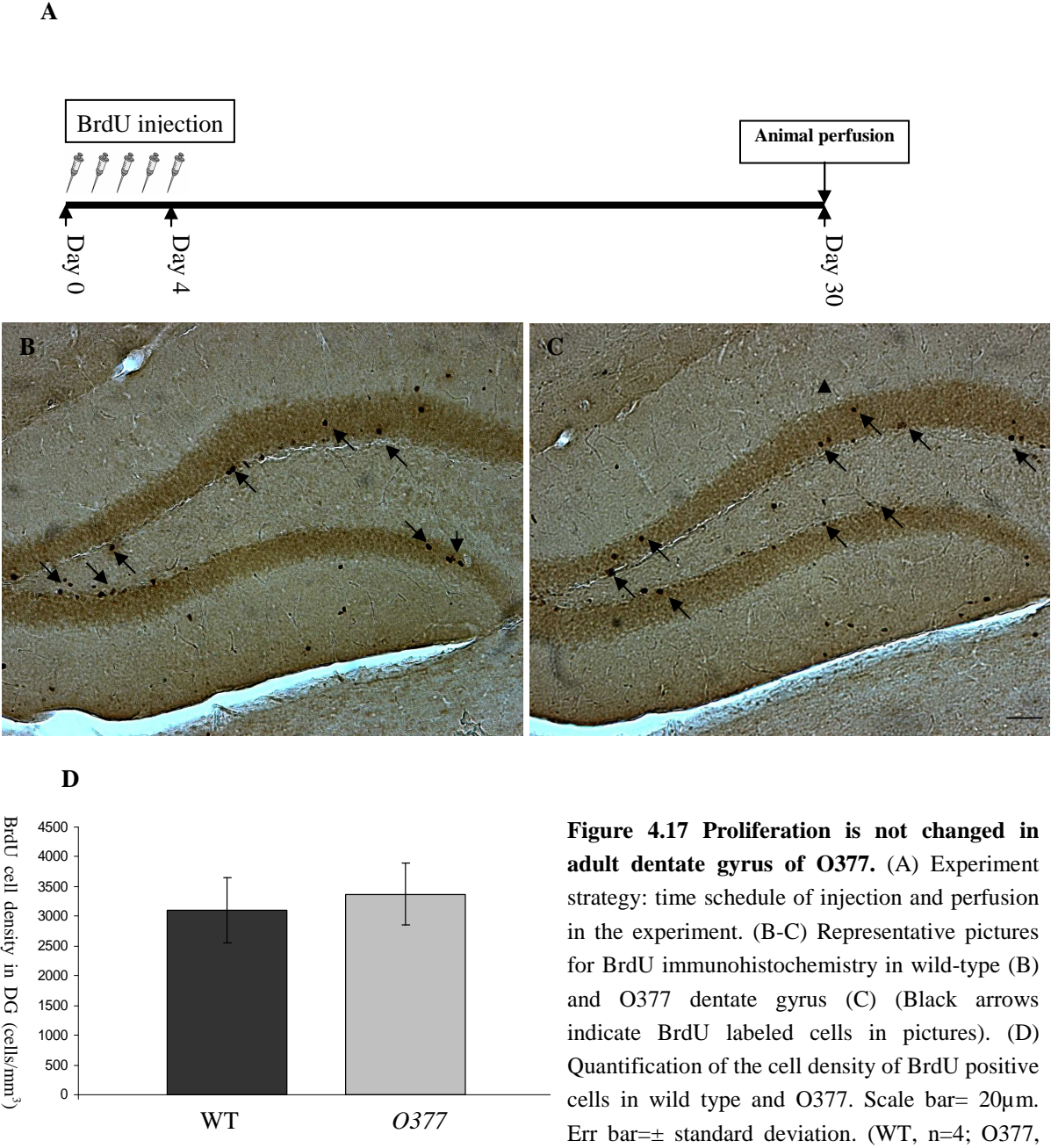
Figure 4.17 Proliferation is not changed in adult dentate gyrus of O377. (A) Experiment strategy: time schedule of injection and perfusion in the experiment. (B-C) Representative pictures for BrdU immunohistochemistry in wild-type (B) and O377 dentate gyrus (C) (Black arrows indicate BrdU labeled cells in pictures). (D) Quantification of the cell density of BrdU positive cells in wild type and O377. Scale bar= 20µm. Err bar=± standard deviation. (WT, n=4; O377, n=5)

4.6.2 No change in maturation is observed in *O377* mutants

Sections from wild type and *O377* mutants were triple-labeled with BrdU, doublecortin (DCX) and Neuronal Nuclei (NeuN) antibody in order to explore the

maturation in wild type and *O377* (Figure 4.18 A, B). DCX and NeuN were used as markers for immature neurons and mature neurons respectively as previously described (Ehm *et al.*, 2010). The ratios of BrdU colocalized with DCX (DCX/BrdU) or with NeuN (NeuN/BrdU) or with DCX and NeuN (DCX+NeuN/BrdU) were determined. 6.01±4.01% of DCX/BrdU in wild type and 2.57±2.82% of DCX/BrdU in *O377* mutants was observed; 26.64±7.93% of NeuN/BrdU in wild type and 28.75±5.96% of NeuN/BrdU in *O377* mutants were quantified; while 49.53±8.36% of triple labled DCX+NeuN/BrdU in wild type and 52.05±10.67% of triple labled DCX+NeuN/BrdU in *O377* was found. No significant difference was observed between wild type (Figure 4.18 A) and *O377* mutants (Figure 4.18 B) among these 3 groups, which indicated no significant difference in maturation between wild type and *O377* mutants.
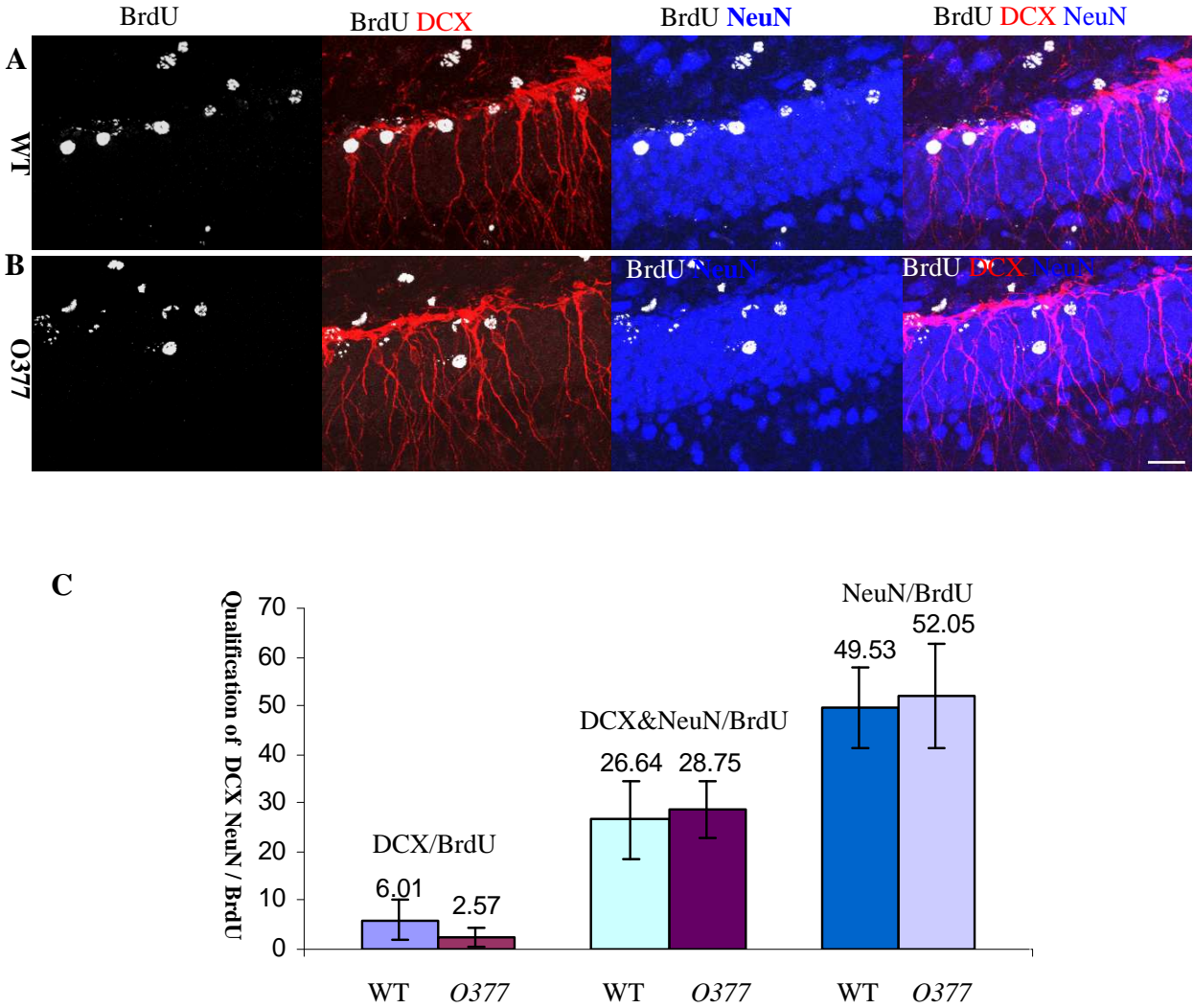
Figure 4.18 Maturation is not changed in adult dentate gyrus of *O377*. (A-B) Representative confocal imaging of wild type (A) and O377 (B) dentate gyrus labeled with BrdU (white), DCX (red) and NeuN (blue). (C) Quantification of DCX/BrdU, DCX+NeuN/BrdU and NeuN/BrdU in wild type and O*377* mutants. Scale bar, 20µm. Err bar=± Standard deviation. (WT, n=4; *O377*, n=5)

Sections from wild type and *O377* mutants were triple-labeled with BrdU, Sex determining region Y-box 2 (Sox2) and Glial fibrillary acidic prot Gfap ein () antibody to study the differentiation of adult stem cells. Sox2 and Gfap were used as stem cell marker and astrocyte marker as previously described (Zhao et al., 2008; Ehm *et al.*, 2010). The ratios of BrdU colocalized with Sox2 (Sox2/BrdU) and with Gfap (Sox2+Gfap/BrdU) were determined.19.73±5.2% of Sox2/BrdU was detected in wild type, while 15.30±2.78% of Sox2/BrdU was detected in *O377* mutants. Tree-shaped Gfap positive neurons and star-shaped Gfap positive neurons were detected by Gfap staining. No overlapping of tree-shape Gfap positive neurons and BrdU positive neurons could be detected (Figure 4.19 A, B). Significantly increased star-shaped Gfap positive cells with BrdU and Sox2 labeling were detected in wild type (10.09%±2.67%) (Figure 4.19 A) compared with *O377* mutants (4.95%±1.82%) (Figure 4.19 B). It means that *O377* mutants generated about 51% fewer astrocytes than wild type at adult age. It indicates that the differentiation of the adult stem cell is changed in *O377* compared with wild type.
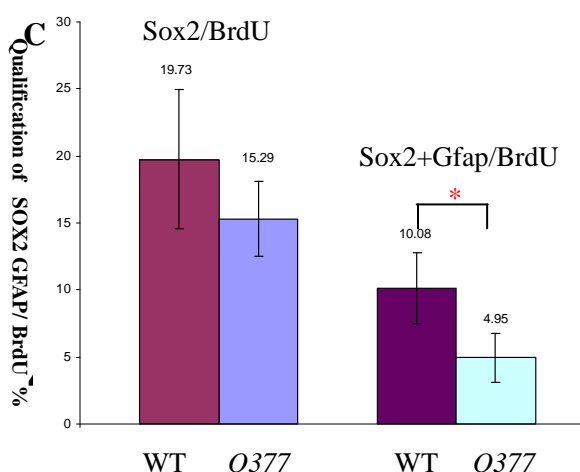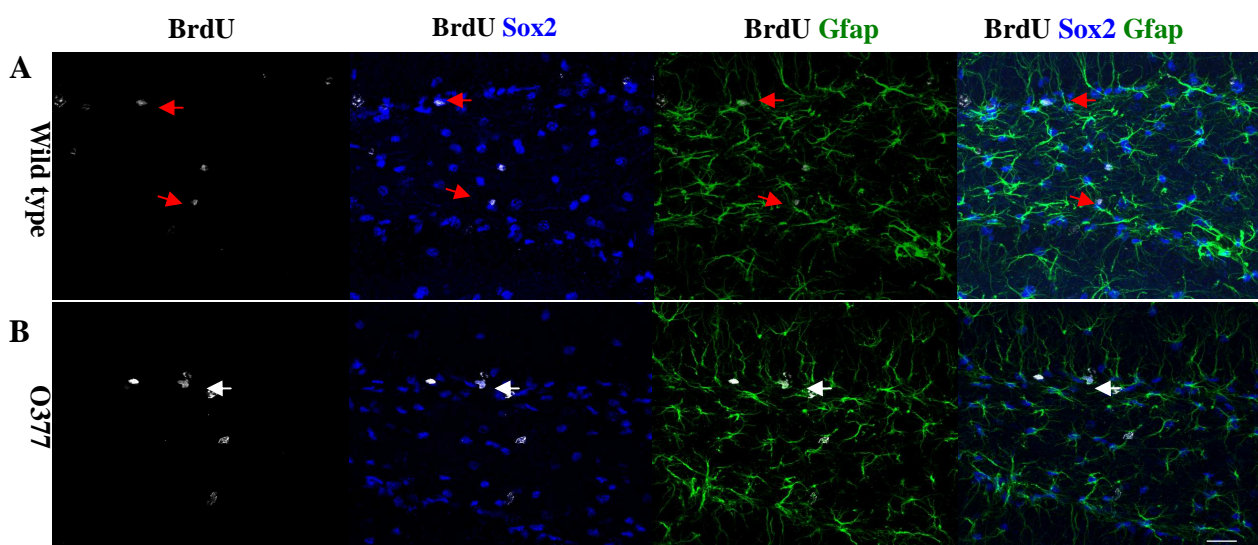
Figure 4.19 Less star-shaped Gfap neuron is generated in the dentate gyrus of *O377* mutants. (A-B) Representative confocal picture of wild type (A) and *O377* (B) dentate gyrus labeled with BrdU (white), Sox2 (blue) and Gfap (green). Cells Co-labeled with Sox2 and BrdU were marked with white arrow, and triple labeled neurons were marked by red arrow (C): Quantification of Sox2/BrdU, Sox2 +Gfap/BrdU in wild type and *O377*. * P≤0.05, student T-test, (WT, n=4; *O377*, n=5). Scale bar, 20μm. Err bar=± Standard deviation.

4.7.1 Reduced dendritic complexity in dentate gyrus neurons of *O377* mutants

To investigate the neuronal morphology, we used the Golgi staining to label neurons in 3-month-old wild-type (Figure 20 A) and *O377* mutant brains (Figure 20 B), and analyzed the neuronal morphology in dentate gyrus using Neurolucida software (Figure 20 C, D).
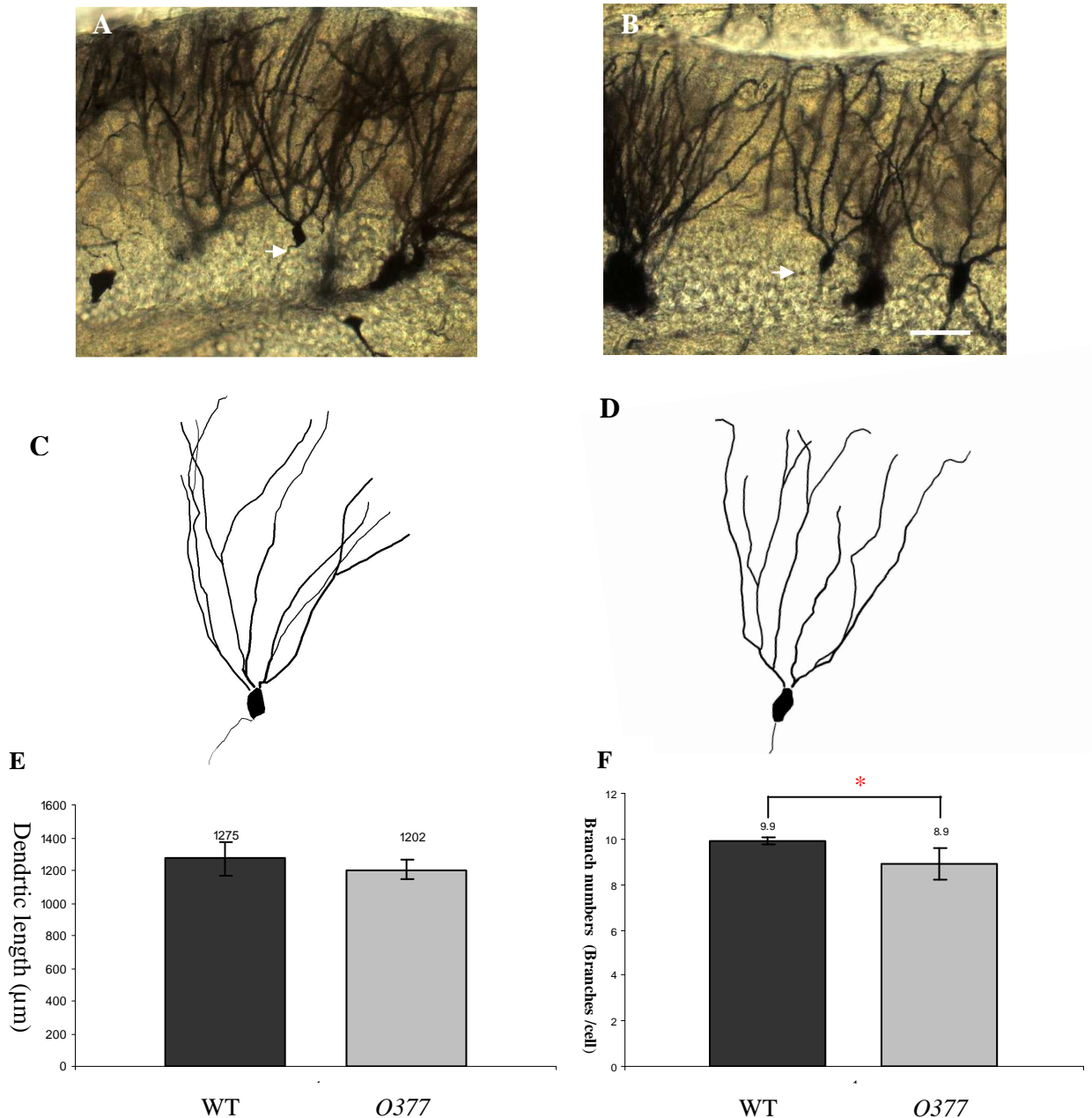

Figure 4.20 Dendritic complexity is reduced in *O377* dentate gyrus neuron. (A, B) Golgi staining of wild-type (A) and *O377* (B) dentate gyrus neurons. (C, D) Lucida trace of representative neurons in wild type (C) and *O377* (D) which are marked in (A) and (B). (E) Total dendrite length of wild-type and *O377* dentate gyrus neuron. (F) Total dendrite number of wild type and *O377* dentate gyrus neuron.* P≤0.05, student t-test, n=4-5. Scale bar, 20µm. Err bar=± standard deviation.

Within these two groups more than 4 animals were stained and in each animal 15-25 neurons were analyzed. To get more homogenous neurons, only the mature neurons in the ventral dentate gyrus were selected. Classification of mature neuron is based on previous publications (Green et al 1985, Wang et al 2000, Fujioka et al 2004): only neurons having more than 2 primary dendrites are considered to be mature neurons. The average number of branches of neurons at the dentate gyrus in *O377* mutants (8.91±0.71 branches/cell) (Figure 4.20 B, D) is less compared with the wild type (9.91±0.18 branches/cell) (Figure 4.20 A, C). However, total lengths of neurons at the dentate gyrus of *O377* (1202 ± 58µm) (Figure 4.20 B, D) was not significantly changed compared with wild type (1275 ±103 µm) (Figure 4.20 A, C).

4.7.2 Disturbance of Microtubule-associated protein 2 staining in *O377* mutants

Tmsb4x is actin monomer (G-actin) sequestering protein coding gene (for more detail see chapter 2.2.6). As it is up-regulated in *O377* mutants, expression of other cytoskeleton proteins in *O377* mutant neurons may be also changed. Therefore, I also performed the Microtubule-associated protein 2 (MAP2) staining to check whether there were variations in MAP2 staining in *O377* mutants compared with wild type. I could nicely detect MAP2 expression in the cell processes at dentate gyrus of wild type and *O377* mutants at 3-month and 1-year (Figure 4.21). Minor changes in the cell processes at dentate gyrus of 3-month-old *O377* mutants were observed (Figure 4.21 B) compared with wild type (Figure 4. 21 A). However, increased MAP2 staining intensity and disarrangement of cell processes were detected at dentate gyrus in one-year-old *O377* mutants (Figure 4.21 D) compared with wild type (Figure 4.21 C).

Abnormalities in MAP2 staining in granular cells of the dentate gyrus and of neurons in the hilus were also observed. MAP2 staining was observed in the cell bodies of wild type and *O377* mutants granular cell layer at 3-month-old, while strong staining in the cell bodies and dendrites of neurons in the hilus (Figure 4.22 A, B) was detected. Loss of MAP2 immunoreactivity was found in 1-year-old wild-type dentate granular cells and neurons in hilus, however granular cells and neurons in hilus at 1-year-old *O377* mutants almost maintained the immunoactivity as in 3-month-old mice (Figure 4.22 D). Small populations of granular cells with a bigger cell body were also observed in *O377* mutants with MAP2 staining (Figure 4.22 E).
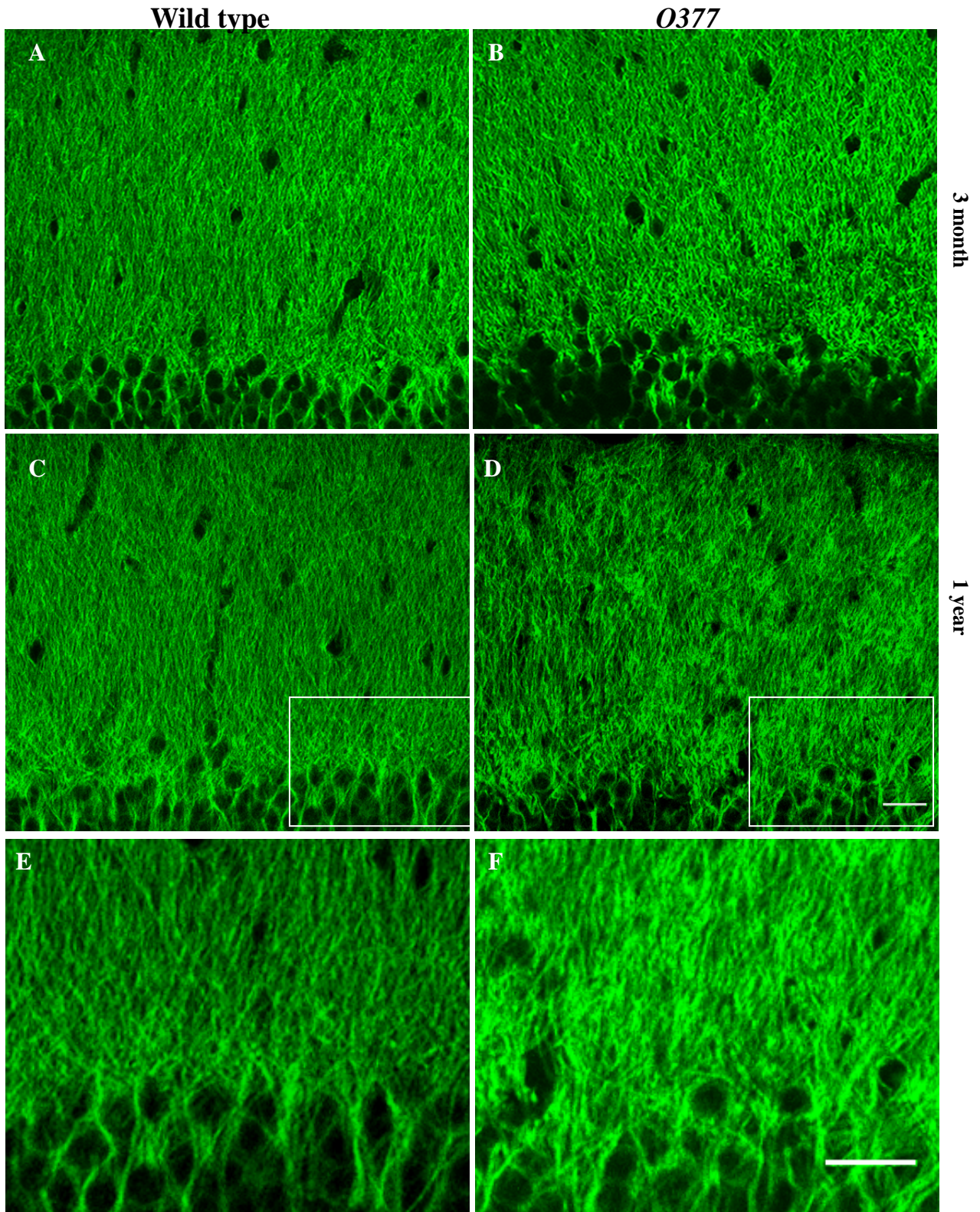
Figure 4.21 MAP2 staining shows increased staining intensity and irregular cell processes in one-year-old *O377* mice . (A-D) MAP2 staining of the cell processes in dentate gyrus of wild type at 3-month-old (A) and 1-year-old (C), *O377* at 3-month-old (B) and 1-year-old (D). (E-F) (E) Larger view of framed area in (C); (F) larger view of framed area in (D). Scale bar, 20µm.
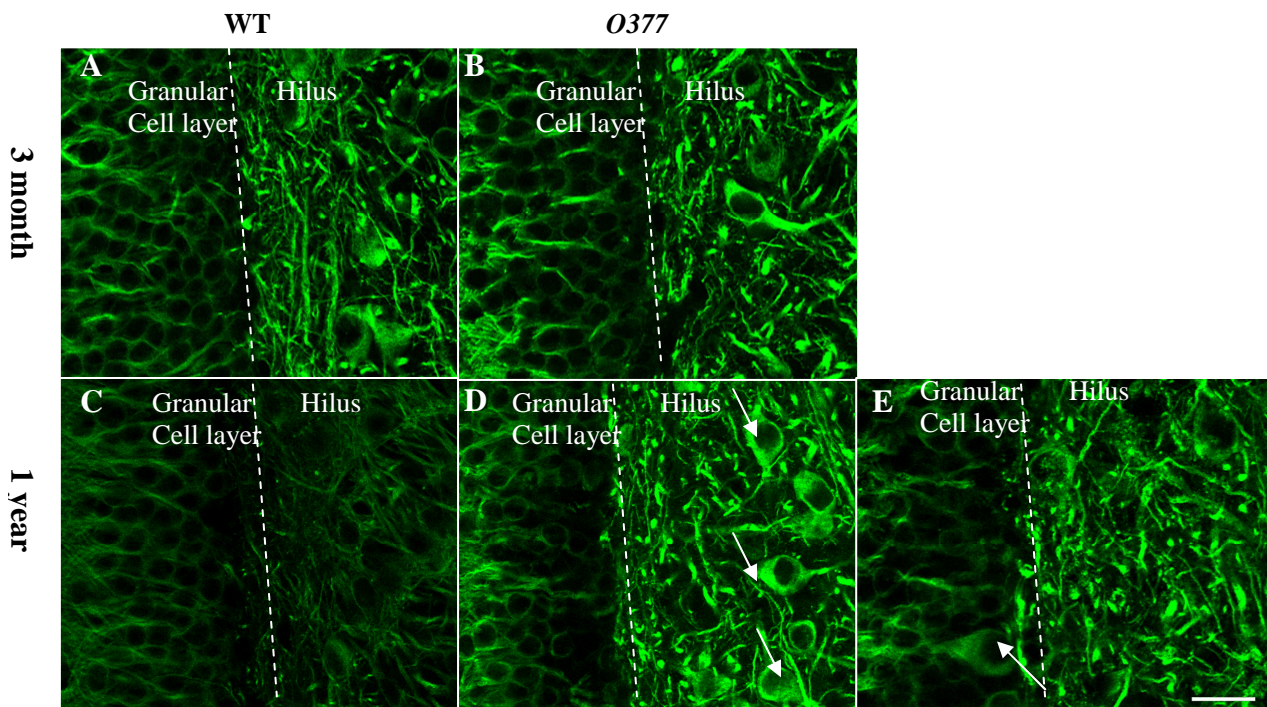
Figure 4.22 Abnormal MAP2 staining in granular cell layer and hilus. (A-D) MAP2 staining at the granular cell layer and hilus of 3-month-old wild type (A) and 1-year-old wild type (C), 3-month-old (B) and 1-year-old (D, E) *O377*. White arrow shows granular cell with bigger area of MAP2 staining (E). Scale bar, 20µm. White lines indicate boundaries of granular cell layers and hilus; white arrows indicate the cells with brilliant MAP2 stainings.

4.8 *Crybb2* is co-expressed with different GABAergic interneuron markers

Defects in GABAergic function leads to an unbalance of inhibitory and excitatory circuit. One of the most constant observations found in psychiatric disorders is the loss of GABAergic interneurons (Tooney *et al.*, 2004; Reynolds *et al.*, 2001). To discuss the possibility that *Crybb2* might play a role in development of GABAergic interneuron, we did immunohistochemistry labeling *Crybb2* and either parvalbumin, calretinin or somatostatin (for more details about GABAerigic interneuron markers see chapter 2.3.3). Co-expression of *Crybb2* and parvalbumin were counted in three different areas in the brain: prefrontal cortex, dentate gyrus and CA1. *Crybb2* was detected to be expressed in 96.7% of parvalbumin positive GABAergic interneurons at the prefrontal cortex (Figure 4.23 A); in 94.9% of parvalbumin, positive GABAergic interneurons at CA1 (Figure 4.23 B) and in 97.8% of parvalbumin positive GABAergic interneurons at dentate gyrus (Figure 4.23 C).
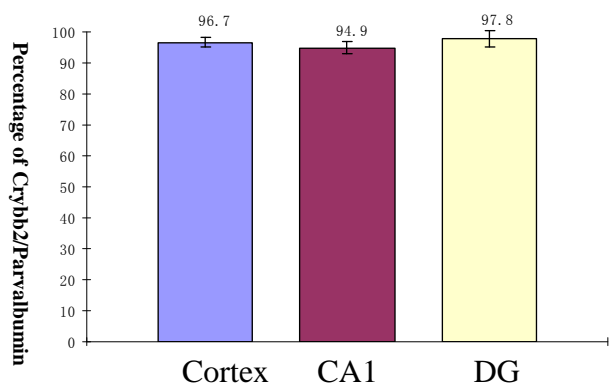
	Parvalbumin	*Crybb2*	Parvalbumin *Crybb2*	
A				Prefrontal cortex
B				CA1
C				DG
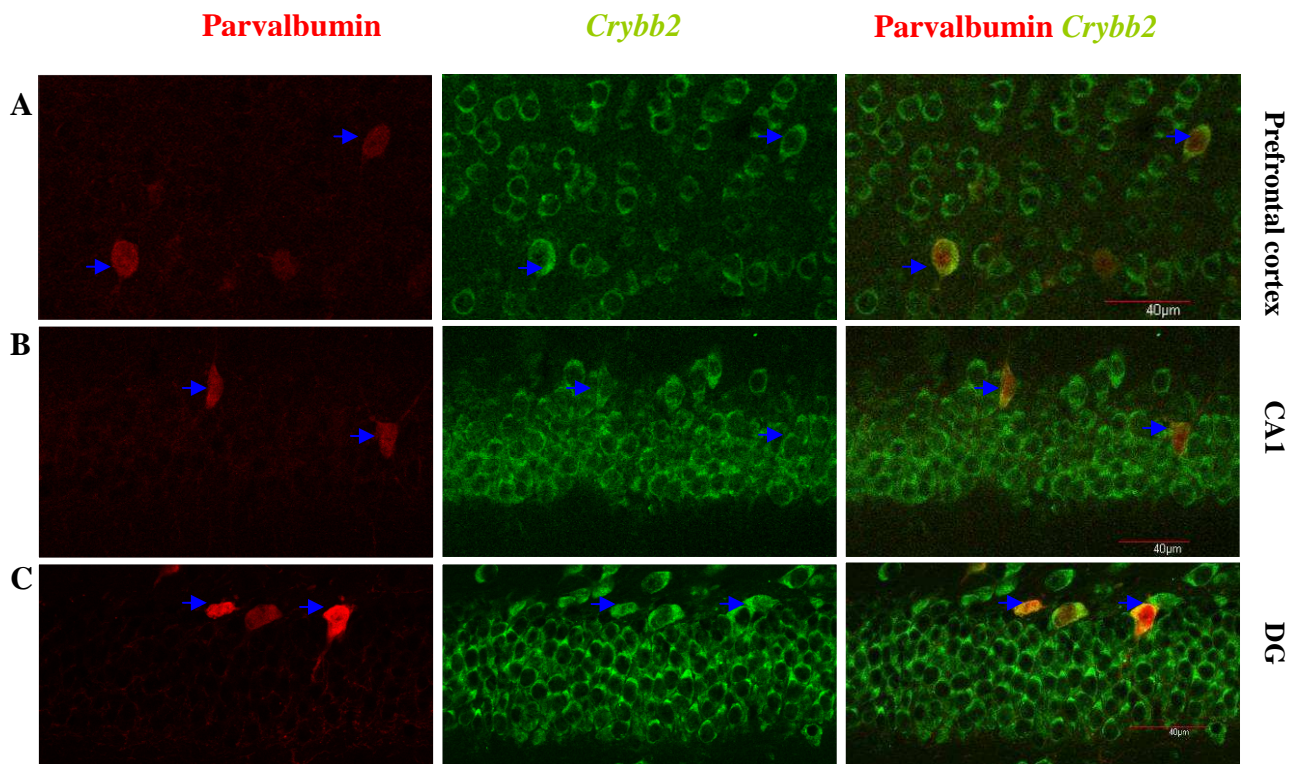
D

Figure 4.23 *Crybb2* is co-expressed with parvalbumin positive GABAergic interneuron. (A-C) *Crybb2* expression (green) overlaps with parvalbumin positive GABAergic interneurons (red) in prefrontal cortex (A), CA1 (B) and dentate gyrus (C). (D) Percentage of *Crybb2* positve cells in parvalbumin positive GABAergic interneuron in prefrontal cortex (96.7±1.5%), CA1 (94.9±2.0%) and dentate gyrys (97.8±2.6%) (n=3). Scale bar, 40µm. Err bar= ± standard deviation.

Double staining of *Crybb2* and calretinin was determined at three different brain areas: prefrontal cortex, dentate gyrus and CA1. Quantification of co-expression of *Crybb2* and calretinin revealed that *Crybb2* was expressed in 75.0% of calretinin positive GABAergic interneurons at prefrontal cortex (Figure 4.24 A), in 69.6% of calretinin positive GABAergic interneurons at CA1 (Figure 4.24 B), and in 46.3% of calretinin positive GABAergic interneurons at dentate gyrus (Figure 4.24 C).
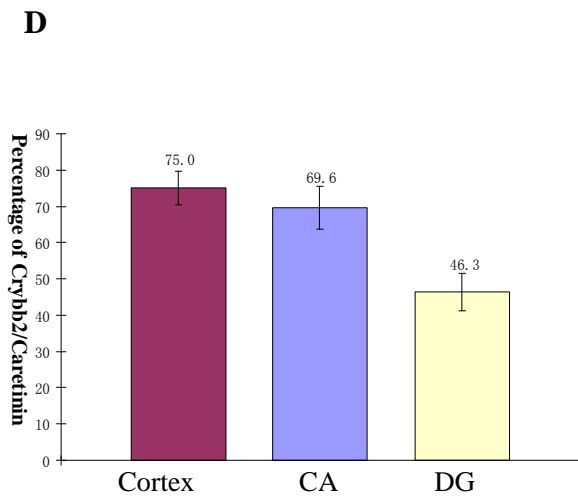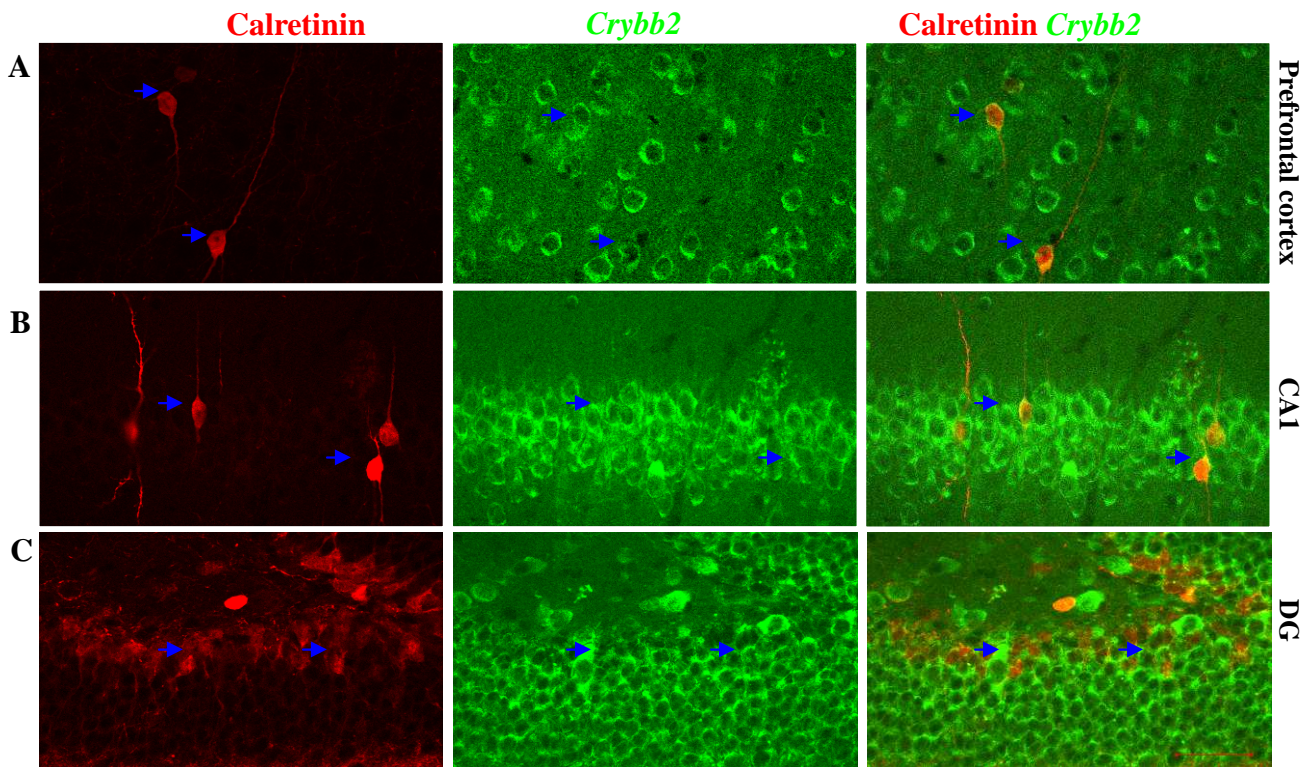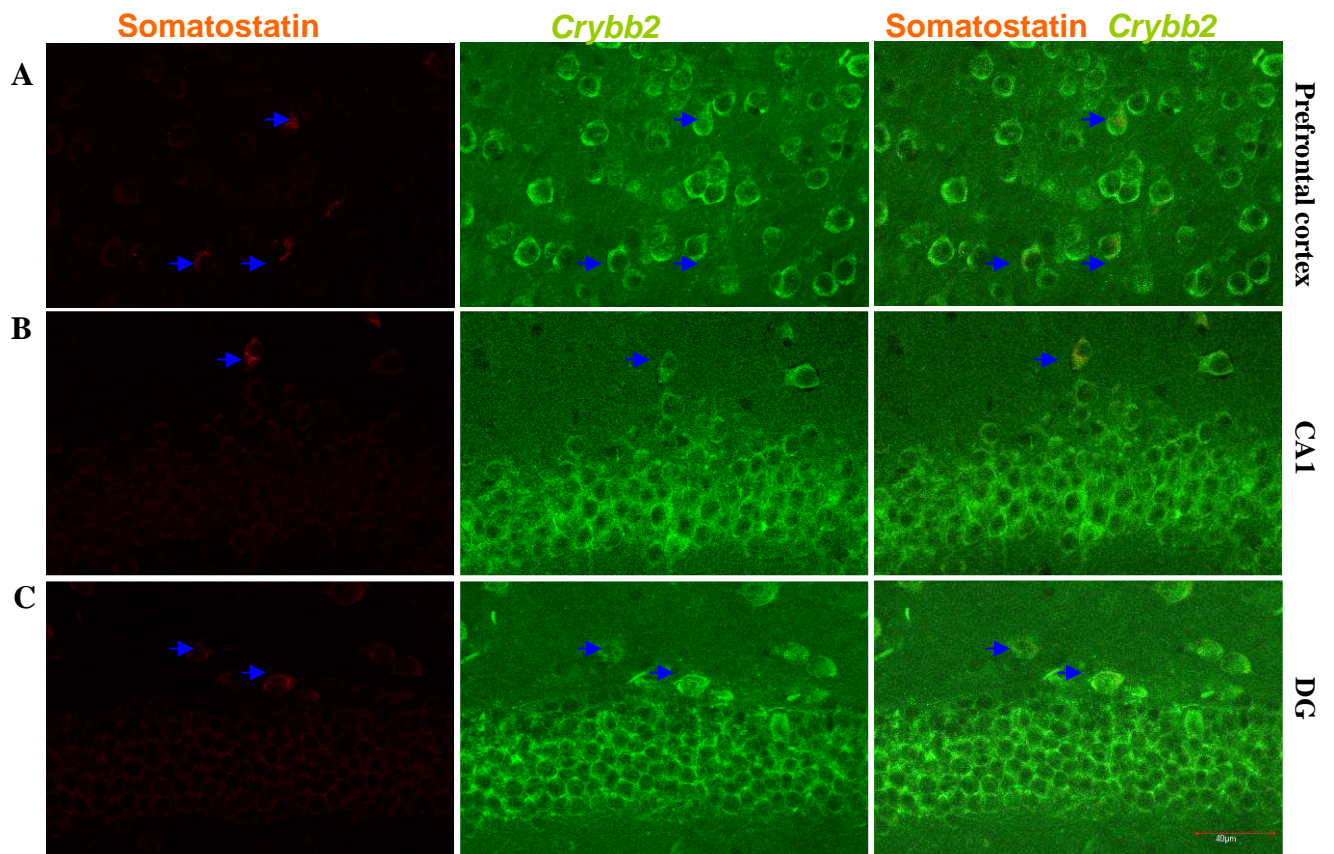
Figure 4.24 ***Crybb2*** **is co-expressed with calretinin positive GABAergic interneuron.** (A-C) *Crybb2* (Green) is co-expressed with calretinin positive GABAergic interneurons (red) in prefrontal cortex (A), CA (B) and dentate gyrus (C). (D) Percentage of *Crybb2* positve cells in calretinin positive GABAergic interneurons at prefrontal cortex (75±2.6%), CA1 (69.6±5.9%) and dentate gyrus (46.3±5.2%) (n =3). Scale bar, 40µm. Err bar= ± standard deviation.

Co-expression of *Crybb2* and somatostatin was also examined at three different brain areas: prefrontal cortex, dentate gyrus and CA1. *Crybb2* was expressed in 90.5% of somatostatin positive GABAergic interneurons in prefrontal cortex (Figure 4.25 A), 90 % of somatostatin positive GABAergic interneurons in CA1 (Figure 4.25 B) and 92.6% of somatostatin positive GABAergic interneurons in dentate gyrus (Figure 4.25 C).

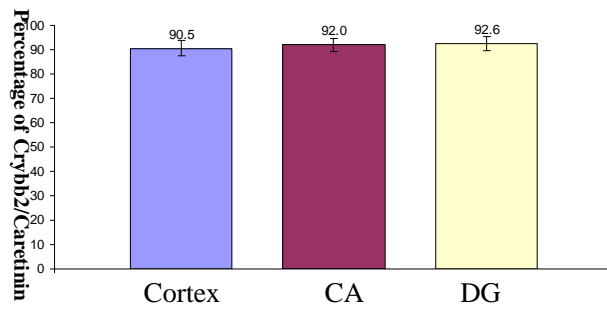**Figure 4.25 *Crybb2* is co-expressed with somatostatin positive GABAergic interneurons**. (A-C) *Crybb2* (Green) were detected to be co-expressed with somatostatin positive GABAergic interneurons (red) in prefrontal Cortex (A), CA1 (B) and dentate gyrus (C). (D) Percentage of *Crybb2* positve cell in 90.5±3.1% of somatostatin positive cells at prefrontal cortex, 92±2.8% of somatostatin positive cells at CA1, and 92.6±3.0% of somatostatin positive cells at dentate gyrus (n=3). Scal bar, 40µm. Err bar= ± standard deviation.

4.9 GABAergic interneuron subtype-specific loss in the hippocampus of *O377* mutants

As *Crybb2* is detected in distinct subtypes of GABAergic neurons, it is quit possible that mutation in *Crybb2* could lead to reduction of GABAergic interneurons in *O377* mutants. I employed three different types of GABAergic interneuron markers to check the differences in GABAergic interneurons of *O377* mutants and wild-type mice at the hippocampus and the prefrontal cortex.

4.9.1 Parvalbumin positive GABAergic interneurons are reduced in ventral hippocampal in *O377* mutants but not in prefrontal cortex

The cell density of parvalbumin positive GABAergic neurons was examined in the ventral dentate gyrus (DG) and CA of wild type and *O377* mutants at different ages (Table 4.3). The cell density of parvalbumin positive GABAgeric interneuron was significantly reduced in *O377* mutant (Figure 4.26 B, D) compared with wild type (Figure 4.26 A, C) in both dentate gyrus and CA region. The cell density of parvalbumin positive GABAergic interneuron at the dentate gyrus and CA region was reduced with aging both in wild type and *O377* mutant, however, the cell density was reduced more and more pronounced from P14 to 3-month-old at dentate gyrus (Figure 4.26 E) and CA region of *O377* (Figure 4.26 F) compared with wild type.

Table 4.3 The cell density of Wild type and *O377* parvalbumin positive GABAergic interneuron (cells/mm^3) in ventral dentate gyrus and CA at P14, 1-month and 3-month.

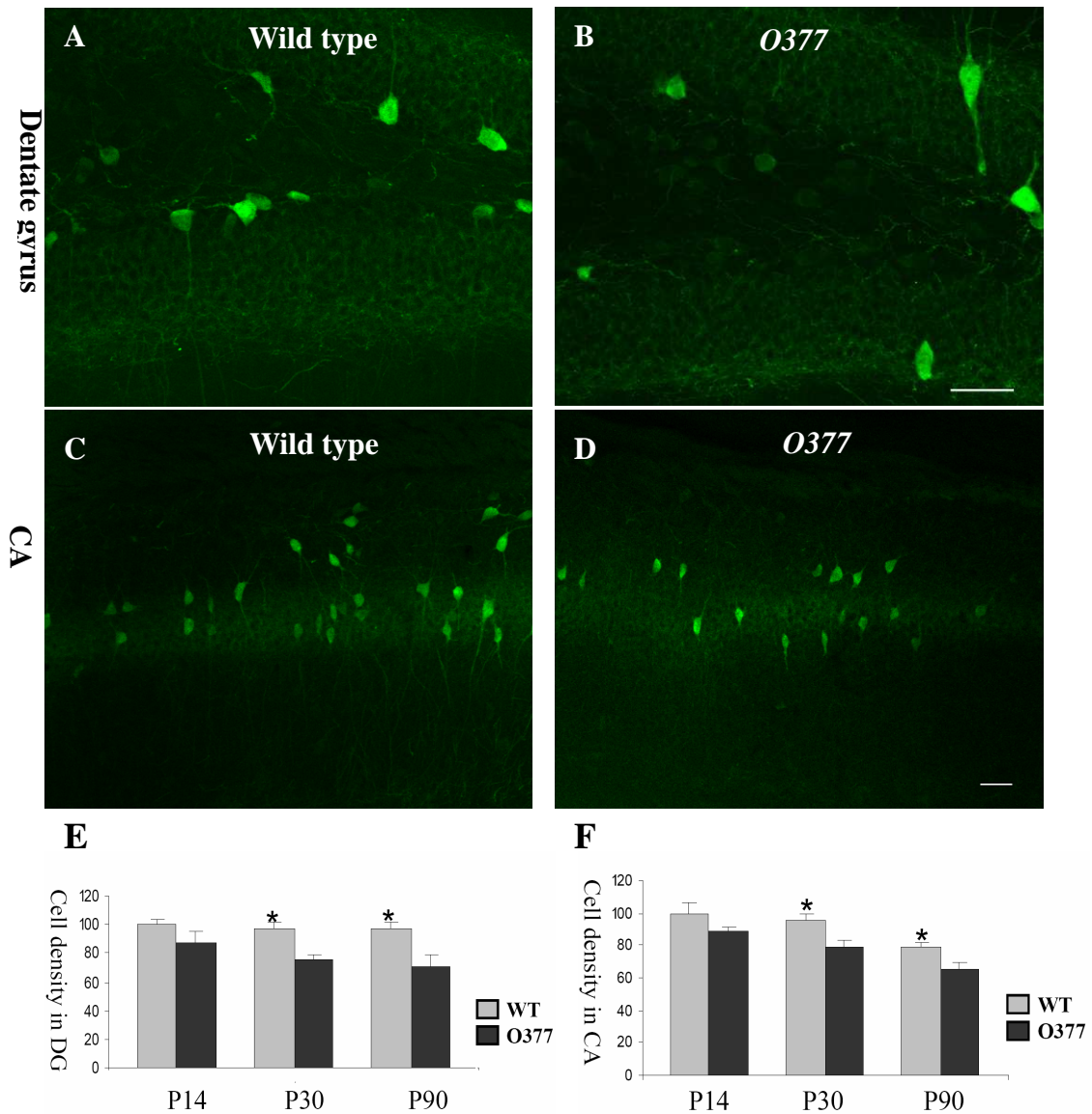|	P14	1-month-old	3-month-old
WT DG	3308.9±252.5	3214.24±264.5	3199.21±295.2
O377 DG	2886.1±558.8	2517.72±183.0	2366.02±478.6
WT CA	5127.3±688.3	4909.9±456.7	4062.7±278.2
O377 CA	4576.8±247.4	4076.3±344.6	3328.1±427.0

Figure 4.26 Parvalbumin positive GABAergic interneuron loss in ventral hippocampus of *O377* (A-B) Parvalbumin positive GABAergic interneurons in dentate gyrus of 3-month-old wild type (A) and *O377* mutant (B). (C-D) Parvalbumin positive GABAergic interneuron in CA1 of 3 month old wild type and *O377.* (E) Cell density of parvalbumin positive GABAergic interneuron in dentate gyrus. (F) Cell density of parvalbumin positive GABAergic interneuron in CA. In (E) (F) values are normalized to P14 wild type (WT=100), (*P< 0.05, student t-test, n=4). Scale bar, 40µm. Err bar= ± standard deviation.

The cell density of positive GABAergic neurons in the prefrontal cortex of 3-month-old wild type and *O377* mutants was also calculated. No significant difference was detected in cell density of parvalbumin positive GABAergic neurons between wild type (2425.7±173.4cells/mm^3) (Figure 4.27 A) and *O377* mutants (2519.9±248.6cells/mm^3) (Figure 4.27 B).
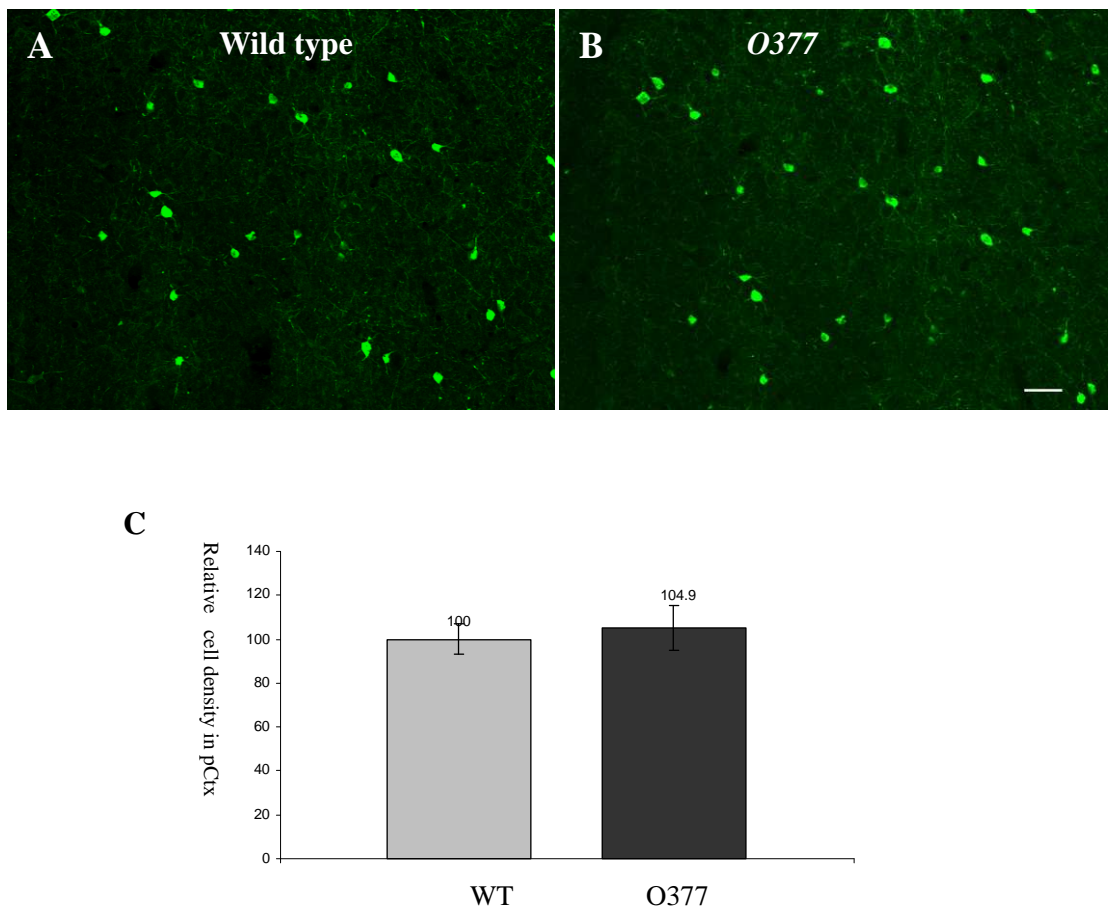
Figure 4.27 Cell density of parvalbumin positive GABAergic interneurons is not significantly altered in prefrontal cortex of *O377* mutants. (A-B) Parvalbumin positive GABAergic neurons in prefrontal cortex of 3-month-old wild type (A) and *O377* (B). (C) Normalized cell density in prefrontal cortex of 3-month-old wild type and *O377*. Cell density of 3-month-old wild type =100 (n=4). Scale bar, 40µm. Err bar= ± standard deviation.

4.9.2 The cell density of Calretinin positive GABAergic interneurons are not significantly altered in *O377* mutants.

The cell density of calretinin positive GABAergic interneurons at ventral dentate gyrus, ventral CA and prefrontal cortex of 3-month-old wild type and *O377* mutant was counted (Table 4.4). No significant difference was detected in cell density of calretinin positive GABAergic neurons at ventral dentate gyrus (Figure 4.28 A, B), ventral CA (Figure 4.28 C, D), and prefrontal cortex (Figure 4.28 E, F) between wild type (Figure 4.28, A, C, E) and *O377* mutants (Figure 4.28 B, D, F).
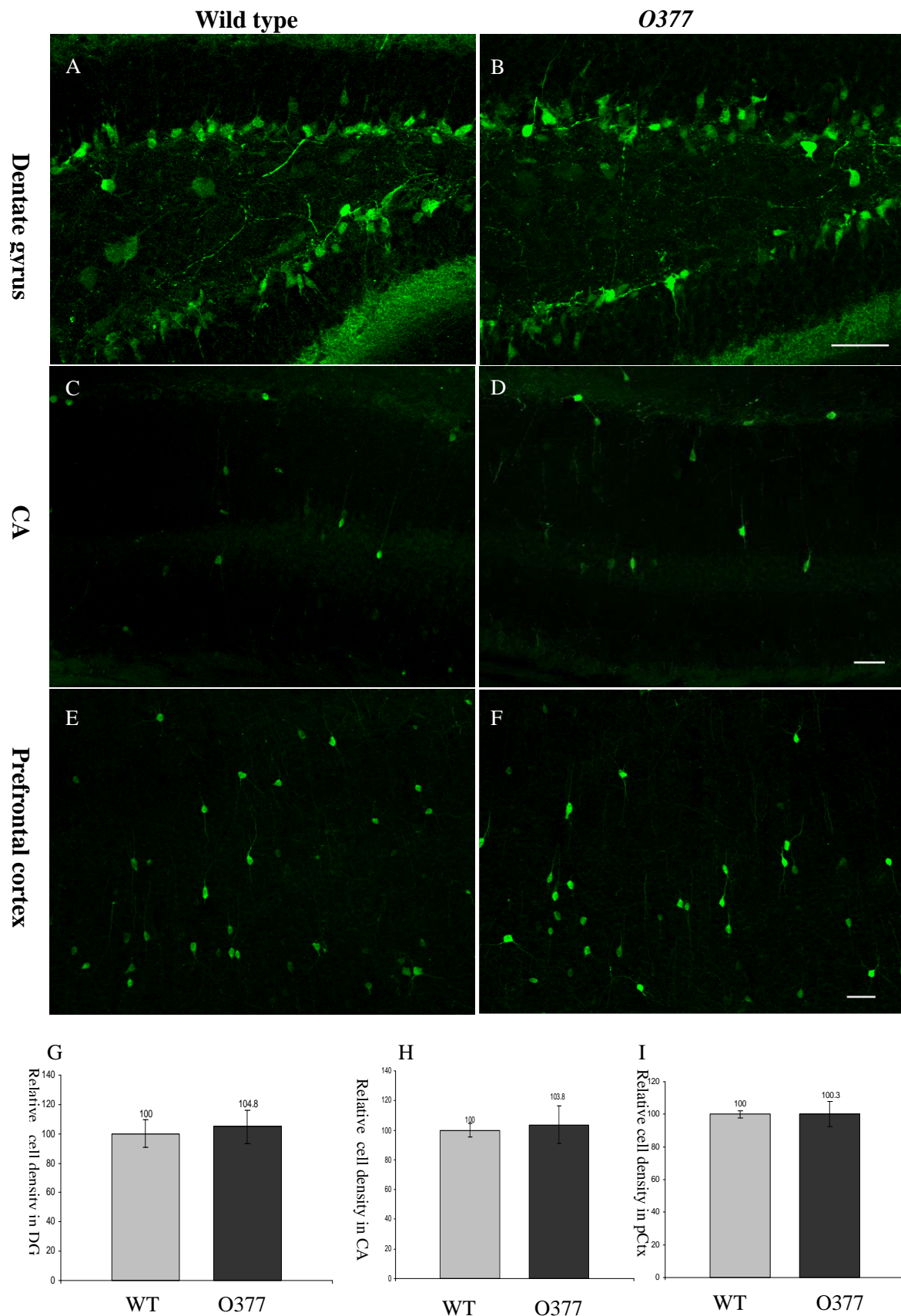
Figure 4.28 Cell density of calretinin positive GABAergic interneurons was not significantly altered in O377. (A-B) Calretinin positive GABAergic interneurons in ventral dentate gyrus of 3-month-old wild type (A) and O377 (B). (C-D) Calretinin positive GABAergic interneurons in CA1 of 3-month-old wild type (C) and O377 (D). (E-F) Calretinin positive GABAergic interneurons in prefrontal cortex of 3-month-old wild type (E) and O377 (F). (G-I) Cell density of calretinin positive GABAergic interneurons in dentate gyrus (G), in CA (H) and in prefrontal cortex (I). In (G), (H), (I) values were normalized to 3-month-old wild type (WT=100), n=4. Scale bar=40µm. Err bar= ± standard deviation.

Table 4.4 Cell density of calretinin postsitive GABAergic interneurons (cells/mm³) at ventral dentate gyrus (DG), ventral CA and prefrontal cortex of 3-month-old wild type and *O377*.

	Wild type 3M	*O377* 3M
Cell density DG	22322.3±2094.4	23391.1±2550.0
Cell density in pCtx	804.2±18.5	806.9 ±62.9
Cell density CA	3354.9±154.9	3482.1±421.7

4.9.3 Somatostatin positive GABAergic interneurons are not significantly changed in *O377* mutants.

Another kind of important GABAergic interneurons, somatostatin positive GABAergic interneurons, were also checked by immmunohistochemistry at 3-month-old wild type and *O377* mutants. Cell density in ventral dentate gyrus, ventral CA and prefrontal cortex of wild type and *O377* was determined (Table 4.5). No significant alteration was detected in cell density of somatostatin positive GABAergic interneuron at dentate gyrus (Figure 4.11 A, B), CA (Figure 4.29 C, D), and prefrontal cortex (Figure 4.29 E, F) between wild type (Figure 4.29, A, C, E) and *O377* mutants (Figure 4.29 B, D, F).

Table 4.5 Cell density of somatostatin postsitive GABAergic interneurons (cells/mm³) at ventral dentate gyrus (DG), ventral CA and prefrontal cortex (pCtx) of 3-month-old wild type and *O377* mutants.

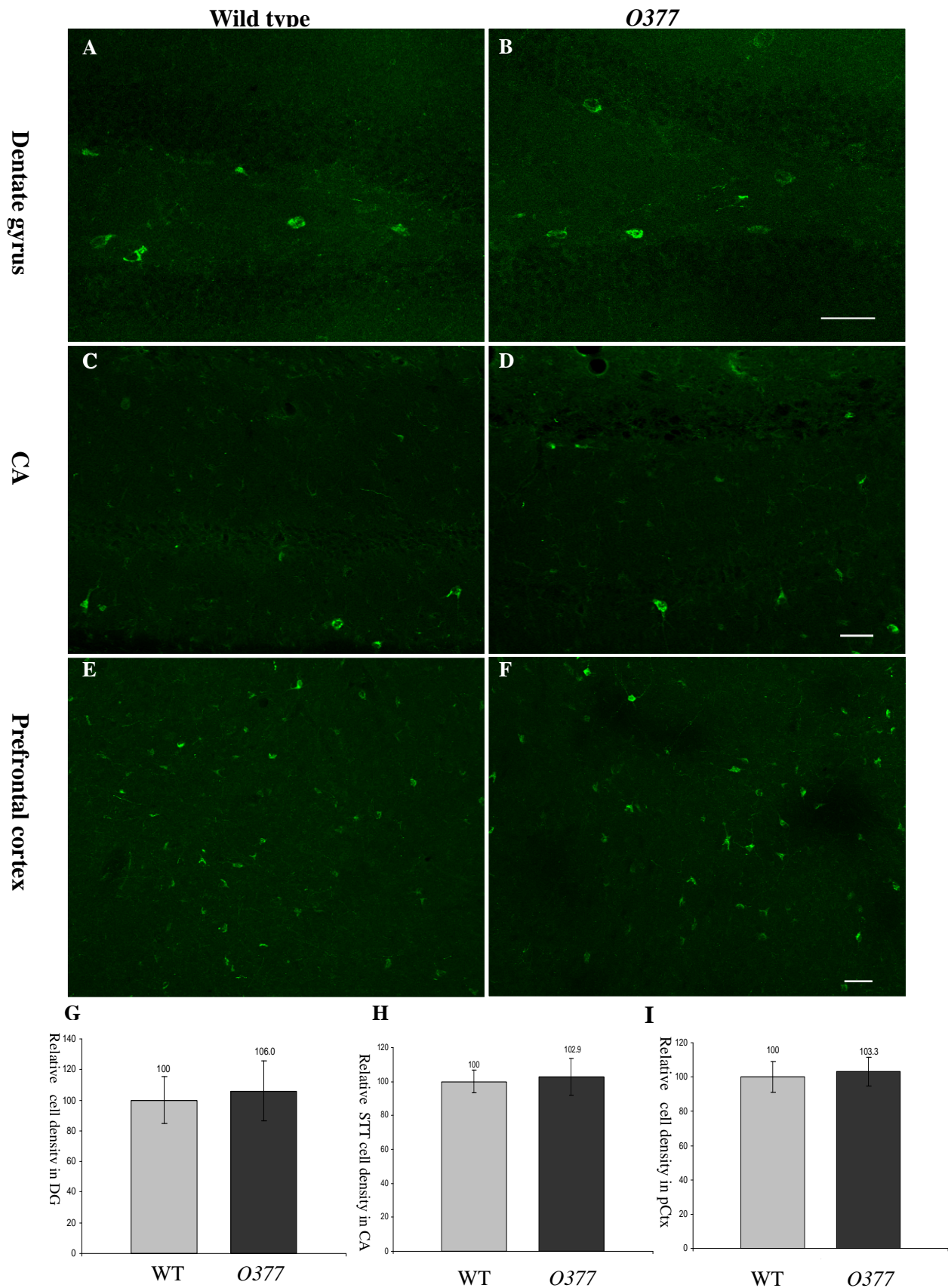|	Wild type 3M	*O377* 3M
Cell density DG	4699.4±729.8	4979.4±908.8
Cell density CA	3666.8±242.0	3771.6±401.8
Cell density in pCtx	2857.2±256.5/	2951.8±240.3

Figure 4.29 Cell density of Somatostatin positive GABAergic interneurons was not significantly altered in 3-month-old O377. (A-B) Somatostatin positive GABAergic neurons in dentate gyrus of 3 month old wild type (A) and O377 (B). (C-D) Somatostatin positive GABAergic neurons in CA1 of 3 month old wild type (C) and *O377* (D). (E-F) Somatostatin positive GABAergic neurons in prefrontal cortex of 3-month-old wild type (E) and *O377* (F). (G-I) Cell density of somatostatin positive GABAergic neurons in dentate gyrus (G), in CA (H) and in prefrontal cortex (I) In (G) (H) (I) values were normalized to 3-month-old wild type (WT=100), n=4. Scale bar=40μm. Err bar= ± standard deviation.

4.10 No changes in synaptic inhibition in *O377* mutants

To verify whether a decrease in parvalbumin positive GABAergic interneuron number and neurons with reduced dendrite complexity would result in functional changes in the dentate gryrus, I performed whole-cell patch-clamp recording.
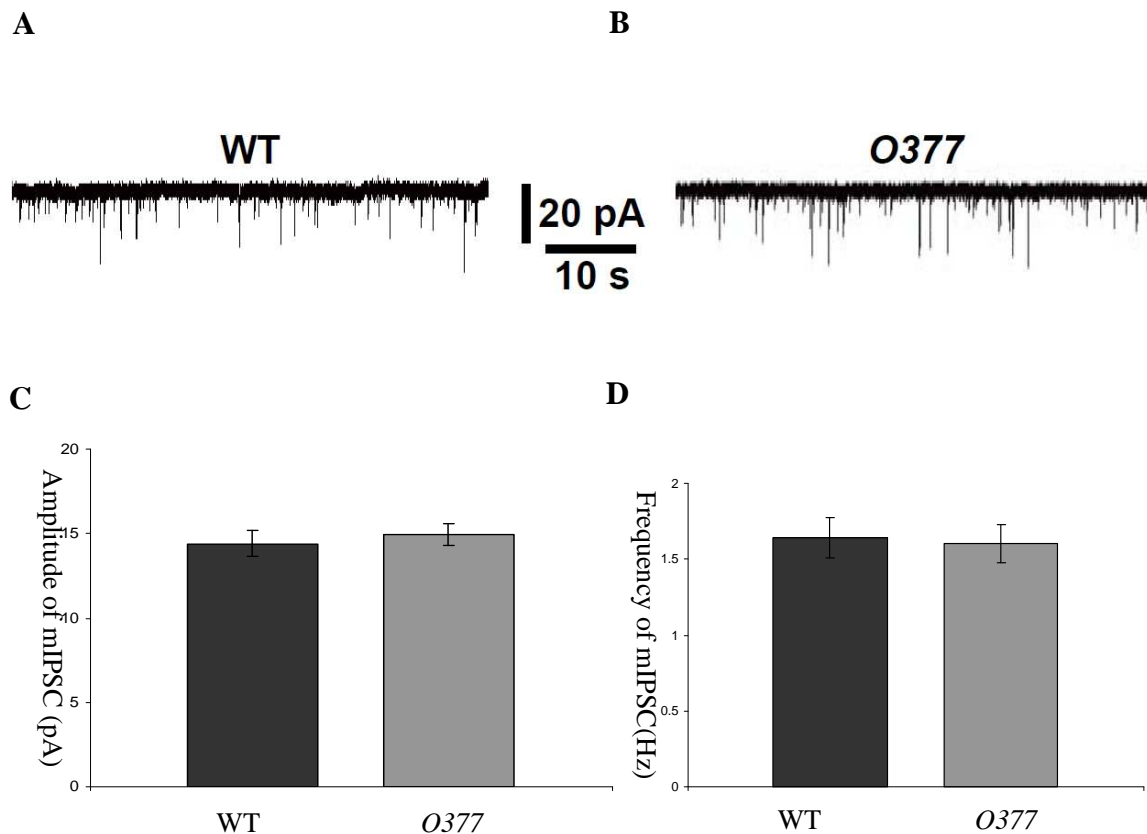
A **B**

C **D**

Figure 4.30 GABAergic synaptic inhibition is not significantly altered in *O377* mutant. (A) Representative trace of miniIPSC from wild-type dentate gyrus. (B) Representative trace of miniIPSC from O377 dentate gyrus. (C) Average amplitude of *O377* (1.60±0.12 pA) is not significantly changed compared with wild type (1.64±0.13 pA). (D) Average frequency of wild type (14.40±0.78 Hz) and O377 (14.95±0.65 Hz) is almost identical. Over 20 cells from more than 5 mice were recorded in each group. Err bar=±standard err mean.

Cells in the ventral dentate gryrus were selected for whole cell miniature inhibitory postsynaptic currents (IPSCs). Miniature IPSCs recordings were made at holding potential of 70 mV in the artificial cerebrospinal fluid (ACSF) with 5µM NBQX (2, 3-dihydroxy-6-nitro-7-sulfamoyl-benzo[f]quinoxaline-2,3-dione, an AMPA Glutamate receptor antagonists), 50µM AP5 ((2R)-amino-5-phosphonovaleric acid; (2R)-amino-5- phosphonopentanoate, a NMDA channel blocker) and 1µM TTX (tetrodotoxin, an action potential blocker). The average mIPSCs frequency in the *O377* mutants (1.60±0.12 Hz) (Figure 4.30 B, D) was almost identical with the wild-type IPSC

frequency (1.64±0.13 Hz) (Figure 4.30 A, D), while the amplitude of the mIPSCs in *O377* mutants (14.95±0.65 pA) (Figure 4.30 B,C) was also not significantly altered in comparison to the wild type (14.40±0.78 pA) (Figure 4.30 A,C).

4.11 Increased apoptosis in the ventral hippocampal region at early postnatal stage

As parvalbumin positive GABAergic interneurons were lost in the ventral hippocampus of *O377* mutant from P14 to 3-month and hippocampus volume is decreased in 3-month-old *O377* mutants, I tested for apoptosis by immunohistochemistry against cleaved caspase-3 in wild-type and *O377* mutant sections. The cell density of apoptotic cells in the ventral dentate gyrus of *O377* mutant (1356.0±126.0cells/mm^3) (Figure 4.31 B, D) was found to be increased by 75.2% compared with wild-type (775.6±126.9cells/mm^3) (Figure 4.31 A, C). The cell density of cleaved caspase-3 positive cells in ventral CA at P14 was also determined. The cell density of apoptotic cells in the ventral CA region of *O377* mutants (405.8±55.1cells/mm^3) (Figure 32 B, D) was found to be increased by 99.4% compared with wild type (203.5±45.9cells/mm^3) (Figure 32 A, C).

I also checked apoptosis at 1-month-old wild-type and *O377* mutant sections. The cell density of apoptotic cells in *O377* mutant ventral dentate gyrus (610.6±122.7cells/mm^3) was found to be increased by 46.3% compared with wild type (417.2±53.5cells/mm^3) (Figure 4.33 A). The cell density of apoptotic cells in *O377* mutant ventral CA (165.0±27.1cells/mm^3) was found to be increased by 53.2% compared with wild type (252.8±34.33cells/mm^3) (Figure 4.33 B).

In addition, I also detected apoptosis by immunohistochemistry with an antibody against cleaved caspase-3 at 3-month-old wild-type and *O377* mutant sections. The cell density of apoptotic cells in *O377* mutant ventral dentate gyrus (281.3±35.4cells/mm^3) (Figure 4.34 B) was not significantly altered compared with wild type (276.2±48.2 cells/mm^3) (Figure 4.34 A). In addition, the apoptotic cells density in the ventral CA of *O377* mutant (117.4±22.0cells/mm^3) (Figure 4.34 D) was found to be almost identical with wild-type (115.3±18.2cells/mm^3) (Figure 4.34 B). It indicates the increase of apoptosis in *O377* appears within a short period after birth.
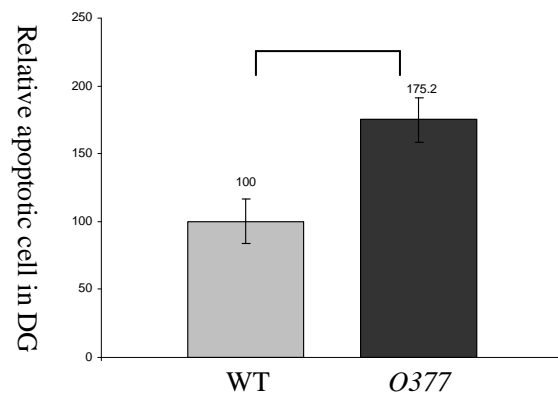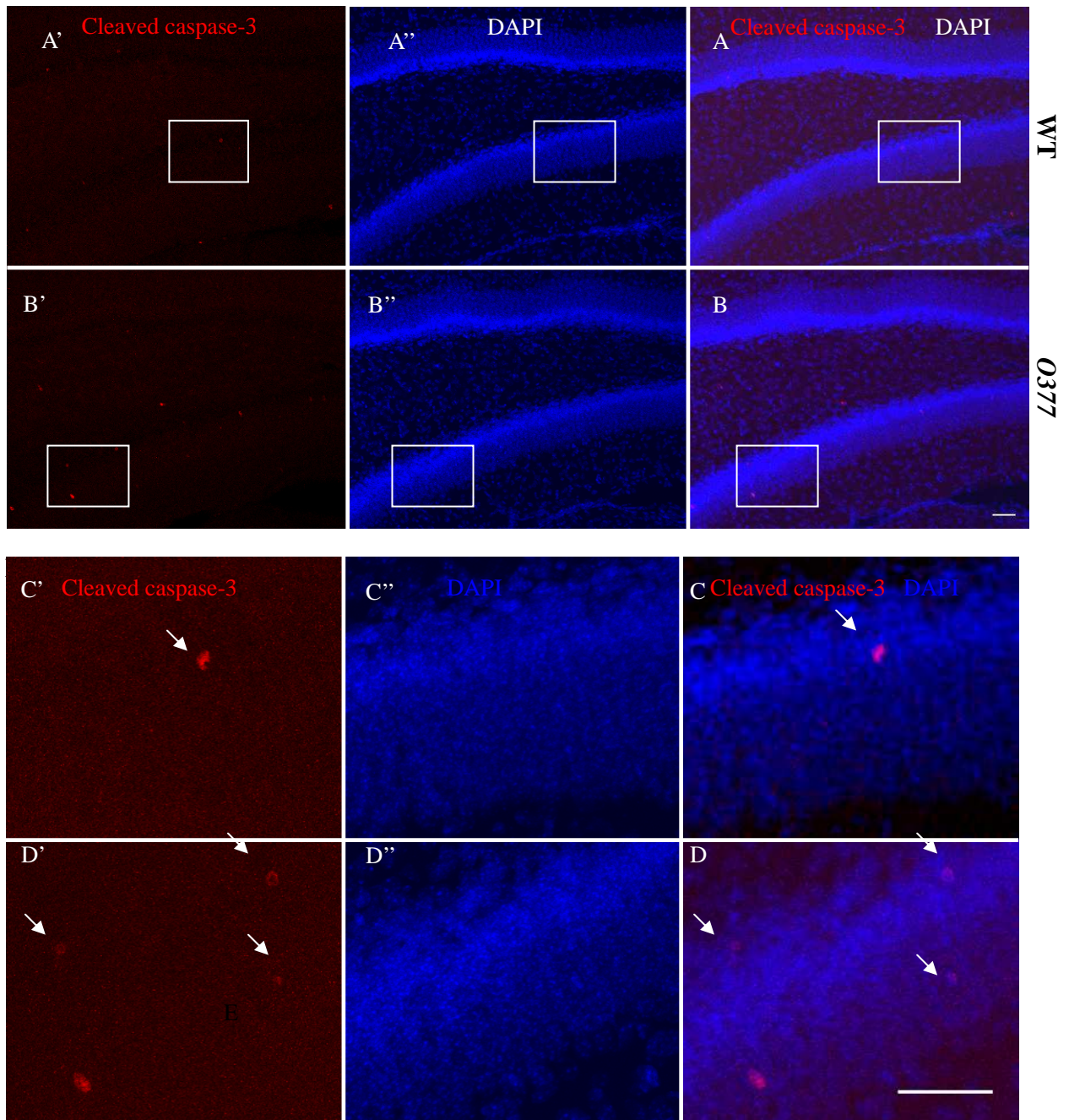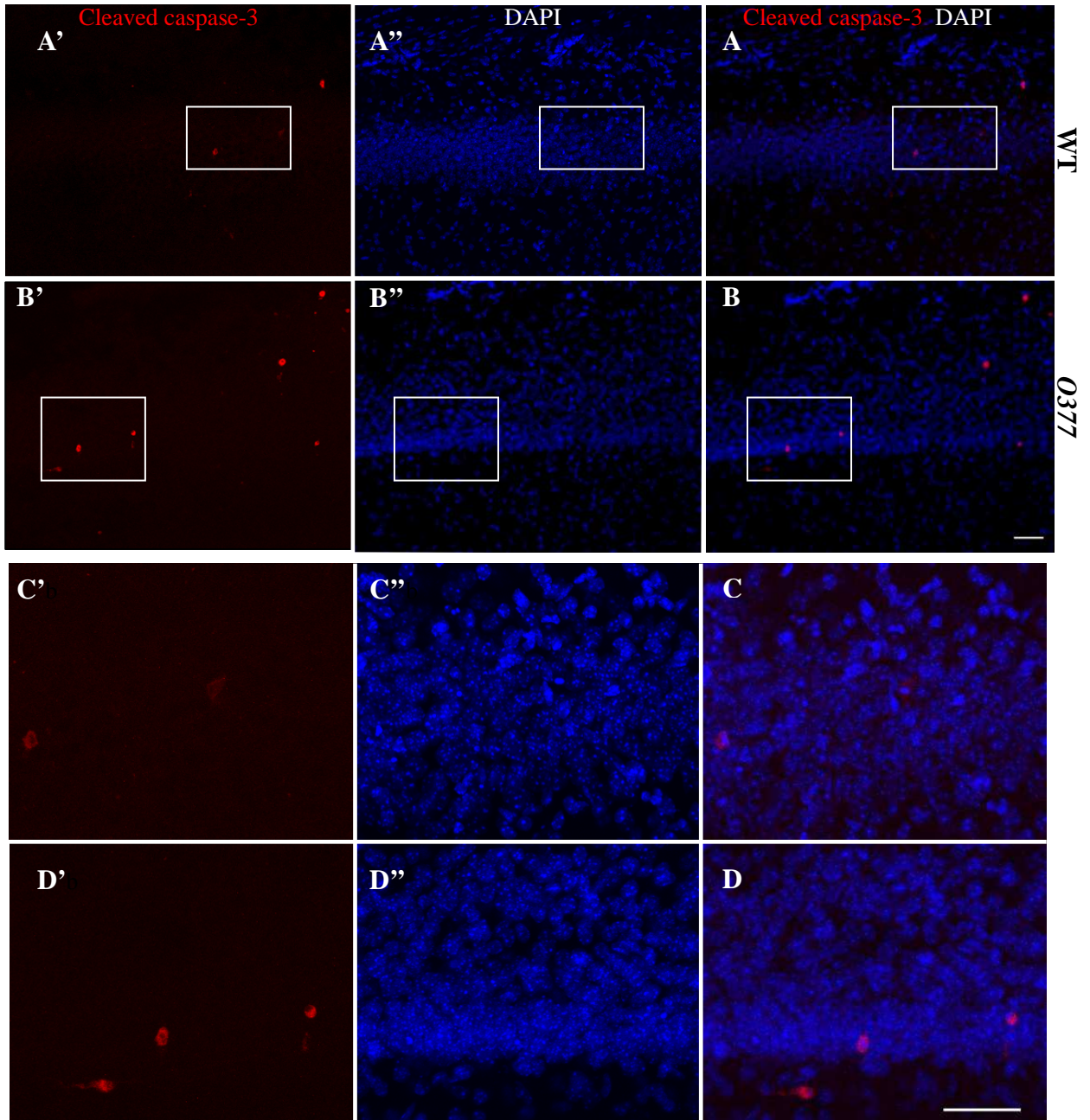
P14 ventral dentate gyrus

Figure 4.31   Apoptotic cell death is increased in P14 *O377* ventral dentate gyrus. Confocal image of anti-cleaved caspase-3 staining in wild type (A') and O377 (B') P14 ventral dentate gyrus. (A'', B'') Confocal image of DAPI staining in wild-type (A'') and O377 (B'') P14 ventral dentate gyrus. (A, B) Confocal merge image of anti-cleaved caspase-3 staining with DAPI staining in P14 wild type (A) and O377 (B) ventral dentate gyrus. (C', D', C'', D'' C, D) Larger image of selected area in A', B', A'', B'', A, B. (E) Relative positive anti-cleaved caspase-3 cell density in wild type and O377 (Wild type =100). * P≤0.05, student t-test, n=4. Scale bar, 40µm. Err bar=± Standard deviation.
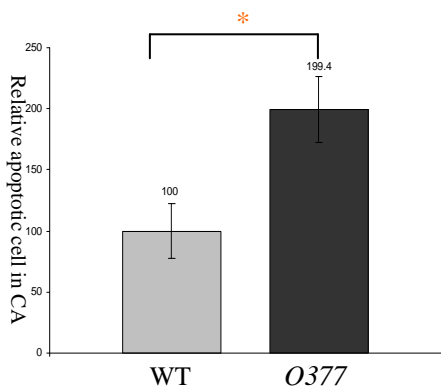
Figure 4.32   Apoptotic cells are increased in P14 O377 ventral CA. Confocal image of anti-cleaved caspase-3 staining in wild type (A') and O377 (B') P14 ventral CA. (A'', B'') Confocal image of DAPI staining in wild type (A'') and O377 (B'') P14 ventral CA. (A, B) Confocal merge image of anti-cleaved caspase-3 staining with DAPI staining in P14 wild-type (A) and O377 (B) ventral CA. (C', D', C'', D'' C, D) Larger image of selected area in A', B', A'', B'', A, B. (E) Relative positive anti-cleaved caspase-3 cell density in wild type and O377 (wild type =100). * P≤0.05, student t-test, n=4.Scale bar, 40μm. Err bar=± standard deviation.
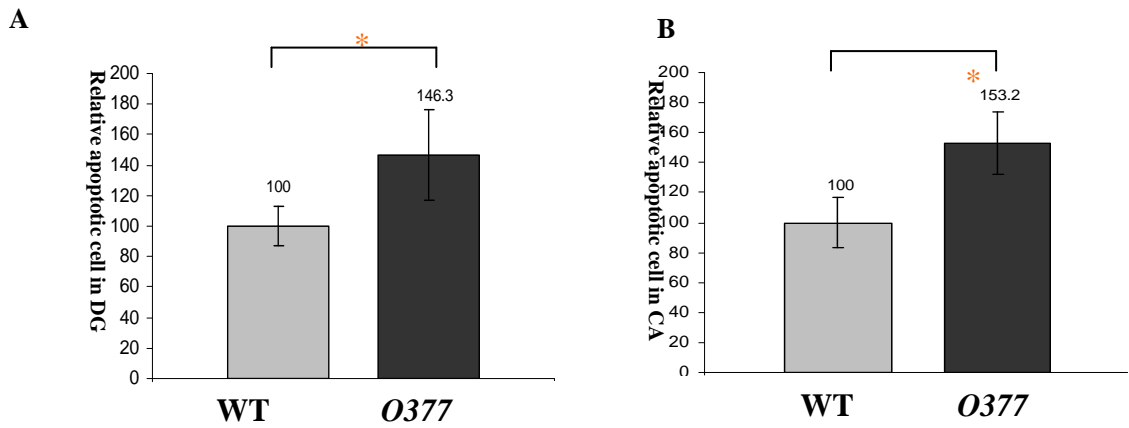
A

B

Figure 4.33 Apoptotic cells are increased in 1-month-old *O377* ventral hippocampus. Relative positive anti-cleaved caspase-3 cell density in one-month-old wild type and O377 (wild type =100) in dentate gyrus (A) and CA region (B).). * P≤0.05, student T-test, n=3. Err bar=± standard deviation.

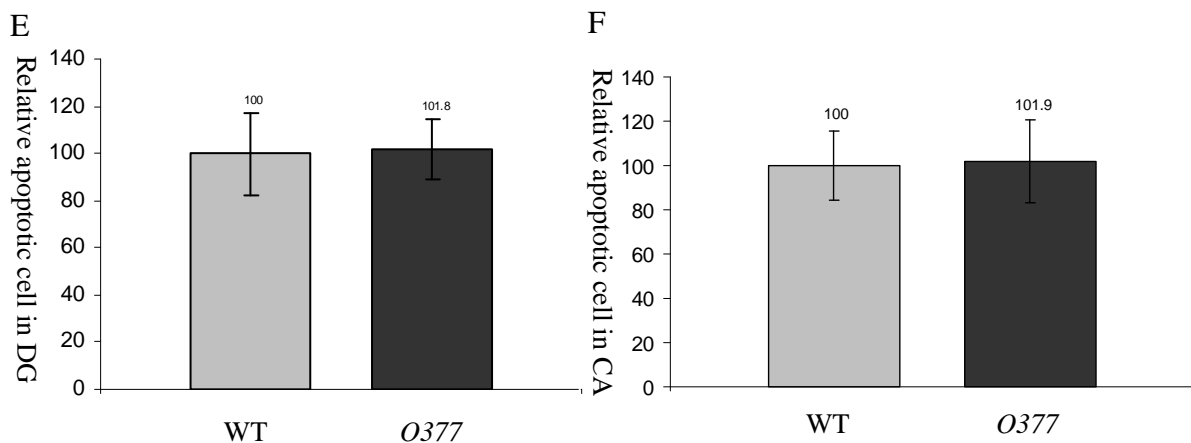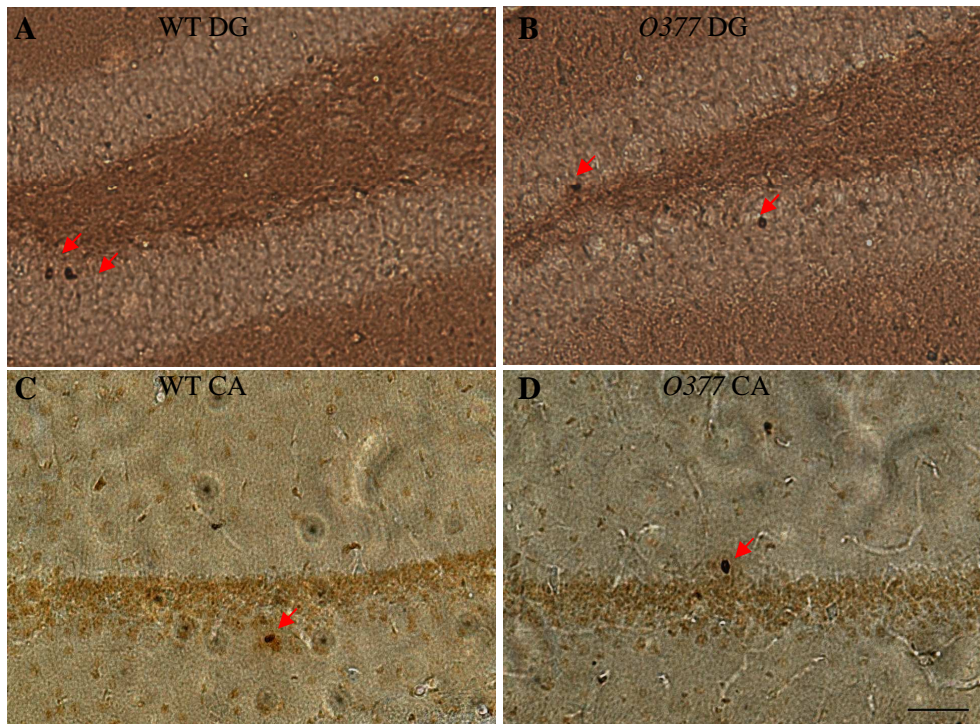**Figure 4.34 Apoptotic cells are not significantly changed in 3-month-old *O377* ventral hippocampus.** (A-D) Image of anti-cleaved caspase-3 immunohistochemistry staining in wild-type DG (A), O377 DG (B), wild-type CA (C), O377 CA (D). (E-F) Relative positive anti-cleaved caspase-3 cell density in 3-month-old wild type and O377 (wild type =100) in dentate gyrus (E) and CA region (F). Scale bar, 50µm. Err bar=± standard deviation.

4.12 *Capn3* is up-regulated in *O377* hippocampus.

Apoptosis is increased in the hippocampus of *O377* mutants compared with wild type. In addition, *Capn3* is expressed in the hippocampus (see chapter 4.3.1), and it plays important roles in apoptotic cell death (Verkhratsky, 2007; Liu et al., 2008). Therefore, I want to quantify the expression level of *Capn3* in the hippocampus of *O377* mutants compared with wild type. As in the ages checked, P14 is the most severe apoptotic stage, so I measured the relative expression level of *Capn3* in the hippocampus of *O377* mutants compared with wild type by relative quantitative real-time PCR using cDNA from hippocampi of wild type and *O377* mutants at the age of P14. The relative *Capn3* expression level is calculated by mRNA level of *Capn3* /mRNA level of *Tuba1a*. *Capn3* expression was found to be significantly increased (132%) in *O377* hippocampus compared with wild type (Figure 4.35). It is consentent with the results of previous chip experiment (for more details see chapter 2.2.6) that *Capn3* is up-regulated in 1-month-old *O377* mutants compared with wild type.

A
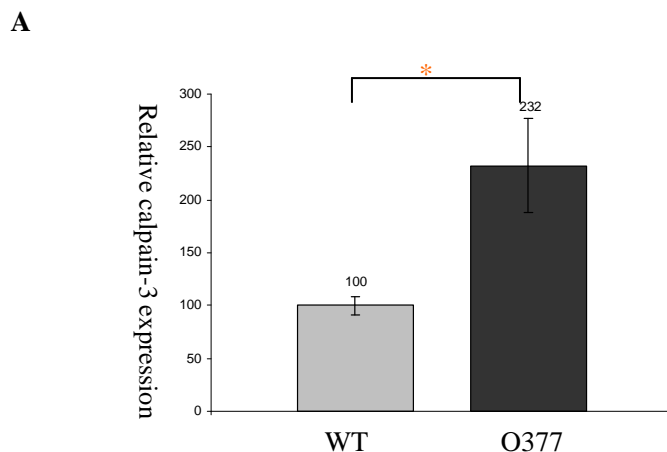
Fig 4.35 *Capn3* **is up-regulated in O377 hippocampus.** (A) Normalized ratio of *Capn3* expression level in wild-type and *O377* mutant hippocampus at P14 (wild type =1), The expression ratios in real-time PCR were calculated according to the $2^{-\Delta\Delta ct}$ method. * P≤0.05, student t-test, n=4-6. Err Bars=±standard err mean.

4.13 NMDA receptor subunits were down-regulated in *O377* mutants

N-methyl-D-aspartate (NMDA) receptors are major synaptic plasticity mediators that play very important roles in learning, memory and cognition in the central nervous system (Okiyama *et al.*, 1997; Hillman *et al.*, 2011). NMDA receptor subunits are suggested to be substrates of the calpain family (Bi *et al.*, 1998; Araújo *et al.*, 2005). Therefore, I performed relative quantitative real-time PCR to check the expression

profiling of four different subunits of NMDA receptor (NR1 encoded by *Grin1*, NR2A encoded by *Grin2a*, NR2B encoded by *Grin2b*, NR2C encoded by *Grin2c*) in hippocampus of *O377* mutants and wild type. The relative gene expression level is determined by the mRNA level of the gene/mRNA level of *Tuba1a*. *Grin1* expression was found to be significantly decreased in 0377 by 37.4%, while *Grin2a*, *Grin2b* and *Grin2c* expression were significantly decreased 50.0%, 46.8% and 45.4%, respectively (Figure 4.36).

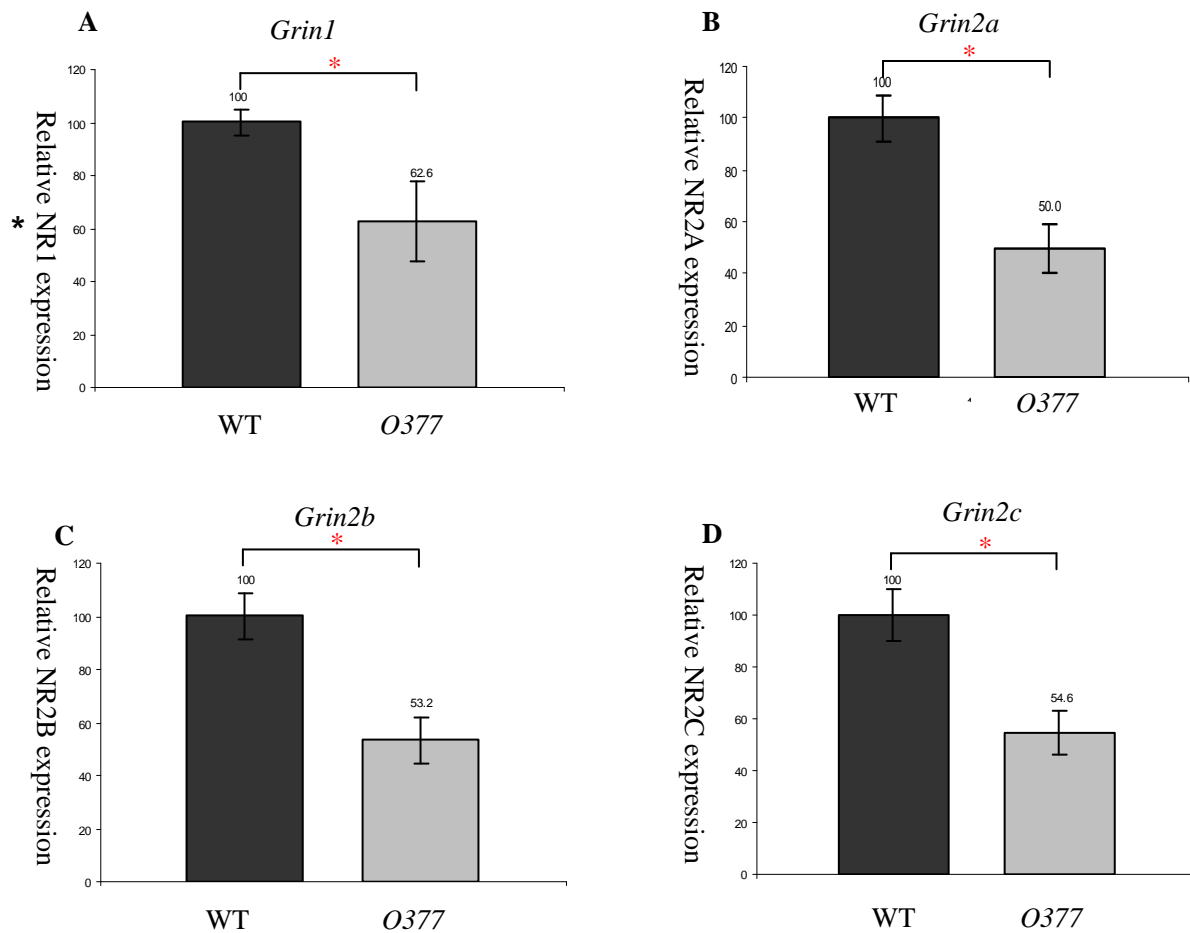**Figure 4.36 Real-time PCR illustrates down-regulation of *Grin1, Grin2a, Grin2b, Grin2c*.** (A-D) Relative expression ratios of *Grin1* (A), *Grin2a* (B), *Grin2b* (C) and *Grin2c* (D) in wild type and O377 at P14 were determined by real-time PCR. The expression ratios are calculated according to the $2^{-\Delta\Delta ct}$ method. * P≤0.05, student T-test, n=4-6.Err bar=± standard err mean.

5 Discussion

5.1 *Crybb2* expression in the brain of wild type and *O377* mutants

By *in situ* hybridization, *Crybb2* is found to be expressed in the Purkinje cells and the granular cells (GC) of the cerebellum; in all layers of the cerebral cortex; in the CA1, CA2, CA3 and the dentate gyrus of the hippocampus; in the glomerular layer, the mitral cell layer and the granule cells of olfactory bulb in 3-month-old wild-type and *O377* brain (see chapter 4.2). In a previous study, Ganguly demonstrated that *Crybb2* is expressed in neurons of the olfactory bulb (mitral cell layer and glomerular layer), hippocampus (pyramidal cells of the CAI, CAII, CAIII regions and granule cells of the dentate gyrus), cerebral cortex (pyramidal cells throughout all layers), and cerebellum (Purkinje cells and stellate cells of the molecular layers) (Ganguly *et al.,* 2008). Compared with previous immunohistochemistry study; I have detected *Crybb2* in more regions (like granlular cells of cerebellum and granule cells of olfactory bulb). However, it should be mentioned that I detected *Crybb2* expression at different ages (present study: 3-month-old; Ganguly's study: 1-month-old), and in different mouse strains (present study: C57BL/6 mice; Ganguly's study: C3H mice). Furthermore, *in situ* hybridization is for mRNA detection, while the immunohistochemistry is for protein.

Crybb2 is also detected at different stages in brain, including E14.5, E16.5, E18.5, P0, P7, P14, P30, and P90 at both *O377* and wild type (see chapter 4.2). This is in contrast to the previous report by Ganguly (Ganguly *et al.*, 2008), who could not detect *Crybb2* transcripts at embryonic stages of the mouse brain. The low level of *Crybb2* mRNA in the embryonic brain, different materials and experimental methods may contribute to these different results. For example, we used different primers in amplifing the *Crybb2* by PCR.

Moreover, βb2 crystallin was demonstrated to be a moderate calcium binding protein (see chapter 4.4). However, only when *Crybb2* is expressed in embryonic stage that I can detect the increase of calcium concentration in the hippocampal neuron of *O377* mutants compared with wild type. Therefore, the increased calcium concentration in embryonic hippocampal neuron of O377 mutants indicates that *Crybb2* is expressed in the embryonic brain and hippocampus.

5.2 Hippocampus structural and function abnormality in *O377* mutants

In many different psychiatric disorders, such as depression (Bremner *et al.*, 2000), Alzheimer's disease (Sparks *et al.,* 2008; Jernigan *et al.,* 1991), epilepsy (Pulsipher *et al.,* 2007; Lawson *et al.,* 2000) and schizophrenia, hippocampal volume reductions have been described.

The hippocampus is located in the medial temporal lobe, beneath the cortical surface. The hippocampus is a paired structure, with mirror-image halves in the left and right sides of the brain. It is composed of cornu amonis (CA) and dentate gyrus, and its morphology is analogous to a seahorse. It has been known for a while that the hippocampus is important for memory formation in spatial navigation (O'Keefe *et al.*, 1978) and certain forms of learning and memory (Eichenbaum, 2000; Squire *et al.*, 2004). In addition, there is increasingly number of evidences that the hippocampus is also involved in anxiety-related behavior (David *et al.*, 2010; Brambilla *et al.*, 2002; Caetano *et al.*, 2001; Trimble *et al.*, 1988).

In the *Philly* mouse, no significant morphological changes are detected compared with wild type, while in *O377* mutant, ventral hippocampus is smaller compared with wild type. Additiionally, volume of dentate gyrus, CA volume and hippocampal volume is found to be significantly decreased by 12% to 20% in the *O377* mutants (see chapter 4.1). These results indicate that the volume of the whole hippocampus and of its sub-regions is reduced, and the reduction in volume increased from 1 month to 3 months. The reduction of the hippocampus volume of *O377* mutant is most likely caused by the increased apoptosis and reduced dendritic complexity observed in the ventral hippocampus (see chapter 4.7 and 4.11).

Interestingly, one of the most consistent brain morphological changes in schizophrenia patients is the reduction in hippocampal volume (Steen *et al.*, 2006; Nelson *et al.*, 1998), even though other parts of the brain also have been reported to be reduced compared with the healthy control. Meta-analyses of schizophrenia patients suggest that reducation in hippocampal volume is about 6% to 8% (Wright *et al.*, 2000; Steen *et al.*, 2006). Compared with present study, the reduction in ratio of hippocamal volume in human schizophrenia patient is not as pronounced as in our *O377* mutants. However, it should be mentioned that mice and human would have different response to the same defect. On the other side, the genetic background of

the human patient is much more complicated, and the environment is also much more different.

The most prominent behavioral alteration in the male *O377* mutants is observed in the prepulse inhibition analysis. Assessment of prepulse inhibition revealed a clear increase in homozygous male *O377* mutants at different pre-pulse intensities (personal communication by Dr. Sabine Hölter-Koch, unpublished data).

The observed prepulse inhibition change indicates altered sensorimotor gating. Sensorimotor gating means the ability of a weak sensory event to inhibit ("gate") the response to an intense sensory stimulus. Deficits of prepulse inhibition reveals in the inability to filter out unnecessary information. Many brain areas have been reported to be involved in regulating the prepulse inhibition including hippocampus (Swerdlow *et al.*, 2001; Koch *et al.*, 1999).

Caine and colleagues demonstrated that infusion of the cholinergic agonist carbachol into the dentate gyrus disrupts prepulse inhibition in the rat (Caine *et al.*, 1991). In addition, they microinjected carbachol into CA1 and dentate gyrus caused depressing startle. Carbachol infusion decreased prepulse inhibition with regional rank-order potency CA1 greater than dentate gyrus. CA1 infusions depressed the startle reflex more potently, while dentate gyrus infusions preferentially decreased prepulse inhibition. In rat with a lesion in the ventral hippocampus, the acoustic startle response was increased and the prepulse inhibition was impaired compared with the animal without lesion (Daenen *et al.*, 2003). More recently, mice with ablation of the expression of the *GluR4* at hippocampus showed impaired prepulse inhibition (Sagata *et al.*, 2010). In addition, the forebrain-specific *Smad4* knock-out mice, which ablated the expression of *Smad4* at hippocampus and cortex, also demonstrated a deficit of prepulse inhibition (Sun *et al.*, 2010). These results demonstrate that the hippocampus is associated to acoustic startle reflex and prepulse inhibition.

A growing number of studies now suggest that the hippocampus may be functionally separated into different subregions (Fanselow *et al.*, 2010; Engin *et al.*, 2007). There is evidence for at least two distinct functional domains, dorsal and ventral regions, each associated with a distinct set of behaviors. Dorsal hippocampus has a role in learning and memory, especially in spatial learning, while ventral hippocampus may have a role in brain processes associated with anxiety-related behaviors.

There is increasing evidence that ventral hippocampus is also associated with prepulse inhibition. Prepulse inhibition of the acoustic startle response and open-field locomotor activity was measured after infusion of *N*-methyl-D-aspartate into the ventral and dorsal hippocampus of Wistar rats. Dose-dependent hyperactivity and disruption of prepulse inhibition were observed after ventral infusions but not after dorsal infusions (Zhang *et al.*, 2002). This study indicates the susceptibility of prepulse inhibition to NMDA-induced overactivity of the ventral hippocampus. The susceptibility of prepulse inhibition to disruption activity of ventral hippocampus was also confirmed by injection of the dopamine agonist apomorphine and psychotomimetic drugs like phencyclidine and amphetamine (Kusljic, 2004; Swerdlow *et al.*, 2004).

Therefore, it can be concluded here that the reduced volume of the ventral hippocampus is very consistent with the deficiency in *O377* mutants prepulse inhibition test. These results indicate that *O377* mutants show structural and functional abnormalities in hippocampus.

5.3 Calcium homeostasis in *O377* mutants

In the γβ-crystallin family, β-crystallins were first reported to have calcium binding ability (Sharma *et al.*, 1989). γ-crystallins were also proved to have calcium binding ability by the same group, and the Greek key motif in the protein were suggested as a potential binding site for calcium. Carver and colleagues did a ^{1}H-NMR spectroscopic study of homodimer of βB2-crystallin suggesting that terminal extension of βB2-crystallin is not involved in calcium binding (Carver *et al.*, 1993). However, by using calcium assays, isothermal titration calorimetry, and ^{15}N-^{1}H heteronuclear single quantum correlation NMR spectroscopy, Jobby and Sharma demonstrated that βb2-crystallin is a calcium binding protein (Jobby *et al.*, 2007).

To confirm the calcium binding ability of βB2-crystallin, I used NMR spectroscopy to determine the changes in ^{15}N-^{1}H HSQC spectra of the βB2-crystallin caused by calcium binding. Two spectra of ^{15}N-^{1}H HSQC, recording free calcium and calcium saturated protein, have been overlapped for comparison. The addition of Ca^{2+} resulted in the alteration and shift of the spectra, suggesting calcium binding of βB2-crystallin (see chapter 4.4).

To analyze the effect of the mutation in *O377* mutants in calcium homeostatsis, I analyzed the calcium concentration in embryonic hippocampal neurons of *O377*

mutants and wild type. Basal free calcium concentration in the *O377* hippocampal neurons is higher compared with wild type (see chapter 4.4). This indicates that the mutation in the *O377* mutants leads to a loss of calcium binding ability, at least in part, thus more free calcium is present in the hippocampal neurons.

Increase in calcium concentration mediates a wide range of cellular responses. Calcium signal-transduction mechanisms are central to the development and plasticity of the nervous system, including activity-dependent cell survival, modulation of synaptic strength, and calcium-mediated cell death (Di *et al.*, 2007; LaFerla *et al.*, 2002). In *O377* mutants, I detected an up-regulation of *Capn3* (encoding calpain-3 protein, a calcium-depend protease), compared with wild type at early postnatal age. Interaction of calpain and NMDA receptors has been reported in many diseases (GoniOliver *et al.*, 2009; Bevers 2009; Nimmrich 2008), and NMDA receptor subunits are reported as substrates of the calpain family (Bi *et al.,* 1998; Araújo *et al.*, 2005; Wu *et al.*, 2005). Using quantitative real-time PCR, the expression of four different subunits of NMDA receptor (NR1, NR2A, NR2B, NR2C) in the hippocampus of *O377* mutants was found to be significantly decreased compared with wild type. The down-regulation of NMDA receptors may be the response to functional changes of NMDA receptors.

NMDA receptors are highly permeable to Ca^{2+}, and Ca^{2+} influx through NMDA receptors is essential for synaptogenesis and synaptic transmission in the central nervous system (Bi *et al.,* 1998; Wu *et al.*, 2005). When I stimulated hippocampal neurons by NMDA, calcium increment in *O377* hippocampal neurons was increased compared to wild type. It is consistent with previous reports that the hypofunction of NMDA receptors in the hippocampus is a common phenotype of schizophrenia (Belforte *et al.*, 2010; Rejesuce *et al.,* 2006).

My second conclusion is that the increase in free calcium concentration in hippocampal neurons caused by the mutation in *Crybb*2 might activate the calcium-dependent protease calpain-3, and the activated calpain-3 could diminish NMDA receptor by digestion. Loss of the NMDA receptors might disturb normal calcium influx in hippocampal neurons, which might further deteriorate the calcium homeostasis.

5.4 Neuronal morphology change in *O377* mutants

A variety of studies has documented considerable evidence that dendritic complexity (dendritic length and branches) is relatively dynamic (Leuner and Gould, 2010; Gao *et al.*, 2007). Moreover, dendrite complexity is the major indication how neurons integrate and process incoming information, and thus, they play a vital role in the functional properties of neural circuits (Kolb and Whishaw, 1998).

In the present study, average number of branches is found to be significantly reduced in the neurons of the dentate gyrus in *O377* mutants compared with wild type, and total length of neurons at dentate gyrus of *O377* mutants is reduced but not significantly changed compared with wild type. This is consistent with a previous Golgi staining study in human schizophrenia patients. Broadbelt and colleagues described a significant decrease in the number of both primary and secondary basilar dendrites in both layer III and layer V of pyramidal neurons (Broadbelt *et al.*, 2002). In schizophrenia related mouse models, hippocampal neuronal complexity is also reported to be reduced compared with wild type control (Kvajo *et al* 2008). However, it should be mentioned that alterations in dendritic complexity also have been observed in other psychiatry disordes like Rett syndrome and posttraumatic stress disorders (Jentarra *et al.*, 2010; McEwen, 2003; Armstrong *et al.*, 1998). Changes in dendritic complexity may be only an indicator of altered information processes and integration in neurons rather than a specific and typical phenotype in schizophrenia.

Crybb2 was found to be strongly up-regulated in regenerating retinal ganglion cells (RGCs) (Liedtke *et al.*, 2007). *Crybb2* was demonstrated to be expressed in the retinal and hippocampal neurons by immunohistochemistry. Over-expression of *Crybb2* promotes axonal outgrowth in RGCs and hippocampcal neurons, suggesting that βB2-crystalline plays an important role in axonal growth. Therefore, it is not surprising that I found the reduced complexity of hippocampus dendrites in the *O377* mutants

The expression pattern of *Tmsb4X* in *O377* mutants was not altered compared with wild type. However, a higher expression of *Tmsb4x* in *O377* mutants was observed (see chapter 4.3). In addition, β-thymosins are a family of actin monomer (G-actin) sequestering proteins widely expressed in the mouse and human (Ericksson-Viitanen *et al.,* 1983). *Tmsb4x* (thymosin β4) is a small polypeptide having one of the highest expression levels among the thymosin family (Yu *et al.*, 1993). As a cytoskeleton

protein, Thymosin β4 was reported to be involved in axonal outgrowth (Yang *et al.*, 2008). Down regulation of thymosin β4 was reported to lead to enhanced neurite outgrowth (Mollinari *et al.*, 2009). The role of *Crybb2* and thymosin β4 in axonal outgrowth and up-regulation of thymosin β4 in *O377* mutants suggest that *Crybb2* mediates the axonal outgrowth by thymosin β4. However, controversial results about thymosin β4 also suggested that thymosin β4 overexpression would also greatly promote axonal outgrowth (Yang *et al.*, 2008). Further studies are required to investigate the role of thymosin β4 in the reorganization of actin cytoskeleton (depolymerization or polymerization) that occurs during axon outgrowth of *O377* mutant and wild type neurons. However, it is conceivable that in *O377* mutants neurons the effects of overexpressed thymosin β4 inhibit the axonal outgrowth and branching by directly binding to G-actin and promote depolymerization of filament actin.

Microtubule associated protein 2 (MAP2) is a cytoskeleton protein, which is closely related to the neuronal elongation, branching and neuronal plasticity (Chamak *et al.*, 1987; Jochson *et al.*, 1992). Therefore, MAP2 protein level is a very good indicator for neuronal morphology and plasticity. Loss of MAP2 immunoreactivity is observed in hippocampus and cortex area in aged rats (Chuahan *et al.*, 1997), which suggests MAP2 is related to hippocampus and cortical functional impairment with aging.

In the present study, increase of MAP2 staining intensity and disarrangement of cell processes were detected at dentate gyrus in one-year-old *O377* mutants compared with wild-type (Figure 4.21). Increase of MAP2 immunoreactivity was also detected in granular cells and neurons in the hilus at 1-year-old *O377* mutants (Figure 4.22). A small population of granular cells with bigger cell body with MAP2 staining was also observed in *O377* mutants (Figure 4.22). My results are consistent with the results of Cotter and his colleagues showing an elevated in MAP2 immunoreactivity in schizophrenic subjects in the hippocampus region (Cotter *et al* 2000). However, the opposite results have also been observed; reduced MAP2 immunoactiviety has often been observed in schizophrenia patients (Somenarain *et al.*, 2010; Rioux *et al.*, 2004; Cotter *et al.,* 1997). Altered expression of MAP2 also has been detected in other psychiatry disorders like Huntington's disease and autism (Diprospero, *et al.*, 2004, Mukaetova-Ladinska *et al.*, 2004). This suggests that MAP2 protein level is closely related to the neuronal plasticity and neuron morphology, but it is not a specific indicator for schizophrenia.

My finding of changes in the neuronal morphology is focused on the dentate gyrus of hippocampus; in further experiments, it would be necessary to expand to other regions of the brain like the CA region of hippocampus and the prefrontal cortex. Furthermore, to analyze the functional consequence of reduction in dendrite complexity, further experiments like electroencephalography would be necessary.

Therefore, my third conclusion is that the reduction in neuronal dendritic complexity and increase in MAP2 is an indication of an alteration in synaptic plasticity and hippocampus function. It is associated with the observation that there is an impairment in prepulse inhibition in *O377* mutant, which is consistent with a previous observation (Quach *et al.,* 2008). In this study, they also found an alteration of prepulse inhibition and dendritic abnormalities in mouse hippocampus with targeted disruption of the collapsin response mediator protein-3 (*Crmp3*) gene.

5.5 Specific loss of parvalbumin positive GABAergic interneurons in *O377* mutants

The most robust pathological change observed in schizophrenia patients is a decrease in GABAergic interneurons, especially parvalbumin positive GABAergic interneurons (Tooney *et al.*, 2004; Reynolds *et al.*, 2001; Beasley *et al.,* 1997). As a promising schizophrenia mouse model, I also examined parvalbumin positive GABAergic interneurons together with calretinin positive GABAergic interneurons and cell density of somatostatin positive GABAergic interneurons in the prefrontal cortex and the hippocampal region of *O377* mutants and wild type. In our study, the cell density of parvalbumin positive GABAergic interneurons in the ventral hippocampus of *O377* mutants is significantly reduced compared with wild type mice, while the cell density in prefrontal cortex is not changed. In addition, the reduction in parvalbumin positive GABAergic interneurons appears to be age-dependent (see chapter 4.9).

This is consistent with a previous study showing that in schizophrenia patients parvalbumin positive GABAergic interneurons are reduced only in the hippocampus but not in the prefrontal cortex (Tooney *et al.*, 2004). However, others also observed that parvalbumin positive GABAergic interneurons are also detected to be reduced at prefrontal cortex region in schizophrenia patients (Reynolds *et al.,* 2001; Beasley *et al.,* 1997). The difference might be caused by the environment or genetic background of the schizophrenia patients. Different counting methods like unbiased stereological

counting would be greatly improving the reliability of data (Dorph-Peterson *et al.*, 2011; West *et al.*, 1999).

A decrease in parvalbumin positive GABAergic interneurons is also observed in many animal models of schizophrenia, including methylazoxymethanol acetate (MAM) treated rats (Lodge *et al.*, 2009; Penschuck *et al.*, 2006), phencyclidine (PCP) treated rats (Rujescu *et al.*, 2006), in rats treated by social isolation (Harte *et al.*, 2007) and the amygdala activation model (Berretta *et al.*, 2004). In addition, the loss of parvalbumin positive GABAergic interneurons is also observed in a postnatal NMDA ablation mouse model for schizophrenia (Belforte *et al.*, 2010). These studies clearly demonstrate the reduction of parvalbumin positive GABAergic interneurons being closely related to schizophrenia.

Loss of parvalbumin positive GABAergic interneurons have also been observed in the hilus of hippocampus in patients with epilepsy (Gill *et al.*, 2010; Zhu *et al.*, 1997). However, in patients of epilepsy or mouse models of epilepsy, loss of GABAergic interneurons is not limited to the parvalbumin positive subtype. Loss of calretinin positive GABAergic interneurons and somatostatin positive GABAergic interneurons could also be observed in epilepsy (Cobos *et al.*, 2005; Treiman, 2001). Compared with epilepsy, loss of parvalbumin positive GABAergic interneurons in schizophrenia patients and mouse models is more specific and typical.

In the current study, four different NMDA receptor subunits are significantly down-regulated in *O377* hippocampus compared with the wild type (see chapter 4.13). It has been reported that animals treated with NMDA receptor antagonists show a loss of parvalbumin positive GABAergic interneurons resulting in a syndrome that highly mimics clinical features of schizophrenia (Lodge *et al.,* 2009; Penschuck *et al.*, 2006; Rujescu *et al.*, 2006). In addition, the *Grin1* knock out mice model also reminisce the schizophrenia phenotype and is associated with the reduction of parvalbumin positive GABAergic interneurons. This may be able to be explained, at least in part, by blockade of the NMDA receptors that are located on GABAergic neurons, which have been shown to be 10-fold more sensitive to NMDA receptor antagonists than the NMDA receptor on pyramidal neurons (Green *et al.*, 2000; Grunze *et al.*, 1996). In addition, NMDA receptor (NR2A) was observed to be expressed five times more in parvalbumin positive GABAergic interneurons than in pyramidal neurons (Kinney *et al.*, 2006). Moreover, blocking of NMDA receptors was reported to release an

excessive amount of glutamate, which is toxic to the blocked neurons (Moghaddam *et al.*, 1997). All these informations illustrate that the down-regulation of NMDA receptor subunits found in early postnatal age of *O377* mutants is associated with reduction of parvabumin positive GABAergic interneurons.

Parvalbumin positive GABAergic interneurons predominantly innervate the perisomatic regions of projection neurons, so that most of their synaptic contacts cluster around the somata and the proximal portion of target primary dendrites (Freund *et al.*, 1996). Therefore, parvalbumin positive GABAergic interneurons were suggested to be important for neuronal synchronization (Freund *et al.*, 2003). In addition, parvalbumin positive GABAergic interneurons have been suggested to be involved in gamma oscillations (Fuchs *et al.*, 2007; Freund *et al.*, 2003; Sohal *et al.*, 2009), which are suggested to enhance information processing (Womelsdorf *et al.*, 2007). Therefore, it is not surprising that the *O377* mutant show an impairment of prepulse inhibition in behavior test, which is an indication for an unsuccessful information process (Swerdlow *et al.*, 2001; Koch *et al.*, 1999).

The *O377* mutants showed no differences in GABA-receptor mediated postsynaptic inhibition in whole cell patch clamp recording, which is out of our expectation. It may be due to the intense innervation of granule cells by numerous types of GABAergic interneurons (Ribak and Shapiro, 2007).

My fourth conclusion is that loss of parvalbumin positive GABAergic interneurons in *O377* mutants is a very special phenotype in schizophrenia patients. It is strong evidence that *O377* mouse is a very promising schizophrenia mouse model.

5.6 *O377* mutant and glutamate hypothesis of schizophrenia

In the present study, the NMDA receptor subunits are down regulated in *O377* mutants compared with wild type. In addition, the increment of calcium concentration in the hippocampal neurons of *O377* mutants after stimulation by NMDA is significantly higher than in the wild type, which indicates that *O377* mutants show a functional abnormality of NMDA receptor. NMDA receptors are a major subtype of glutamate receptors and mediate slow excitatory postsynaptic potentials. Inhibition of NMDA receptors or reduction of NMDA receptor could produce schizophrenia like phenotypes in human and in mouse models (Belforte *et al.*, 2010; Rujescu *et al.*, 2006; Moghaddam *et al.*, 1997).

Postmortem studies in schizophrenia patients showed changes in glutamate receptor related genes, like *Grin1*, *Grin2a* encoding NMDA receptor subunits. Some NMDA receptor-affiliated intracellular proteins such as PSD95 and SAP102 are changed in different regions of the brain (Kristiansen *et al.,* 2010; Clinton *et al.*, 2004). Many studies have also been done by administration of a single low dose of NMDA receptor antagonists such as phencyclidine (PCP) or ketamine producing "schizophrenia like" symptoms in healthy individuals (Krystal *et al.,* 1994; Javitt *et al.,* 1991). The range of symptoms produced by these agents resembles positive (delusion and hallucination), negative (avolition, apathy, and blunted affect), and cognitive (deficits in attention, memory, and abstract reasoning) symptoms of schizophrenia, as well as disruptions in smooth-pursuit eye movements and prepulse inhibition of startle. After ketamine administration, healthy volunteers show similar disruptions in working memory and thought disorders like schizophrenia patients (Adler *et al.*, 1999). Further administration of ketamine in schizophrenia patients could profoundly exacerbate symptoms (Lahti *et al.,* 1995).

In addition, many animal models of schizophrenia are produced by administration of NMDA antagonists including methylazoxymethanol acetate (MAM) (Lodge *et al.,* 2009; Penschuck *et al.*, 2006), phencyclidine (PCP) (Rujescu *et al.*, 2006) (for more detail please see chapter 5.5). These animals showed reduced gamma-band response to a conditioned tone, deficits of oscillatory activity in the medial prefrontal cortex and in the ventral hippocampus. The *O377* mutants also show deficits in prepluse inhibition compared with wild type, which indicates altered sensorimotor gating, which is consistent with the observation in animal models as well as schizophrenia patients.

The observed loss of parvalbumin positive GABAergic interneurons is an evidence that our mouse model is in agreement with the glutamate hypothesis of schizophrenia, since the loss of parvalbumin positive GABAergic interneuron is consistently observed in NMDA hypofunction mouse model for schizophrenia (Belforte *et al.*, 2010; Rujescu *et al.*, 2006) (For more details please see chapter 5.3).

Therefore, my fifth conclusion is that the observation in *O377* mice fits very well with the glutamate hypothesis of schizophrenia. It is another evidence that *O377* mouse is a very promising schizophrenia mouse model.

5.7 *Crybb2* is a new candidate gene for schizophrenia

In the present study, loss of parvalbumin positive GABAergic interneurons, abnormality in hippocampal morphology, reduction in neuronal dendritic complexity, increase in MAP2 staining and down-regulation of the expression of NMDA receptor coding genes are observed in the *O377* mutant mouse. In addition, the mutation in *Crybb*2 leads to an imbalance in the calcium homeostasis, which activates the calcium-depend protease calpain-3 and *Tmsb4x* that contribute to the abnormalities observed in *O377* mutants. Moreover, in the behavior test, the *O377* mice show impairment in prepulse inhibition (personal communication with Dr.Sabine Hölter, unpublished data).

Additionally, the genome scan meta-analysis of schizophrenia in 2003 shows that the human chromosomal region harbouring *CRYBB2* (22q11.2) is linked to schizophrenia, as well as to schizophrenia-related intermediate phenotypes of reduced P50 suppression (sensory gating) and altered antisaccade eye movement (Lewis *et al.*, 2003). In this region, the *COMT* gene (catechol-O-methyltransferase) has often been reported to be involved in schizophrenia and schizophrenia related phenotypes (DeRosse *et al.*, 2006; Quednow *et al.*, 2010). Harbouring in 22q11.2, *CRYBB2* gene is close to *COMT* gene in the human chromosome 22. In addition, the linkage analysis conducted by Dr. Rujescu showed that polymorphic sites in *CRYBB2* are associated with schizophrenia related intermediate phenotypes (personal communication, unpublished data). All these data together make the *Crybb2* gene a good candidate for schizophrenia research.

However, my observation is not necessarily limited to the model of schizophrenia. Many other diseases like depression (Bremner *et al.*, 2000), Alzheimer's disease (Sparks *et al.*, 2008; Jernigan *et al* 1991) and epilepsy (Pulsipher *et al* 2007, Lawson *et al.*, 2000) are also associated with hippocampal volume reduction. In addition, the neuronal dendritic complexity, and MAP2 staining abnormality is common within the neurological diseases, as dendrite and cytoskeleton of neurons itself is very dynamic (Leuner and Gould 2010; Gao *et al.*, 2007). The specific loss of parvalbumin positive GABAergic interneurons in hippocampus can also be observed in a few cases of epilepsy, even though in patients with epilepsy, the loss of parvalbumin positive GABAergic interneurons is only found in the hilus of the hippocampus (Gill *et al.*, 2010; Zhu *et al.*, 1997). Moreover, alteration in expression of NMDA receptors is a

very common finding in Huntington's disease, Parkinson's disease and Alzheimer's disease (Fernandes *et al.,* 2009; Bustos *et al.*, 2009; Geddes et al., 1986). In addition, prepulse inhibition is a measure of sensorimotor gating and is reduced in patients with many neuropsychiatric disorders like Huntington's diseases and Parkinson's disease (Swerdlow *et al.*, 2001). Furthermore, the *O377* mouse shows unexpected results in the whole cell recording in the ventral dentate gyrus.

In a further study, we may also check the GABAergic interneuron cell density in other regions, which are involved in the prepulse inhibition. Although I detected the specific loss of parvalbumin positive GABAergic interneurons, the functional consequences of this deficit are still largely unknown. Therefore, electroencephalography recordings for the analysis of the functional changes in the hippocampus should be performed. In addition, calcium homestasis changed in the *O377* may cause other calcium signalling alterations which also need to be classified.

Nevertheless, it should be noted that no animal model could fully reproduce all facets of the corresponding human disease. The *O377* mutant resembles many important features that could be observed in postmortem schizophrenia brains and established schizophrenia animal models. Therefore, it is very valuable for psychiatric research, especially for schizophrenia research.

6 References

Aarts, H.J., Lubsen, N.H., and Schoenmakers, J.G. (1989). Crystallin gene expression during rat lens development. Eur J Biochem *183*, 31-36.

Abe, S., Katagiri, T., Saito-Hisaminato, A., Usami, S., Inoue, Y., Tsunoda, T., and Nakamura, Y. (2003). Identification of CRYM as a candidate responsible for nonsyndromic deafness, through cDNA microarray analysis of human cochlear and vestibular tissues. Am J Hum Genet *72*, 73-82.

Adler, C.M., Malhotra, A.K., Elman, I., Goldberg, T., Egan, M., Pickar, D., and Breier, A. (1999). Comparison of ketamine-induced thought disorder in healthy volunteers and thought disorder in schizophrenia. Am J Psychiatry *156*, 1646-1649.

Anadon, R., Rodriguez Moldes, I., Carpintero, P., Evangelatos, G., Livianou, E., Leondiadis, L., Quintela, I., Cervino, M.C., and Gomez-Marquez, J. (2001). Differential expression of thymosins beta(4) and beta(10) during rat cerebellum postnatal development. Brain Res *894*, 255-265.

Arai, H., and Atomi, Y. (1997). Chaperone activity of alpha B-crystallin suppresses tubulin aggregation through complex formation. Cell Struct Funct *22*, 539-544.

Araujo, I.M., Xapelli, S., Gil, J.M., Mohapel, P., Petersen, A., Pinheiro, P.S., Malva, J.O., Bahr, B.A., Brundin, P., and Carvalho, C.M. (2005). Proteolysis of NR2B by calpain in the hippocampus of epileptic rats. Neuroreport *16*, 393-396.

Aravind, P., Mishra, A., Suman, S.K., Jobby, M.K., Sankaranarayanan, R., and Sharma, Y. (2009). The betagamma-crystallin superfamily contains a universal motif for binding calcium. Biochemistry *48*, 12180-12190.

Armstrong, D.D., Dunn, K., and Antalffy, B. (1998). Decreased dendritic branching in frontal, motor and limbic cortex in Rett syndrome compared with trisomy 21. J Neuropathol Exp Neurol *57*, 1013-1017.

Arnold, S.E., Lee, V.M., Gur, R.E., and Trojanowski, J.Q. (1991). Abnormal expression of two microtubule-associated proteins (MAP2 and MAP5) in specific subfields of the hippocampal formation in schizophrenia. Proc Natl Acad Sci U S A *88*, 10850-10854.

Bateman, J.B., von-Bischhoffshaunsen, F.R., Richter, L., Flodman, P., Burch, D., and Spence, M.A. (2007). Gene conversion mutation in crystallin, beta-B2

(CRYBB2) in a Chilean family with autosomal dominant cataract. Ophthalmology *114*, 425-432.

Beasley, C.L., and Reynolds, G.P. (1997). Parvalbumin-immunoreactive neurons are reduced in the prefrontal cortex of schizophrenics. Schizophr Res *24*, 349-355.

Belforte, J.E., Zsiros, V., Sklar, E.R., Jiang, Z., Yu, G., Li, Y., Quinlan, E.M., and Nakazawa, K. (2010). Postnatal NMDA receptor ablation in corticolimbic interneurons confers schizophrenia-like phenotypes. Nat Neurosci *13*, 76-83.

Benes, F.M., and Berretta, S. (2001). GABAergic interneurons: implications for understanding schizophrenia and bipolar disorder. Neuropsychopharmacology *25*, 1-27.

Berretta, S., Lange, N., Bhattacharyya, S., Sebro, R., Garces, J., and Benes, F.M. (2004). Long-term effects of amygdala GABA receptor blockade on specific subpopulations of hippocampal interneurons. Hippocampus *14*, 876-894.

Berridge, M.J. (1993). Inositol trisphosphate and calcium signalling. Nature *361*, 315-325.

Bettelheim, F.A., and Chen, A. (1998). Thermodynamic stability of bovine alpha-crystallin in its interactions with other bovine crystallins. Int J Biol Macromol *22*, 247-252.

Bevers, M.B., Lawrence, E., Maronski, M., Starr, N., Amesquita, M., and Neumar, R.W. (2009). Knockdown of m-calpain increases survival of primary hippocampal neurons following NMDA excitotoxicity. J Neurochem *108*, 1237-1250.

Bhat, S.P. (2003). Crystallins, genes and cataract. Prog Drug Res *60*, 205-262.

Bi, X., Rong, Y., Chen, J., Dang, S., Wang, Z., and Baudry, M. (1998). Calpain-mediated regulation of NMDA receptor structure and function. Brain Res *790*, 245-253.

Black, J.E., Kodish, I.M., Grossman, A.W., Klintsova, A.Y., Orlovskaya, D., Vostrikov, V., Uranova, N., and Greenough, W.T. (2004). Pathology of layer V pyramidal neurons in the prefrontal cortex of patients with schizophrenia. Am J Psychiatry *161*, 742-744.

Bluhm, W.F., Martin, J.L., Mestril, R., and Dillmann, W.H. (1998). Specific heat shock proteins protect microtubules during simulated ischemia in cardiac myocytes.

Am J Physiol *275*, H2243-2249.

Borras, T., and Rodokanaki, A. (1989). Primary structure of zeta-crystallin protein from guinea pig. Its similarity to the enzyme alcohol dehydrogenase. Lens Eye Toxic Res *6*, 795-805.

Braak, H., Del Tredici, K., Sandmann-Kiel, D., Rub, U., and Schultz, C. (2001). Nerve cells expressing heat-shock proteins in Parkinson's disease. Acta Neuropathol *102*, 449-454.

Brady, J.P., Garland, D.L., Green, D.E., Tamm, E.R., Giblin, F.J., and Wawrousek, E.F. (2001). AlphaB-crystallin in lens development and muscle integrity: a gene knockout approach. Invest Ophthalmol Vis Sci *42*, 2924-2934.

Brakenhoff, R.H., Aarts, H.J., Schuren, F., Lubsen, N.H., and Schoenmakers, J.G. (1992). The second human beta B2-crystallin gene is a pseudogene. Exp Eye Res *54*, 803-806.

Brambilla, P., Barale, F., Caverzasi, E., and Soares, J.C. (2002). Anatomical MRI findings in mood and anxiety disorders. Epidemiol Psichiatr Soc *11*, 88-99.

Bremner, J.D., Narayan, M., Anderson, E.R., Staib, L.H., Miller, H.L., and Charney, D.S. (2000). Hippocampal volume reduction in major depression. Am J Psychiatry *157*, 115-118.

Broadbelt, K., Byne, W., and Jones, L.B. (2002). Evidence for a decrease in basilar dendrites of pyramidal cells in schizophrenic medial prefrontal cortex. Schizophr Res *58*, 75-81.

Buchanan, R.W., Vladar, K., Barta, P.E., and Pearlson, G.D. (1998). Structural evaluation of the prefrontal cortex in schizophrenia. Am J Psychiatry *155*, 1049-1055.

Bustos, G., Abarca, J., Bustos, V., Riquelme, E., Noriega, V., Moya, C., and Campusano, J. (2009). NMDA receptors mediate an early up-regulation of brain-derived neurotrophic factor expression in substantia nigra in a rat model of presymptomatic Parkinson's disease. J Neurosci Res *87*, 2308-2318.

Caetano, S.C., Sassi, R., Brambilla, P., Harenski, K., Nicoletti, M., Mallinger, A.G., Frank, E., Kupfer, D.J., Keshavan, M.S., and Soares, J.C. (2001). MRI study of thalamic volumes in bipolar and unipolar patients and healthy individuals.

Psychiatry Res *108*, 161-168.

Caine, S.B., Geyer, M.A., and Swerdlow, N.R. (1991). Carbachol infusion into the dentate gyrus disrupts sensorimotor gating of startle in the rat. Psychopharmacology (Berl) *105*, 347-354.

Carlsson, A., and Lindqvist, M. (1963). Effect of Chlorpromazine or Haloperidol on Formation of 3methoxytyramine and Normetanephrine in Mouse Brain. Acta Pharmacol Toxicol (Copenh) *20*, 140-144.

Carpintero, P., Anadon, R., Diaz-Regueira, S., and Gomez-Marquez, J. (1999). Expression of thymosin beta4 messenger RNA in normal and kainate-treated rat forebrain. Neuroscience *90*, 1433-1444.

Carver, J.A., Cooper, P.G., and Truscott, R.J. (1993). 1H-NMR spectroscopy of beta B2-crystallin from bovine eye lens. Conformation of the N- and C-terminal extensions. Eur J Biochem *213*, 313-320.

Chamak, B., Fellous, A., Glowinski, J., and Prochiantz, A. (1987). MAP2 expression and neuritic outgrowth and branching are coregulated through region-specific neuro-astroglial interactions. J Neurosci *7*, 3163-3170.

Chambers, C., and Russell, P. (1991). Deletion mutation in an eye lens beta-crystallin. An animal model for inherited cataracts. J Biol Chem *266*, 6742-6746.

Chauhan, N., and Siegel, G. (1997). Age-dependent organotypic expression of microtubule-associated proteins (MAP1, MAP2, and MAP5) in rat brain. Neurochem Res *22*, 713-719.

Chen, J.M., Cooper, D.N., Chuzhanova, N., Ferec, C., and Patrinos, G.P. (2007). Gene conversion: mechanisms, evolution and human disease. Nat Rev Genet 8, 762-775.

Chen, Y., Hancock, M.L., Role, L.W., and Talmage, D.A. (2010). Intramembranous valine linked to schizophrenia is required for neuregulin 1 regulation of the morphological development of cortical neurons. J Neurosci *30*, 9199-9208.

Cheng, C., Xia, C.H., Huang, Q., Ding, L., Horwitz, J., and Gong, X. (2010). Altered chaperone-like activity of alpha-crystallins promotes cataractogenesis. J Biol Chem *285*, 41187-41193.

Clinton, S.M., and Meador-Woodruff, J.H. (2004). Abnormalities of the NMDA

Receptor and Associated Intracellular Molecules in the Thalamus in Schizophrenia and Bipolar Disorder. Neuropsychopharmacology *29*, 1353-1362.

Cobos, I., Calcagnotto, M.E., Vilaythong, A.J., Thwin, M.T., Noebels, J.L., Baraban, S.C., and Rubenstein, J.L. (2005). Mice lacking Dlx1 show subtype-specific loss of interneurons, reduced inhibition and epilepsy. Nat Neurosci *8*, 1059-1068.

Cotter, D., Kerwin, R., Doshi, B., Martin, C.S., and Everall, I.P. (1997). Alterations in hippocampal non-phosphorylated MAP2 protein expression in schizophrenia. Brain Res *765*, 238-246.

Cotter, D., Wilson, S., Roberts, E., Kerwin, R., and Everall, I.P. (2000). Increased dendritic MAP2 expression in the hippocampus in schizophrenia. Schizophr Res *41*, 313-323.

Coyle, J.T. (2006). Glutamate and schizophrenia: beyond the dopamine hypothesis. Cell Mol Neurobiol *26*, 365-384.

Creese, I., Burt, D.R., and Snyder, S.H. (1976). Dopamine receptor binding predicts clinical and pharmacological potencies of antischizophrenic drugs. Science *192*, 481-483.

Crockford, D., Turjman, N., Allan, C., and Angel, J. (2010). Thymosin beta4: structure, function, and biological properties supporting current and future clinical applications. Ann N Y Acad Sci *1194*, 179-189.

Daenen, E.W., Wolterink, G., Van Der Heyden, J.A., Kruse, C.G., and Van Ree, J.M. (2003). Neonatal lesions in the amygdala or ventral hippocampus disrupt prepulse inhibition of the acoustic startle response; implications for an animal model of neurodevelopmental disorders like schizophrenia. Eur Neuropsychopharmacol *13*, 187-197.

David, D.J., Wang, J., Samuels, B.A., Rainer, Q., David, I., Gardier, A.M., and Hen, R. (2010). Implications of the functional integration of adult-born hippocampal neurons in anxiety-depression disorders. Neuroscientist *16*, 578-591.

Davis, K.L., Kahn, R.S., Ko, G., and Davidson, M. (1991). Dopamine in schizophrenia: a review and reconceptualization. Am J Psychiatry *148*, 1474-1486.

Del Vecchio, P.J., MacElroy, K.S., Rosser, M.P., and Church, R.L. (1984). Association of alpha-crystallin with actin in cultured lens cells. Curr Eye Res *3*,

1213-1219.

DeRosse, P., Funke, B., Burdick, K.E., Lencz, T., Goldberg, T.E., Kane, J.M., Kucherlapati, R., and Malhotra, A.K. (2006). COMT genotype and manic symptoms in schizophrenia. Schizophr Res *87*, 28-31.

Devi, R.R., Yao, W., Vijayalakshmi, P., Sergeev, Y.V., Sundaresan, P., and Hejtmancik, J.F. (2008). Crystallin gene mutations in Indian families with inherited pediatric cataract. Mol Vis *14*, 1157-1170.

Di Garbo, A., Barbi, M., Chillemi, S., Alloisio, S., and Nobile, M. (2007). Calcium signalling in astrocytes and modulation of neural activity. Biosystems *89*, 74-83.

Diaz-Hernandez, M., Pereira, M.F., Pintor, J., Cunha, R.A., Ribeiro, J.A., and Miras-Portugal, M.T. (2002). Modulation of the rat hippocampal dinucleotide receptor by adenosine receptor activation. J Pharmacol Exp Ther *301*, 441-450.

DiProspero, N.A., Chen, E.Y., Charles, V., Plomann, M., Kordower, J.H., and Tagle, D.A. (2004). Early changes in Huntington's disease patient brains involve alterations in cytoskeletal and synaptic elements. J Neurocytol *33*, 517-533.

Dirks, R.P., Kraft, H.J., Van Genesen, S.T., Klok, E.J., Pfundt, R., Schoenmakers, J.G., and Lubsen, N.H. (1996). The cooperation between two silencers creates an enhancer element that controls both the lens-preferred and the differentiation stage-specific expression of the rat beta B2-crystallin gene. Eur J Biochem *239*, 23-32.

Dodt, H.U., Eder, M., Schierloh, A., and Zieglgansberger, W. (2002). Infrared-guided laser stimulation of neurons in brain slices. Sci STKE *2002*, pl2.

Doerwald, L., Nijveen, H., Civil, A., van Genesen, S.T., and Lubsen, N.H. (2001). Regulatory elements in the rat betaB2-crystallin promoter. Exp Eye Res *73*, 703-710.

Dorph-Petersen, K.A., and Lewis, D.A. (2011). Stereological approaches to identifying neuropathology in psychosis. Biol Psychiatry *69*, 113-126.

Duan, X., Chang, J.H., Ge, S., Faulkner, R.L., Kim, J.Y., Kitabatake, Y., Liu, X.B., Yang, C.H., Jordan, J.D., Ma, D.K.*, et al.* (2007). Disrupted-In-Schizophrenia 1 regulates integration of newly generated neurons in the adult brain. Cell *130*, 1146-1158.

Duguid, J.R., Rohwer, R.G., and Seed, B. (1988). Isolation of cDNAs of scrapie-

modulated RNAs by subtractive hybridization of a cDNA library. Proc Natl Acad Sci U S A *85*, 5738-5742.

Duprey, K.M., Robinson, K.M., Wang, Y., Taube, J.R., and Duncan, M.K. (2007). Subfertility in mice harboring a mutation in betaB2-crystallin. Mol Vis *13*, 366-373.

Ecroyd, H., and Carver, J.A. (2009). Crystallin proteins and amyloid fibrils. Cell Mol Life Sci *66*, 62-81.

Ehm, O., Goritz, C., Covic, M., Schaffner, I., Schwarz, T.J., Karaca, E., Kempkes, B., Kremmer, E., Pfrieger, F.W., Espinosa, L.*, et al.* (2010). RBPJkappa-dependent signaling is essential for long-term maintenance of neural stem cells in the adult hippocampus. J Neurosci *30*, 13794-13807.

Eichenbaum, H. (2000). A cortical-hippocampal system for declarative memory. Nat Rev Neurosci *1*, 41-50.

Engin, E., and Treit, D. (2007). The role of hippocampus in anxiety: intracerebral infusion studies. Behav Pharmacol *18*, 365-374.

Erickson-Viitanen, S., Ruggieri, S., Natalini, P., and Horecker, B.L. (1983). Distribution of thymosin beta 4 in vertebrate classes. Arch Biochem Biophys *221*, 570-576.

Fanselow, M.S., and Dong, H.W. (2010). Are the dorsal and ventral hippocampus functionally distinct structures? Neuron *65*, 7-19.

Farkas, N., Lendeckel, U., Dobrowolny, H., Funke, S., Steiner, J., Keilhoff, G., Schmitt, A., Bogerts, B., and Bernstein, H.G. (2010). Reduced density of ADAM 12-immunoreactive oligodendrocytes in the anterior cingulate white matter of patients with schizophrenia. World J Biol Psychiatry *11*, 556-566.

Fernandes, H.B., and Raymond, L.A. (2009). NMDA Receptors and Huntington's Disease.

Fernstrom, R.C. (1958). A durable Nissl stain for frozen and paraffin sections. Stain Technol 33, 175-176.

Francis, A.N., Bhojraj, T.S., Prasad, K.M., Kulkarni, S., Montrose, D.M., Eack, S.M., and Keshavan, M.S. (2010). Abnormalities of the corpus callosum in non-psychotic high-risk offspring of schizophrenia patients. Psychiatry Res *191*, 9-15.

Freund, T.F. (2003). Interneuron Diversity series: Rhythm and mood in perisomatic

inhibition. Trends Neurosci *26*, 489-495.

Freund, T.F., and Buzsaki, G. (1996). Interneurons of the hippocampus. Hippocampus *6*, 347-470.

Fuchs, E.C., Zivkovic, A.R., Cunningham, M.O., Middleton, S., Lebeau, F.E., Bannerman, D.M., Rozov, A., Whittington, M.A., Traub, R.D., Rawlins, J.N., and Monyer, H. (2007). Recruitment of parvalbumin-positive interneurons determines hippocampal function and associated behavior. Neuron *53*, 591-604.

Fujioka, T., Fujioka, A., and Duman, R.S. (2004). Activation of cAMP signaling facilitates the morphological maturation of newborn neurons in adult hippocampus. J Neurosci *24*, 319-328.

Ganguly, K., Favor, J., Neuhauser-Klaus, A., Sandulache, R., Puk, O., Beckers, J., Horsch, M., Schadler, S., Vogt Weisenhorn, D., Wurst, W., and Graw, J. (2008). Novel allele of crybb2 in the mouse and its expression in the brain. Invest Ophthalmol Vis Sci *49*, 1533-1541.

Gao, F.B. (2007). Molecular and cellular mechanisms of dendritic morphogenesis. Curr Opin Neurobiol *17*, 525-532.

Garland, D., Rao, P.V., Del Corso, A., Mura, U., and Zigler, J.S., Jr. (1991). zeta-Crystallin is a major protein in the lens of Camelus dromedarius. Arch Biochem Biophys *285*, 134-136.

Geddes, J.W., Chang-Chui, H., Cooper, S.M., Lott, I.T., and Cotman, C.W. (1986). Density and distribution of NMDA receptors in the human hippocampus in Alzheimer's disease. Brain Res *399*, 156-161.

George, A.J., Gordon, L., Beissbarth, T., Koukoulas, I., Holsinger, R.M., Perreau, V., Cappai, R., Tan, S.S., Masters, C.L., Scott, H.S., and Li, Q.X. (2010). A serial analysis of gene expression profile of the Alzheimer's disease Tg2576 mouse model. Neurotox Res *17*, 360-379.

Ghosh, A., and Greenberg, M.E. (1995). Calcium signaling in neurons: molecular mechanisms and cellular consequences. Science *268*, 239-247.

Giger, R.J., Wolfer, D.P., De Wit, G.M., and Verhaagen, J. (1996). Anatomy of rat semaphorin III/collapsin-1 mRNA expression and relationship to developing nerve tracts during neuroembryogenesis. J Comp Neurol *375*, 378-392.

Gill, D., Klose, R., Munier, F.L., McFadden, M., Priston, M., Billingsley, G., Ducrey, N., Schorderet, D.F., and Heon, E. (2000). Genetic heterogeneity of the Coppock-like cataract: a mutation in CRYBB2 on chromosome 22q11.2. Invest Ophthalmol Vis Sci *41*, 159-165.

Gill, D.A., Ramsay, S.L., and Tasker, R.A. (2010). Selective reductions in subpopulations of GABAergic neurons in a developmental rat model of epilepsy. Brain Res *1331*, 114-123.

Goni-Oliver, P., Avila, J., and Hernandez, F. (2009). Memantine inhibits calpain-mediated truncation of GSK-3 induced by NMDA: implications in Alzheimer's disease. J Alzheimers Dis *18*, 843-848.

Gonzalez, P., Rao, P.V., and Zigler, J.S., Jr. (1994). Organization of the human zeta-crystallin/quinone reductase gene (CRYZ). Genomics *21*, 317-324.

Gopalakrishnan, S., and Takemoto, L. (1992). Binding of actin to lens alpha crystallins. Curr Eye Res *11*, 929-933.

Gothelf, D., Soreni, N., Nachman, R.P., Tyano, S., Hiss, Y., Reiner, O., and Weizman, A. (2000). Evidence for the involvement of the hippocampus in the pathophysiology of schizophrenia. Eur Neuropsychopharmacol *10*, 389-395.

Graff-Guerrero, A., Mizrahi, R., Agid, O., Marcon, H., Barsoum, P., Rusjan, P., Wilson, A.A., Zipursky, R., and Kapur, S. (2009). The dopamine D2 receptors in high-affinity state and D3 receptors in schizophrenia: a clinical [11C]-(+)-PHNO PET study. Neuropsychopharmacology *34*, 1078-1086.

Graw, J. (1997). The crystallins: genes, proteins and diseases. Biol Chem *378*, 1331-1348.

Graw, J. (1999). Mouse models of congenital cataract. Eye (Lond) *13 (Pt 3b)*, 438-444.

Graw, J. (2004). Congenital hereditary cataracts. Int J Dev Biol *48*, 1031-1044.

Graw, J. (2009). Genetics of crystallins: cataract and beyond. Exp Eye Res *88*, 173-189.

Graw, J., Liebstein, A., Pietrowski, D., Schmitt-John, T., and Werner, T. (1993). Genomic sequences of murine gamma B- and gamma C-crystallin-encoding genes: promoter analysis and complete evolutionary pattern of mouse, rat and human

gamma-crystallins. Gene *136*, 145-156.

Graw, J., Loster, J., Soewarto, D., Fuchs, H., Reis, A., Wolf, E., Balling, R., and Hrabe de Angelis, M. (2001). Aey2, a new mutation in the betaB2-crystallin-encoding gene of the mouse. Invest Ophthalmol Vis Sci *42*, 1574-1580.

Green, E.J., and Juraska, J.M. (1985). The dendritic morphology of hippocampal dentate granule cells varies with their position in the granule cell layer: a quantitative Golgi study. Exp Brain Res *59*, 582-586.

Grunze, H.C., Rainnie, D.G., Hasselmo, M.E., Barkai, E., Hearn, E.F., McCarley, R.W., and Greene, R.W. (1996). NMDA-dependent modulation of CA1 local circuit inhibition. J Neurosci *16*, 2034-2043.

Grynkiewicz, G., Poenie, M., and Tsien, R.Y. (1985). A new generation of Ca2+ indicators with greatly improved fluorescence properties. J Biol Chem *260*, 3440-3450.

Hansen, L., Yao, W., Eiberg, H., Kjaer, K.W., Baggesen, K., Hejtmancik, J.F., and Rosenberg, T. (2007). Genetic heterogeneity in microcornea-cataract: five novel mutations in CRYAA, CRYGD, and GJA8. Invest Ophthalmol Vis Sci *48*, 3937-3944.

Hansen, L., Yao, W., Eiberg, H., Kjaer, K.W., Baggesen, K., Hejtmancik, J.F., and Rosenberg, T. (2007). Genetic heterogeneity in microcornea-cataract: five novel mutations in CRYAA, CRYGD, and GJA8. Invest Ophthalmol Vis Sci *48*, 3937-3944.

Harrison, P.J. (2004). The hippocampus in schizophrenia: a review of the neuropathological evidence and its pathophysiological implications. Psychopharmacology (Berl) *174*, 151-162.

Harrison, P.J., and Owen, M.J. (2003). Genes for schizophrenia? Recent findings and their pathophysiological implications. Lancet *361*, 417-419.

Harte, M.K., Powell, S.B., Swerdlow, N.R., Geyer, M.A., and Reynolds, G.P. (2007). Deficits in parvalbumin and calbindin immunoreactive cells in the hippocampus of isolation reared rats. J Neural Transm *114*, 893-898.

Head, M.W., and Goldman, J.E. (2000). Small heat shock proteins, the cytoskeleton, and inclusion body formation. Neuropathol Appl Neurobiol *26*, 304-312.

Heydebrand, G. (2006). Cognitive deficits in the families of patients with schizophrenia. Curr Opin Psychiatry *19*, 277-281.

Hilgenberg, L.G., and Smith, M.A. (2007). Preparation of dissociated mouse cortical neuron cultures. J Vis Exp, 562.

Hillman, B.G., Gupta, S.C., Stairs, D.J., Buonanno, A., and Dravid, S.M. (2011). Behavioral analysis of NR2C knockout mouse reveals deficit in acquisition of conditioned fear and working memory. Neurobiol Learn Mem *95*, 404-414.

Hoe, H.S., Lee, K.J., Carney, R.S., Lee, J., Markova, A., Lee, J.Y., Howell, B.W., Hyman, B.T., Pak, D.T., Bu, G., and Rebeck, G.W. (2009). Interaction of reelin with amyloid precursor protein promotes neurite outgrowth. J Neurosci *29*, 7459-7473.

Horwitz, J. (2003). Alpha-crystallin. Exp Eye Res *76*, 145-153.

Huang, Q.L., Du, X.Y., Stone, S.H., Amsbaugh, D.F., Datiles, M., Hu, T.S., and Zigler, J.S., Jr. (1990). Association of hereditary cataracts in strain 13/N guinea-pigs with mutation of the gene for zeta-crystallin. Exp Eye Res *50*, 317-325.

Huang, Q.L., Russell, P., Stone, S.H., and Zigler, J.S., Jr. (1987). Zeta-crystallin, a novel lens protein from the guinea pig. Curr Eye Res *6*, 725-732.

Huber, G., and Matus, A. (1984). Differences in the cellular distributions of two microtubule-associated proteins, MAP1 and MAP2, in rat brain. J Neurosci *4*, 151-160.

Hulsebos, T.J., Jenkins, N.A., Gilbert, D.J., and Copeland, N.G. (1995). The beta crystallin genes on human chromosome 22 define a new region of homology with mouse chromosome 5. Genomics *25*, 574-576.

Hutchinson, E.G., and Thornton, J.M. (1993). The Greek key motif: extraction, classification and analysis. Protein Eng *6*, 233-245.

Iwaki, T., Iwaki, A., Tateishi, J., and Goldman, J.E. (1994). Sense and antisense modification of glial alpha B-crystallin production results in alterations of stress fiber formation and thermoresistance. J Cell Biol *125*, 1385-1393.

Jaenicke, R., and Slingsby, C. (2001). Lens crystallins and their microbial homologs: structure, stability, and function. Crit Rev Biochem Mol Biol *36*, 435-499.

James, A.C., James, S., Smith, D.M., and Javaloyes, A. (2004). Cerebellar, prefrontal cortex, and thalamic volumes over two time points in adolescent-onset schizophrenia. Am J Psychiatry *161*, 1023-1029.

Javitt, D.C., and Zukin, S.R. (1991). Recent advances in the phencyclidine model of

schizophrenia. Am J Psychiatry *148*, 1301-1308.

Jentarra, G.M., Olfers, S.L., Rice, S.G., Srivastava, N., Homanics, G.E., Blue, M., Naidu, S., and Narayanan, V. (2010). Abnormalities of cell packing density and dendritic complexity in the MeCP2 A140V mouse model of Rett syndrome/X-linked mental retardation. BMC Neurosci *11*, 19.

Jentsch, J.D., and Roth, R.H. (1999). The neuropsychopharmacology of phencyclidine: from NMDA receptor hypofunction to the dopamine hypothesis of schizophrenia. Neuropsychopharmacology *20*, 201-225.

Jernigan, T.L., Salmon, D.P., Butters, N., and Hesselink, J.R. (1991). Cerebral structure on MRI, Part II: Specific changes in Alzheimer's and Huntington's diseases. Biol Psychiatry *29*, 68-81.

Jobby, M.K., and Sharma, Y. (2007). Calcium-binding to lens betaB2- and betaA3-crystallins suggests that all beta-crystallins are calcium-binding proteins. FEBS J *274*, 4135-4147.

Johnson, G.V., and Jope, R.S. (1992). The role of microtubule-associated protein 2 (MAP-2) in neuronal growth, plasticity, and degeneration. J Neurosci Res *33*, 505-512.

Kador, P.F., Fukui, H.N., Fukushi, S., Jernigan, H.M., Jr., and Kinoshita, J.H. (1980). Philly mouse: a new model of hereditary cataract. Exp Eye Res *30*, 59-68.

Kato, K., Ito, H., Inaguma, Y., Okamoto, K., and Saga, S. (1996). Synthesis and accumulation of alphaB crystallin in C6 glioma cells is induced by agents that promote the disassembly of microtubules. J Biol Chem *271*, 26989-26994.

Kawaguchi, Y., and Kubota, Y. (1997). GABAergic cell subtypes and their synaptic connections in rat frontal cortex. Cereb Cortex *7*, 476-486.

Kendler, K.S., Gruenberg, A.M., and Strauss, J.S. (1981). An independent analysis of the Copenhagen sample of the Danish adoption study of schizophrenia. II. The relationship between schizotypal personality disorder and schizophrenia. Arch Gen Psychiatry *38*, 982-984.

Khan, A.O., Aldahmesh, M.A., and Meyer, B. (2007). Recessive congenital total cataract with microcornea and heterozygote carrier signs caused by a novel missense CRYAA mutation (R54C). Am J Ophthalmol *144*, 949-952.

Kim, J.S., Kornhuber, H.H., Schmid-Burgk, W., and Holzmuller, B. (1980). Low cerebrospinal fluid glutamate in schizophrenic patients and a new hypothesis on schizophrenia. Neurosci Lett *20*, 379-382.

Kim, R.Y., Gasser, R., and Wistow, G.J. (1992). mu-crystallin is a mammalian homologue of Agrobacterium ornithine cyclodeaminase and is expressed in human retina. Proc Natl Acad Sci U S A *89*, 9292-9296.

Kim, Y., Zerwas, S., Trace, S.E., and Sullivan, P.F. (2011). Schizophrenia genetics: where next? Schizophr Bull *37*, 456-463.

Kinney, D.K., Jacobsen, B., Jansson, L., Faber, B., Tramer, S.J., and Suozzo, M. (2000). Winter birth and biological family history in adopted schizophrenics. Schizophr Res *44*, 95-103.

Kinney, J.W., Davis, C.N., Tabarean, I., Conti, B., Bartfai, T., and Behrens, M.M. (2006). A specific role for NR2A-containing NMDA receptors in the maintenance of parvalbumin and GAD67 immunoreactivity in cultured interneurons. J Neurosci *26*, 1604-1615.

Koch, M. (1999). The neurobiology of startle. Prog Neurobiol *59*, 107-128.

Kolb, B., and Whishaw, I.Q. (1998). Brain plasticity and behavior. Annu Rev Psychol *49*, 43-64.

Krebs, M.O. (2002). [Genetic hypothesis of schizophrenia]. Rev Prat *52*, 1208-1211.

Kristiansen, L.V., Patel, S.A., Haroutunian, V., and Meador-Woodruff, J.H. (2010). Expression of the NR2B-NMDA receptor subunit and its Tbr-1/CINAP regulatory proteins in postmortem brain suggest altered receptor processing in schizophrenia. Synapse *64*, 495-502.

Krivosheya, D., Tapia, L., Levinson, J.N., Huang, K., Kang, Y., Hines, R., Ting, A.K., Craig, A.M., Mei, L., Bamji, S.X., and El-Husseini, A. (2008). ErbB4-neuregulin signaling modulates synapse development and dendritic arborization through distinct mechanisms. J Biol Chem *283*, 32944-32956.

Krystal, J.H., Karper, L.P., Seibyl, J.P., Freeman, G.K., Delaney, R., Bremner, J.D., Heninger, G.R., Bowers, M.B., Jr., and Charney, D.S. (1994). Subanesthetic effects of the noncompetitive NMDA antagonist, ketamine, in humans. Psychotomimetic, perceptual, cognitive, and neuroendocrine responses. Arch Gen Psychiatry *51*,

199-214.

Kucharska-Pietura, K., Russell, T., and Masiak, M. (2003). Perception of negative affect in schizophrenia--functional and structural changes in the amygdala. Review. Ann Univ Mariae Curie Sklodowska Med *58*, 453-458.

Kusljic, S., and van den Buuse, M. (2004). Functional dissociation between serotonergic pathways in dorsal and ventral hippocampus in psychotomimetic drug-induced locomotor hyperactivity and prepulse inhibition in rats. Eur J Neurosci *20*, 3424-3432.

Kvajo, M., McKellar, H., Arguello, P.A., Drew, L.J., Moore, H., MacDermott, A.B., Karayiorgou, M., and Gogos, J.A. (2008). A mutation in mouse Disc1 that models a schizophrenia risk allele leads to specific alterations in neuronal architecture and cognition. Proc Natl Acad Sci U S A *105*, 7076-7081.

LaFerla, F.M. (2002). Calcium dyshomeostasis and intracellular signalling in Alzheimer's disease. Nat Rev Neurosci *3*, 862-872.

Lahti, A.C., Koffel, B., LaPorte, D., and Tamminga, C.A. (1995). Subanesthetic doses of ketamine stimulate psychosis in schizophrenia. Neuropsychopharmacology *13*, 9-19.

Lapucci, A., Lulli, M., Amedei, A., Papucci, L., Witort, E., Di Gesualdo, F., Bertolini, F., Brewer, G., Nicolin, A., Bevilacqua, A.*, et al.* (2010). zeta-Crystallin is a bcl-2 mRNA binding protein involved in bcl-2 overexpression in T-cell acute lymphocytic leukemia. FASEB J *24*, 1852-1865.

Laruelle, M., Abi-Dargham, A., Gil, R., Kegeles, L., and Innis, R. (1999). Increased dopamine transmission in schizophrenia: relationship to illness phases. Biol Psychiatry *46*, 56-72.

Laskowska, E., Matuszewska, E., and Kuczynska-Wisnik, D. (2010). Small heat shock proteins and protein-misfolding diseases. Curr Pharm Biotechnol 11, 146-157.

Lawson, J.A., Vogrin, S., Bleasel, A.F., Cook, M.J., Burns, L., McAnally, L., Pereira, J., and Bye, A.M. (2000). Predictors of hippocampal, cerebral, and cerebellar volume reduction in childhood epilepsy. Epilepsia *41*, 1540-1545.

Leuner, B., and Gould, E. (2010). Dendritic growth in medial prefrontal cortex and cognitive flexibility are enhanced during the postpartum period. J Neurosci *30*,

13499-13503.

Lewis, C.M., Levinson, D.F., Wise, L.H., DeLisi, L.E., Straub, R.E., Hovatta, I., Williams, N.M., Schwab, S.G., Pulver, A.E., Faraone, S.V.*, et al.* (2003). Genome scan meta-analysis of schizophrenia and bipolar disorder, part II: Schizophrenia. Am J Hum Genet *73*, 34-48.

Li, F.F., Zhu, S.Q., Wang, S.Z., Gao, C., Huang, S.Z., Zhang, M., and Ma, X. (2008). Nonsense mutation in the CRYBB2 gene causing autosomal dominant progressive polymorphic congenital coronary cataracts. Mol Vis *14*, 750-755.

Lie, D.C., Colamarino, S.A., Song, H.J., Desire, L., Mira, H., Consiglio, A., Lein, E.S., Jessberger, S., Lansford, H., Dearie, A.R., and Gage, F.H. (2005). Wnt signalling regulates adult hippocampal neurogenesis. Nature *437*, 1370-1375.

Lieberman, J.A., Kane, J.M., and Alvir, J. (1987). Provocative tests with psychostimulant drugs in schizophrenia. Psychopharmacology (Berl) *91*, 415-433.

Liedtke, T., Schwamborn, J.C., Schroer, U., and Thanos, S. (2007). Elongation of axons during regeneration involves retinal crystallin beta b2 (crybb2). Mol Cell Proteomics *6*, 895-907.

Litt, M., Carrero-Valenzuela, R., LaMorticella, D.M., Schultz, D.W., Mitchell, T.N., Kramer, P., and Maumenee, I.H. (1997). Autosomal dominant cerulean cataract is associated with a chain termination mutation in the human beta-crystallin gene CRYBB2. Hum Mol Genet *6*, 665-668.

Liu, L., Xing, D., Chen, W.R., Chen, T., Pei, Y., and Gao, X. (2008). Calpain-mediated pathway dominates cisplatin-induced apoptosis in human lung adenocarcinoma cells as determined by real-time single cell analysis. Int J Cancer *122*, 2210-2222.

Livak, K.J., and Schmittgen, T.D. (2001). Analysis of relative gene expression data using real-time quantitative PCR and the 2(-Delta Delta C(T)) Method. Methods 25, 402-408.

Lodge, D.J., Behrens, M.M., and Grace, A.A. (2009). A loss of parvalbumin-containing interneurons is associated with diminished oscillatory activity in an animal model of schizophrenia. J Neurosci *29*, 2344-2354.

Lowe, J., Landon, M., Pike, I., Spendlove, I., McDermott, H., and Mayer, R.J. (1990).

Dementia with beta-amyloid deposition: involvement of alpha B-crystallin supports two main diseases. Lancet *336*, 515-516.

Lund, J.S., and Lewis, D.A. (1993). Local circuit neurons of developing and mature macaque prefrontal cortex: Golgi and immunocytochemical characteristics. J Comp Neurol *328*, 282-312.

Magabo, K.S., Horwitz, J., Piatigorsky, J., and Kantorow, M. (2000). Expression of betaB(2)-crystallin mRNA and protein in retina, brain, and testis. Invest Ophthalmol Vis Sci *41*, 3056-3060.

Maric, N., Kamer, T., Schneider Axmann, T., Dani, I., Jasovic Gasic, M., Paunovic, V.R., and Falkai, P. (2003). [Volumetric analysis of gray matter, white matter and cerebrospinal fluid space in schizophrenia]. Srp Arh Celok Lek *131*, 26-30.

McEwen, B.S. (2003). Mood disorders and allostatic load. Biol Psychiatry *54*, 200-207.

Meador-Woodruff, J.H., Clinton, S.M., Beneyto, M., and McCullumsmith, R.E. (2003). Molecular abnormalities of the glutamate synapse in the thalamus in schizophrenia. Ann N Y Acad Sci *1003*, 75-93.

Michiel, M., Duprat, E., Skouri-Panet, F., Lampi, J.A., Tardieu, A., Lampi, K.J., and Finet, S. (2010). Aggregation of deamidated human betaB2-crystallin and incomplete rescue by alpha-crystallin chaperone. Exp Eye Res *90*, 688-698.

Moghaddam, B., Adams, B., Verma, A., and Daly, D. (1997). Activation of glutamatergic neurotransmission by ketamine: a novel step in the pathway from NMDA receptor blockade to dopaminergic and cognitive disruptions associated with the prefrontal cortex. J Neurosci *17*, 2921-2927.

Mollinari, C., Ricci-Vitiani, L., Pieri, M., Lucantoni, C., Rinaldi, A.M., Racaniello, M., De Maria, R., Zona, C., Pallini, R., Merlo, D., and Garaci, E. (2009). Downregulation of thymosin beta4 in neural progenitor grafts promotes spinal cord regeneration. J Cell Sci *122*, 4195-4207.

Moser, M.B., and Moser, E.I. (1998). Functional differentiation in the hippocampus. Hippocampus *8*, 608-619.

Mrzljak, L., Uylings, H.B., Kostovic, I., and van Eden, C.G. (1992). Prenatal development of neurons in the human prefrontal cortex. II. A quantitative Golgi

study. J Comp Neurol *316*, 485-496.

Mukaetova-Ladinska, E.B., Arnold, H., Jaros, E., Perry, R., and Perry, E. (2004). Depletion of MAP2 expression and laminar cytoarchitectonic changes in dorsolateral prefrontal cortex in adult autistic individuals. Neuropathol Appl Neurobiol *30*, 615-623.

Myles-Worsley, M., Coon, H., McDowell, J., Brenner, C., Hoff, M., Lind, B., Bennett, P., Freedman, R., Clementz, B., and Byerley, W. (1999). Linkage of a composite inhibitory phenotype to a chromosome 22q locus in eight Utah families. Am J Med Genet *88*, 544-550.

Nelson, M.D., Saykin, A.J., Flashman, L.A., and Riordan, H.J. (1998). Hippocampal volume reduction in schizophrenia as assessed by magnetic resonance imaging: a meta-analytic study. Arch Gen Psychiatry *55*, 433-440.

Nimmrich, V., Szabo, R., Nyakas, C., Granic, I., Reymann, K.G., Schroder, U.H., Gross, G., Schoemaker, H., Wicke, K., Moller, A., and Luiten, P. (2008). Inhibition of Calpain Prevents N-Methyl-D-aspartate-Induced Degeneration of the Nucleus Basalis and Associated Behavioral Dysfunction. J Pharmacol Exp Ther *327*, 343-352.

Ninkovic, J., Pinto, L., Petricca, S., Lepier, A., Sun, J., Rieger, M.A., Schroeder, T., Cvekl, A., Favor, J., and Gotz, M. (2010). The transcription factor Pax6 regulates survival of dopaminergic olfactory bulb neurons via crystallin alphaA. Neuron *68*, 682-694.

Nord, M., and Farde, L. (2010). Antipsychotic Occupancy of Dopamine Receptors in Schizophrenia. CNS Neurosci Ther.

Nunez, J. (2008). Primary Culture of Hippocampal Neurons from P0 Newborn Rats. J Vis Exp.

O'Keefe, J., and Conway, D.H. (1978). Hippocampal place units in the freely moving rat: why they fire where they fire. Exp Brain Res *31*, 573-590.

Okiyama, K., Smith, D.H., White, W.F., Richter, K., and McIntosh, T.K. (1997). Effects of the novel NMDA antagonists CP-98,113, CP-101,581 and CP-101,606 on cognitive function and regional cerebral edema following experimental brain injury in the rat. J Neurotrauma *14*, 211-222.

Oshima, A., Suzuki, S., Takumi, Y., Hashizume, K., Abe, S., and Usami, S. (2006). CRYM mutations cause deafness through thyroid hormone binding properties in the fibrocytes of the cochlea. J Med Genet *43*, e25.

Pasterkamp, R.J., Giger, R.J., Ruitenberg, M.J., Holtmaat, A.J., De Wit, J., De Winter, F., and Verhaagen, J. (1999). Expression of the gene encoding the chemorepellent semaphorin III is induced in the fibroblast component of neural scar tissue formed following injuries of adult but not neonatal CNS. Mol Cell Neurosci *13*, 143-166.

Pauli, S., Soker, T., Klopp, N., Illig, T., Engel, W., and Graw, J. (2007). Mutation analysis in a German family identified a new cataract-causing allele in the CRYBB2 gene. Mol Vis *13*, 962-967.

Penschuck, S., Flagstad, P., Didriksen, M., Leist, M., and Michael-Titus, A.T. (2006). Decrease in parvalbumin-expressing neurons in the hippocampus and increased phencyclidine-induced locomotor activity in the rat methylazoxymethanol (MAM) model of schizophrenia. Eur J Neurosci *23*, 279-284.

Philp, D., Goldstein, A.L., and Kleinman, H.K. (2004). Thymosin beta4 promotes angiogenesis, wound healing, and hair follicle development. Mech Ageing Dev *125*, 113-115.

Philp, D., St-Surin, S., Cha, H.J., Moon, H.S., Kleinman, H.K., and Elkin, M. (2007). Thymosin beta 4 induces hair growth via stem cell migration and differentiation. Ann N Y Acad Sci *1112*, 95-103.

Piatigorsky, J. (1998). Gene sharing in lens and cornea: facts and implications. Prog Retin Eye Res *17*, 145-174.

Pilowsky, L.S., Bressan, R.A., Stone, J.M., Erlandsson, K., Mulligan, R.S., Krystal, J.H., and Ell, P.J. (2006). First in vivo evidence of an NMDA receptor deficit in medication-free schizophrenic patients. Mol Psychiatry *11*, 118-119.

Ponce, A., and Takemoto, L. (2005). Screening of crystallin-crystallin interactions using microequilibrium dialysis. Mol Vis *11*, 752-757.

Pulsipher, D.T., Seidenberg, M., Morton, J.J., Geary, E., Parrish, J., and Hermann, B. (2007). MRI volume loss of subcortical structures in unilateral temporal lobe epilepsy. Epilepsy Behav *11*, 442-449.

Qiu, F.Y., Song, X.X., Zheng, H., Zhao, Y.B., and Fu, G.S. (2009). Thymosin beta4 induces endothelial progenitor cell migration via PI3K/Akt/eNOS signal transduction pathway. J Cardiovasc Pharmacol *53*, 209-214.

Quach, T.T., Glasper, E.R., Devries, A.C., Honnorat, J., Kolattukudy, P.E., and Duchemin, A.M. (2008). Altered prepulse inhibition in mice with dendrite abnormalities of hippocampal neurons. Mol Psychiatry *13*, 656-658.

Quednow, B.B., Wagner, M., Mossner, R., Maier, W., and Kuhn, K.U. (2010). Sensorimotor gating of schizophrenia patients depends on Catechol O-methyltransferase Val158Met polymorphism. Schizophr Bull *36*, 341-346.

Quinlan, R. (2002). Cytoskeletal competence requires protein chaperones. Prog Mol Subcell Biol *28*, 219-233.

Rajini, B., Shridas, P., Sundari, C.S., Muralidhar, D., Chandani, S., Thomas, F., and Sharma, Y. (2001). Calcium binding properties of gamma-crystallin: calcium ion binds at the Greek key beta gamma-crystallin fold. J Biol Chem *276*, 38464-38471.

Rajkowska, G., Selemon, L.D., and Goldman-Rakic, P.S. (1998). Neuronal and glial somal size in the prefrontal cortex: a postmortem morphometric study of schizophrenia and Huntington disease. Arch Gen Psychiatry *55*, 215-224.

Rao, P.V., Gonzalez, P., Persson, B., Jornvall, H., Garland, D., and Zigler, J.S., Jr. (1997). Guinea pig and bovine zeta-crystallins have distinct functional characteristics highlighting replacements in otherwise similar structures. Biochemistry *36*, 5353-5362.

Rao, P.V., Krishna, C.M., and Zigler, J.S., Jr. (1992). Identification and characterization of the enzymatic activity of zeta-crystallin from guinea pig lens. A novel NADPH:quinone oxidoreductase. J Biol Chem *267*, 96-102.

Reed, P.W., Corse, A.M., Porter, N.C., Flanigan, K.M., and Bloch, R.J. (2007). Abnormal expression of mu-crystallin in facioscapulohumeral muscular dystrophy. Exp Neurol *205*, 583-586.

Ren, S., Liu, T., Jia, C., Qi, X., and Wang, Y. (2010). Physiological expression of lens alpha-, beta-, and gamma-crystallins in murine and human corneas. Mol Vis *16*, 2745-2752.

Reti, R., Kwon, E., Qiu, P., Wheater, M., and Sosne, G. (2008). Thymosin beta4 is

cytoprotective in human gingival fibroblasts. Eur J Oral Sci *116*, 424-430.

Reynolds, G.P., Zhang, Z.J., and Beasley, C.L. (2001). Neurochemical correlates of cortical GABAergic deficits in schizophrenia: selective losses of calcium binding protein immunoreactivity. Brain Res Bull *55*, 579-584.

Ribak, C.E., and Shapiro, L.A. (2007). Ultrastructure and synaptic connectivity of cell types in the adult rat dentate gyrus. Prog Brain Res 163, 155-166.

Rioux, L., Ruscheinsky, D., and Arnold, S.E. (2004). Microtubule-associated protein MAP2 expression in olfactory bulb in schizophrenia. Psychiatry Res *128*, 1-7.

Robinson, M.L., and Overbeek, P.A. (1996). Differential expression of alpha A- and alpha B-crystallin during murine ocular development. Invest Ophthalmol Vis Sci *37*, 2276-2284.

Robinson, T.E., and Kolb, B. (2004). Structural plasticity associated with exposure to drugs of abuse. Neuropharmacology *47 Suppl 1*, 33-46.

Rodokanaki, A., Holmes, R.K., and Borras, T. (1989). Zeta-crystallin, a novel protein from the guinea pig lens is related to alcohol dehydrogenases. Gene *78*, 215-224.

Rodriguez, I.R., Gonzalez, P., Zigler, J.S., Jr., and Borras, T. (1992). A guinea-pig hereditary cataract contains a splice-site deletion in a crystallin gene. Biochim Biophys Acta *1180*, 44-52.

Rosoklija, G., Keilp, J.G., Toomayan, G., Mancevski, B., Haroutunian, V., Liu, D., Malespina, D., Hays, A.P., Sadiq, S., Latov, N., and Dwork, A.J. (2005). Altered subicular MAP2 immunoreactivity in schizophrenia. Prilozi *26*, 13-34.

Rujescu, D., Bender, A., Keck, M., Hartmann, A.M., Ohl, F., Raeder, H., Giegling, I., Genius, J., McCarley, R.W., Moller, H.J., and Grunze, H. (2006). A pharmacological model for psychosis based on N-methyl-D-aspartate receptor hypofunction: molecular, cellular, functional and behavioral abnormalities. Biol Psychiatry *59*, 721-729.

Sagata, N., Iwaki, A., Aramaki, T., Takao, K., Kura, S., Tsuzuki, T., Kawakami, R., Ito, I., Kitamura, T., Sugiyama, H*., et al.* (2010). Comprehensive behavioural study of GluR4 knockout mice: implication in cognitive function. Genes Brain Behav *9*, 899-909.

Sakai, T., Oshima, A., Nozaki, Y., Ida, I., Haga, C., Akiyama, H., Nakazato, Y., and

Mikuni, M. (2008). Changes in density of calcium-binding-protein-immunoreactive GABAergic neurons in prefrontal cortex in schizophrenia and bipolar disorder. Neuropathology *28*, 143-150.

Sandilands, A., Hutcheson, A.M., Long, H.A., Prescott, A.R., Vrensen, G., Loster, J., Klopp, N., Lutz, R.B., Graw, J., Masaki, S.*, et al.* (2002). Altered aggregation properties of mutant gamma-crystallins cause inherited cataract. EMBO J *21*, 6005-6014.

Santhiya, S.T., Manisastry, S.M., Rawlley, D., Malathi, R., Anishetty, S., Gopinath, P.M., Vijayalakshmi, P., Namperumalsamy, P., Adamski, J., and Graw, J. (2004). Mutation analysis of congenital cataracts in Indian families: identification of SNPS and a new causative allele in CRYBB2 gene. Invest Ophthalmol Vis Sci *45*, 3599-3607.

Schaeren-Wiemers, N., and Gerfin-Moser, A. (1993). A single protocol to detect transcripts of various types and expression levels in neural tissue and cultured cells: in situ hybridization using digoxigenin-labelled cRNA probes. Histochemistry *100*, 431-440.

Schobel, S.A., Kelly, M.A., Corcoran, C.M., Van Heertum, K., Seckinger, R., Goetz, R., Harkavy-Friedman, J., and Malaspina, D. (2009). Anterior hippocampal and orbitofrontal cortical structural brain abnormalities in association with cognitive deficits in schizophrenia. Schizophr Res *114*, 110-118.

Seeman, P. (1987). Dopamine receptors and the dopamine hypothesis of schizophrenia. Synapse *1*, 133-152.

Seeman, P., and Lee, T. (1975). Antipsychotic drugs: direct correlation between clinical potency and presynaptic action on dopamine neurons. Science *188*, 1217-1219.

Sergeev, Y.V., David, L.L., Chen, H.C., Hope, J.N., and Hejtmancik, J.F. (1998). Local microdomain structure in the terminal extensions of betaA3- and betaB2-crystallins. Mol Vis *4*, 9.

Sharma, Y., and Balasubramanian, D. (1996). Calcium binding properties of beta-crystallins. Ophthalmic Res *28 Suppl 1*, 44-47.

Sharma, Y., Rao, C.M., Narasu, M.L., Rao, S.C., Somasundaram, T., Gopalakrishna, A., and Balasubramanian, D. (1989). Calcium ion binding to delta- and to beta-

crystallins. The presence of the "EF-hand" motif in delta-crystallin that aids in calcium ion binding. J Biol Chem *264*, 12794-12799.

Sohal, V.S., Zhang, F., Yizhar, O., and Deisseroth, K. (2009). Parvalbumin neurons and gamma rhythms enhance cortical circuit performance. Nature *459*, 698-702.

Somenarain, L., and Jones, L.B. (2010). A comparative study of MAP2 immunostaining in areas 9 and 17 in schizophrenia and Huntington chorea. J Psychiatr Res *44*, 694-699.

Sosne, G., Albeiruti, A.R., Hollis, B., Siddiqi, A., Ellenberg, D., and Kurpakus-Wheater, M. (2006). Thymosin beta4 inhibits benzalkonium chloride-mediated apoptosis in corneal and conjunctival epithelial cells in vitro. Exp Eye Res *83*, 502-507.

Sparks, D.L., Lemieux, S.K., Haut, M.W., Baxter, L.C., Johnson, S.C., Sparks, L.M., Sampath, H., Lopez, J.E., Sabbagh, M.H., and Connor, D.J. (2008). Hippocampal volume change in the Alzheimer Disease Cholesterol-Lowering Treatment trial. Cleve Clin J Med *75 Suppl 2*, S87-93.

Spector, A., Li, S., and Sigelman, J. (1974). Age-dependent changes in the molecular size of human lens proteins and their relationship to light scatter. Invest Ophthalmol *13*, 795-798.

Squire, L.R., Stark, C.E., and Clark, R.E. (2004). The medial temporal lobe. Annu Rev Neurosci *27*, 279-306.

Steen, R.G., Mull, C., McClure, R., Hamer, R.M., and Lieberman, J.A. (2006). Brain volume in first-episode schizophrenia: systematic review and meta-analysis of magnetic resonance imaging studies. Br J Psychiatry *188*, 510-518.

Sun, M., Gewirtz, J.C., Bofenkamp, L., Wickham, R.J., Ge, H., and O'Connor, M.B. (2010). Canonical TGF-beta signaling is required for the balance of excitatory/inhibitory transmission within the hippocampus and prepulse inhibition of acoustic startle. J Neurosci *30*, 6025-6035.

Sun, M., Liu, X., Cao, S., He, Q., Zhou, R., Ye, J., Li, Y., and Chen, H. (2007). Inhibition of porcine circovirus type 1 and type 2 production in PK-15 cells by small interfering RNAs targeting the Rep gene. Vet Microbiol *123*, 203-209.

Swandulla, D., and Misgeld, U. (1990). Development and properties of synaptic

mechanisms in a network of rat hypothalamic neurons grown in culture. J Neurophysiol *64*, 715-726.

Swerdlow, N.R., Geyer, M.A., and Braff, D.L. (2001). Neural circuit regulation of prepulse inhibition of startle in the rat: current knowledge and future challenges. Psychopharmacology (Berl) *156*, 194-215.

Swerdlow, N.R., Shoemaker, J.M., Noh, H.R., Ma, L., Gaudet, I., Munson, M., Crain, S., and Auerbach, P.P. (2004). The ventral hippocampal regulation of prepulse inhibition and its disruption by apomorphine in rats are not mediated via the fornix. Neuroscience *123*, 675-685.

Tamminga, C.A. (1998). Schizophrenia and glutamatergic transmission. Crit Rev Neurobiol *12*, 21-36.

Tamminga, C.A., and Holcomb, H.H. (2005). Phenotype of schizophrenia: a review and formulation. Mol Psychiatry *10*, 27-39.

Tandon, R., Keshavan, M.S., and Nasrallah, H.A. (2008). Schizophrenia, "Just the Facts": what we know in 2008 part 1: overview. Schizophr Res *100*, 4-19.

Tiwari, A.K., Zai, C.C., Muller, D.J., and Kennedy, J.L. (2010). Genetics in schizophrenia: where are we and what next? Dialogues Clin Neurosci *12*, 289-303.

Tooney, P.A., and Chahl, L.A. (2004). Neurons expressing calcium-binding proteins in the prefrontal cortex in schizophrenia. Prog Neuropsychopharmacol Biol Psychiatry *28*, 273-278.

Treiman, D.M. (2001). GABAergic mechanisms in epilepsy. Epilepsia *42 Suppl 3*, 8-12.

Trimble, M.R. (1988). The neurology of anxiety. Postgrad Med J *64 Suppl 2*, 22-26.

Tsuang, M.T., Gilbertson, M.W., and Faraone, S.V. (1991). The genetics of schizophrenia. Current knowledge and future directions. Schizophr Res *4*, 157-171.

Tsuang, M.T., Gilbertson, M.W., and Faraone, S.V. (1991). The genetics of schizophrenia. Current knowledge and future directions. Schizophr Res *4*, 157-171.

van Os, J., and Kapur, S. (2009). Schizophrenia. Lancet *374*, 635-645.

Vanita, Sarhadi, V., Reis, A., Jung, M., Singh, D., Sperling, K., Singh, J.R., and Burger, J. (2001). A unique form of autosomal dominant cataract explained by gene conversion between beta-crystallin B2 and its pseudogene. J Med Genet *38*, 392-

396.

Vartiainen, N., Pyykonen, I., Hokfelt, T., and Koistinaho, J. (1996). Induction of thymosin beta(4) mRNA following focal brain ischemia. Neuroreport *7*, 1613-1616.

Verkhratsky, A. (2007). Calcium and cell death. Subcell Biochem *45*, 465-480.

Vie, M.P., Evrard, C., Osty, J., Breton-Gilet, A., Blanchet, P., Pomerance, M., Rouget, P., Francon, J., and Blondeau, J.P. (1997). Purification, molecular cloning, and functional expression of the human nicodinamide-adenine dinucleotide phosphate-regulated thyroid hormone-binding protein. Mol Endocrinol *11*, 1728-1736.

Vyas, N.S., Patel, N.H., Nijran, K.S., Al-Nahhas, A., and Puri, B.K. (2011). The use of PET imaging in studying cognition, genetics and pharmacotherapeutic interventions in schizophrenia. Expert Rev Neurother *11*, 37-51.

Wang, K., and Spector, A. (1994). The chaperone activity of bovine alpha crystallin. Interaction with other lens crystallins in native and denatured states. J Biol Chem *269*, 13601-13608.

Wang, S., Scott, B.W., and Wojtowicz, J.M. (2000). Heterogenous properties of dentate granule neurons in the adult rat. J Neurobiol *42*, 248-257.

West, M.J. (1999). Stereological methods for estimating the total number of neurons and synapses: issues of precision and bias. Trends Neurosci *22*, 51-61.

Wistow, G., and Kim, H. (1991). Lens protein expression in mammals: taxon-specificity and the recruitment of crystallins. J Mol Evol *32*, 262-269.

Womelsdorf, T., Schoffelen, J.M., Oostenveld, R., Singer, W., Desimone, R., Engel, A.K., and Fries, P. (2007). Modulation of neuronal interactions through neuronal synchronization. Science *316*, 1609-1612.

Woo, T.U., Miller, J.L., and Lewis, D.A. (1997). Schizophrenia and the parvalbumin-containing class of cortical local circuit neurons. Am J Psychiatry *154*, 1013-1015.

Wright, I.C., Rabe-Hesketh, S., Woodruff, P.W., David, A.S., Murray, R.M., and Bullmore, E.T. (2000). Meta-analysis of regional brain volumes in schizophrenia. Am J Psychiatry *157*, 16-25.

Wu, H.Y., Yuen, E.Y., Lu, Y.F., Matsushita, M., Matsui, H., Yan, Z., and Tomizawa, K. (2005). Regulation of N-methyl-D-aspartate receptors by calpain in cortical neurons.

J Biol Chem *280*, 21588-21593.

Wu, J.Y., Wu, H., Jin, Y., Wei, J., Sha, D., Prentice, H., Lee, H.H., Lin, C.H., Lee, Y.H., and Yang, L.L. (2009). Mechanism of neuroprotective function of taurine. Adv Exp Med Biol *643*, 169-179.

Wulff, P., Ponomarenko, A.A., Bartos, M., Korotkova, T.M., Fuchs, E.C., Bahner, F., Both, M., Tort, A.B., Kopell, N.J., Wisden, W., and Monyer, H. (2009). Hippocampal theta rhythm and its coupling with gamma oscillations require fast inhibition onto parvalbumin-positive interneurons. Proc Natl Acad Sci U S A *106*, 3561-3566.

Xi, J., Farjo, R., Yoshida, S., Kern, T.S., Swaroop, A., and Andley, U.P. (2003). A comprehensive analysis of the expression of crystallins in mouse retina. Mol Vis *9*, 410-419.

Xi, J.H., Bai, F., Gross, J., Townsend, R.R., Menko, A.S., and Andley, U.P. (2008). Mechanism of small heat shock protein function in vivo: a knock-in mouse model demonstrates that the R49C mutation in alpha A-crystallin enhances protein insolubility and cell death. J Biol Chem *283*, 5801-5814.

Yang, H., Cheng, X., Yao, Q., Li, J., and Ju, G. (2008). The promotive effects of thymosin beta4 on neuronal survival and neurite outgrowth by upregulating L1 expression. Neurochem Res *33*, 2269-2280.

Yao, K., Li, J., Jin, C., Wang, W., Zhu, Y., Shentu, X., and Wang, Q. (2010). Characterization of a novel mutation in the CRYBB2 gene associated with autosomal dominant congenital posterior subcapsular cataract in a Chinese family. Mol Vis *17*, 144-152.

Yao, K., Tang, X., Shentu, X., Wang, K., Rao, H., and Xia, K. (2005). Progressive polymorphic congenital cataract caused by a CRYBB2 mutation in a Chinese family. Mol Vis *11*, 758-763.

Yu, F.X., Lin, S.C., Morrison-Bogorad, M., Atkinson, M.A., and Yin, H.L. (1993). Thymosin beta 10 and thymosin beta 4 are both actin monomer sequestering proteins. J Biol Chem *268*, 502-509.

Zabel, C., Sagi, D., Kaindl, A.M., Steireif, N., Klare, Y., Mao, L., Peters, H., Wacker, M.A., Kleene, R., and Klose, J. (2006). Comparative proteomics in neurodegenerative and non-neurodegenerative diseases suggest nodal point proteins in regulatory networking. J Proteome Res *5*, 1948-1958.

Zhang, J., Li, J., Huang, C., Xue, L., Peng, Y., Fu, Q., Gao, L., Zhang, J., and Li, W. (2008). Targeted knockout of the mouse betaB2-crystallin gene (Crybb2) induces age-related cataract. Invest Ophthalmol Vis Sci *49*, 5476-5483.

Zhang, W.N., Bast, T., and Feldon, J. (2002). Effects of hippocampal N-methyl-D-aspartate infusion on locomotor activity and prepulse inhibition: differences between the dorsal and ventral hippocampus. Behav Neurosci *116*, 72-84.

Zhao, C., Deng, W., and Gage, F.H. (2008). Mechanisms and functional implications of adult neurogenesis. Cell *132*, 645-660.

Zhu, Z.Q., Armstrong, D.L., Hamilton, W.J., and Grossman, R.G. (1997). Disproportionate loss of CA4 parvalbumin-immunoreactive interneurons in patients with Ammon's horn sclerosis. J Neuropathol Exp Neurol *56*, 988-998.

7 Abbreviations

EGFP	Enhanced green fluorescent protein
A	Ampere
AMPA	2-amino-3-(5-methyl-3-oxo-1,2- oxazol-4-yl)propanoic acid
ACSF	Artificial cerebrospinal fluid
AP5	(2R)-amino-5- phosphonopentanoate
Bp	Base pair
BrdU	Bromodesoxy uridin
BSA	Bovine serum albumin
°C	Degrees Celsius
C	Cytosine
CA	Cornu Ammonis
cDNA	Complementary DNA
DCX	Doublecortin
DG	Dentate gyrus
Dig	Digoxigenin
DNA	Deoxyribonucleic acid
E	Embryonic day
E.coli	Escherichia coli
EDTA	Ethyldiaminetetraacetate
EGFP	Enhanced green fluorescent
et al	*et alteres*
G	Guanine
GABA	γ-Aminobutyric acid
Gapdh	Gyceraldehyde-3-phosphate dehydrogenase
GC	Granule cell
GL	Glomerular layer
Hp	Hippocampus
IPSCs	Inhibitory postsynaptic currents
Kb	Kilo base
kD	Kilo Dalton

L	Litre
MCL	Mitral cell layer
mM	Micro meter
NBQX	2,3-dihydroxy-6-nitro-7-sulfamoyl-benzo[f]quinoxaline-2,3-dione
NeuN	Neuronal Nuclei
NMDA	N-methyl D-aspartate
NMR	Nuclear magnetic resonance
P	Postnatal day
PBS	Phosphate buffer saline
PCR	Polymerase chain reaction
PFA	Paraformaldehyde
PKC	Purkinje cells
RNA	Ribose nucleic acid
rpm	Rotations per minute
RT-PCR	Reverse transcription PCR
SDS	Sodiumdodecylsulphate
Ssc	Sodium chloride-sodium citrate
T	Thymine
TE	Tris-EDTA
TEV	Tobacco Etch Virus
WT	Wild type

8 Acknowledgements

9 Lebenslauf

Minxuan Sun

Geburtsdatum	14. März 1982
Staatsangehörigkeit	Chinesisch
Familienstand	Verheiratet
Handy-Nummer	0049-(0)17685013921
E-mail	sunminxuan@gmail.com

Ausbildung

2007–2011   Doktor rerum naturalium Hauptfach: <u>Genetik</u>

Institut für Entwicklungsgenetik, Helmholtz Zentrum München, Deutschland (Registriert an der Technischen Universität München, in Bearbeitung.)

2004–2007   Master der Agrarwissenschaft   Hauptfach: <u>Präventive Tiermedizin</u>

Tierärztliches und Medizinisches College, Landwirtschaftliche Universität Huazhong, Wuhan, China

2000–2004   Bachelor der Wissenschaften   Hauptfach: <u>Biologie</u>

College der Biowissenschaften und Technik, Landwirtschaftliche Universität Huazhong, Wuhan, China

2002–2004   Bachelor des Managements   Nebenfach: <u>Marketing</u>

Fakultät der Wirtschaftslehre und des Managements, Wuhan – Universität, China

1988–2000   Schulausbildung in "Primarily school" und „High school"

Xiangying, Yueyang, Hunan province, China

Vorbildung

1   Vorlesungsreihe "Environmental Health" 2010

2   Sicherung und Vermarktung des geistigen Eigentums, 20. Mai 2011

3   Zweiter internationaler Workshop "Proteinanalyse im Gewebe", 17. – 18. Februar 2011

Anstellung während der Doktorarbeit

Mitarbeiter im Augenscreen der Deutschen Mausklinik.

Publikationen

1   Morgan H, Beck T, Blake A, Gates H, Adams N, Debouzy G, Leblanc S, Lengger C, Maier H, Melvin D, Meziane H, Richardson D, Wells S, White J, Wood J; **EUMODIC Consortium**, de Angelis MH, Brown SD, Hancock JM, Mallon AM. (2010) EuroPhenome: arepository for high-throughput mouse phenotyping data. Nucleic Acids Res. 38 (Database issue):D577-85. (als Mitglied des EUMODIC – Konsortiums)

2   **Sun M***, Liu X*, Cao S, He Q, Zhou R, Ye J, Li Y, Chen H. (2007) Inhibition of porcine circovirus type 1 and type 2 production in PK-15 cells by small interfering RNAs targeting the Rep gene.Vet Microbiol. 123:203-9.(*gleicher Beitrag)

3   Liu X, Cao S, Zhou R, Xu G, Xiao S, Yang Y, **Sun M**, Li Y, Chen H. (2006) Inhibition of Japanese encephalitis virus NS1 protein expression in cell by small interfering RNAs. Virus Genes. 33:69-75.

4   Cao S, **Sun M**, Liu X, Liu X, Chen H. Construction of molecular clone of chimeric porcine circovirus(PCV1-2) and identification of its infectivity. (2006) Wei Sheng Wu Xue Bao. 46:158-61. (auf chinesisch)

5   Cao S, Liu Z, Liu X, **Sun M**,Chen H. (2006) Genome cloning and infectivity identification of Porcine Circovirus Type 1. China Journal of Virology. 22:66-69. (auf Chinesisch)

Konferenzen und Tagungen

1   1st Annual EuMODIC Meeting, Strasbourg, French. (2008)

2   Annual retreat of Institute of Development Genetics, Helmholtz Zentrum München, Neuherberg, Germany. (2008) *Crybb2* and brain. (Vortrag)

3   Interact 2009-Munich PhD symposium, Ludwig-Maximilians-Universität, München, Germany. (2009)

4   Annual retreat of Institute of Development Genetics, Helmholtz Zentrum München, Neuherberg, Germany. (2009) Identifying novel functions of *Crybb*2 in the brain. Minxuan Sun, Elena Chanina, Chichung Lie, Jochen Graw. (Poster).

5   Annual retreat of Institute of Development Genetics, Helmholtz Zentrum München, Neuherberg, Germany. (2010) *Crybb2*, a new candidate gene for schizophrenia? (Vortrag).

6   Annual Conference of the German Genetics Society, Würzburg, Germany. (2011) Mutations and polymorphisms in *Crybb2* encoding βB2-crystallin are associated with smaller hippocampus volume, reduced sensory gating and altered antisaccade eye movement. Minxuan Sun, Sabine M. Hölter, Jens Stepan, Lillian Garret, Chichung D. Lie, Matthias Eder, Dan Rujescu, and Jochen Graw. (Abstract eingereicht).